Laser Fabrication of Surface Metal Matrix Composites on Aluminum Alloy

By

Chong Pak Hung

A thesis submitted to

The Hong Kong Polytechnic University

for the degree of Master of Philosophy

At

Department of Manufacturing Engineering

The Hong Kong Polytechnic University

2001

Abstract

The creation of a wear resistant surface of metal matrix composite on AA6061 aluminum alloy by laser surface cladding of pre-pasted metal/ceramic powder was successfully achieved using a 2 kW CW Nd-YAG laser. Different ratios of metal and ceramic powder were investigated. Powder mixtures of different compositions of Mo/WC, Mo/TiC, Mo/Si_3N_4 and Si_3N_4/TiC were pre-placed on the aluminum alloy AA6061 and then irradiated by the defocused laser beam. For the Mo/WC laser cladding system, the processing parameters were 17 mm/s beam scanning speed, 3 mm beam diameter and 1.4 kW laser power at the workpiece and 0.3 mm pre-placed layer thickness. For the Mo/TiC laser cladding system, the optimum processing parameters were 3 mm laser beam size, 17 mm/s beam scanning speed, 1.3 kW laser power at the workpiece and 0.25 mm pre-placed layer thickness. Both of 2 systems used 50% overlapping on every single track to produce a surface. Mo/Si_3N_4 and Si_3N_4/TiC systems have a preliminary studied and proved that they are difficult to produce a good clad layer.

The chemical composition, microstructure and surface morphology of the clad layer were analyzed using scanning electron microscopy (SEM), energy dispersive X-ray spectroscopy (EDX) and X-ray diffractometry (XRD). High quality metal matrix composite (MMC) coatings of Mo/WC and Mo/TiC on the Al alloy were obtained. The clad layers were free of porosity and crack. Excellent bonding between the coating and the aluminum alloy substrate was ensured by the strong metallurgical interface. The values of surface hardness of the clad specimens were increased significantly. The samples have been characterized by abrasive pin-on-disc wear test. The results show that all clad specimens have extremely good abrasive wear resistance.

Mostly, fine dendritic structures were observed in the MMC clad layer. Depending on the process parameters, unmelted or partially melted WC particles were also observed. These unmelted particles were found to contribute to the improvement of the wear resistance. The distributions of the dendrites and unmelted or partially melted ceramic phases were found to depend on the process parameters. For the Mo/WC and Mo/TiC MMC cladding systems, the matrix of the MMC layer consisted of alloys of Mo-W-Al and Mo-Ti-Al respectively, which are harder than the Al alloy. Clad layers using Mo/Si_3N_4 and TiC/Si_3N_4 systems were mostly porous and had cracks. Interfacial bonding between the clad surface and the substrate was poor. It was unsuccessful to fabricate a surface large enough for wear test.

List of publications by candidate, Chong Pak Hung, as on September 2001

Conference paper:

1. P. H. Chong, H. C. Man, T. M. Yue, " Laser Surface Cladding of Mo-WC on AA6061 Aluminum Alloy", in the 19th International Congress on the Application of Lasers and Electro-optics, Detroit, USA, October 2000.vol 89, pp.104-113.

JOURNAL PAPERS SUBMITTED:

1. P. H. Chong, H. C. Man, T. M. Yue, " Microstructure and Wear Properties of Laser Surface-cladded Mo-WC MMC on AA6061 Aluminum Alloy", Surface and Coatings Technology, Vol.145, pp.51-59 (2001).
2. P. H. Chong, H. C. Man, T. M. Yue, " Laser Fabrication of Mo-TiC MMC on AA6061 Aluminum Alloy surface" , submitted to the Surface and Coatings Technology.

Acknowledgements

I dedicate this book to my mother, Mrs Chong Li Mee Yuk, who has brought me up and supported me wholeheartedly.

I would like to express my sincere gratitude to my project supervisor Dr. H. C. Man who inspired my work and personality through his attitude, actions, and behaviors. His example inspired me to never give up in the pursuit of all my dreams. Especially, for his invaluable experience and recommendations which are very useful for clarifying some misconceptions and tackling problems. I would like to hold a deep respect for Dr. W. Y. Ng. His talents, patient guidance, encouragement and suggestion throughout this project period were deeply appreciated.

I would like to express my thanks to Dr. T. M Yue, my co-supervisor, for his encouragement and help in many aspects. Also, I am extremely grateful to Dr. F. T. Cheng, Department of Applied Physics, for his constructive advice and encouragement.

I especially appreciate the help from our laboratory technicians for carrying out my experimental work: Mr. T. W. Chan in the Laser laboratory for his experienced technical support, advice and unfailing courtesy; Mr. Rico Cheung of the machine tools laboratory on the tool making and preparation of specimens, and Mr. Lau in the metallurgy laboratory for his help in microhardness test and microstructure analysis. Also, I would like to thank Mr. C.S. Lo and Mr. Yeung in the Department of Applied Physics for their assistance of the SEM work.

At length, I would like to acknowledge the Research Committee of the Hong Kong Polytechnic University for the provision of a research grant (Project No. GV 904).

Table of content

		Page
Abstract		i-ii
Acknowledgement		iii
Table of content		iv-vii
List of figure		viii-xiii
List of table		xiv
Chapter 1	**Introduction**	
1.1	Background	1-2
1.2	Objectives	3
Chapter 2	**Literature Review**	
2.1	Surface engineering techniques	4
2.2	Conventional surface engineering techniques	4-5
2.2.1	Electrochemical treatment	5
2.2.2	Thermal spraying	5-8
2.2.3	Chemical vapour deposition (CVD)	8-9
2.2.4	Ion implantation	9-10
2.3	Comparison between laser and conventional material processing technique	10-11
2.4	Laser surface engineering	11-12
2.4.1	Laser transformation hardening	13-14
2.4.2	Laser surface melting	14-16
2.4.3	Laser glazing	16

2.4.4	Laser surface alloying and laser surface cladding	16-17
2.4.4.1	Difference between laser surface alloying and laser surface cladding	17
2.4.4.2	Dilution ratio between of LSA and LSC	18-19
2.4.4.3	Microstructure formation in laser alloying and laser cladding	19-21
2.4.4.4	Methods of feeding the coating materials	21-23
2.5	Laser alloying or cladding on aluminum alloy	
2.5.1	Surface engineering of aluminum alloys	23-26
2.5.2	Laser alloying / cladding of aluminum alloys with metallic material	26-27
2.5.3	Laser alloying / cladding of aluminum alloys with ceramics material	27-28
2.5.4	Laser alloying / cladding of aluminum alloys with MMC or CMC	29
2.5.5	Problems associated with LSA/LSC of aluminum alloys	29-30
2.6	Laser cladding of WC on various alloys	30-31
2.7	Laser cladding of TiC on various alloys	31-32
2.8	Laser cladding of Si_3N_4 on various alloys	32.-33
2.9	Summary of laser cladding on aluminum alloys	34-37
2.10	Surface engineering and wear	38-40
2.10.1	Abrasive wear	40-41
2.10.2	Adhesive wear	42

Chapter 3 **Methodology**

3.1	Neodymium: YAG laser	43-45
3.1.1	Focusing head	46
3.1.2	Focusing position	46-47
3.1.3	Gas shielding	47
3.2	Material selection	48-49
3.2.1	General characteristics of aluminum alloy	50

3.2.2	General characteristics of molybdenum	50-51
3.2.3	General characteristics of ceramics particles	52-53
3.3	Specimen preparation	53-54
3.4	Laser cladding procedure	54
3.5	Calculation of laser density	54-55
3.6	Microstructures and surface morphology investigation	55
3.6.1	Metallography and structural examination	55
3.6.1.1	Optical microscopy (OM)	56
3.6.1.2	Scanning electron microscopy (SEM)	56
3.6.1.3	Energy dispersive x-ray spectroscopy (EDX)	56-57
3.6.1.4	X-ray diffractometry (XRD)	57-58
3.7	Abrasive pin-on-disc wear test	58-60
3.8	Measurement of Vicker's microhardness	60-61

Chapter 4 Results and Discussions - Laser Cladding of MMC on Al Alloy AA6061

4.1	Introduction	62
4.2	Laser cladding of WC on aluminum alloy AA6061	63-68
4.3	Laser cladding of TiC on aluminum alloy AA6061	68-73
4.4	Laser cladding of Mo on aluminum alloy AA6061	73-82
4.5	Laser cladding of Mo/WC on aluminum alloy AA6061	83-92
4.6	Laser cladding of Mo/TiC on aluminum alloy AA6061	93-103
4.7	Other systems studied	103
4.7.1	Laser cladding of Si_3N_4 on aluminum alloy AA6061	103-109
4.7.2	Laser cladding of Mo/ Si_3N_4 on aluminum alloy AA6061	110-117
4.7.3	Laser cladding of TiC/ Si_3N_4 on aluminum alloy AA6061	118-120

Chapter 5 Results and Discussions - Wear Resistant Properties of the Laser Cladding of MMC on Al Alloy AA6061

5.1	Introduction	121

	5.2	Wear resistance analysis of laser cladding Mo/WC on aluminum alloy	121-126
	5.3	Wear resistance analysis of laser cladding Mo/TiC on aluminum alloy	127-131
	5.4	Wear resistance analysis by using archard equation	132-134
Chapter 6		**Conclusion**	135-136
Chapter 7		**Suggestions for further study**	137
Reference			138-152
Appendix I		**Laser Cladding of WC on various alloys**	153-154
Appendix II		**Laser Cladding of TiC on various alloys**	155-156
Appendix I-III		**Laser Cladding of Si_3N_4 on various alloys**	157

List of Figures

		Page
Figure 2.1	Conventional surface engineering techniques	5
Figure 2.2	Cross sections of typical flame spray guns. (a) Wire or rod. (b) Powder. [15]	7
Figure 2.3	Plasma spray process [15].	8
Figure 2.4	Different laser surface modification method	12
Figure 2.5	Schematic diagram of laser surface treatment process	12
Figure 2.6	Thermal cycle for transformation hardening	14
Figure 2.7	Schematic diagram of cross section through a melted layer showing calculation of dilution ratio.	18
Figure 2.8	Basic categories of wear and specific wear modes [22]	38
Figure 2.9	Illustrations of the three general ways by which materials wear [122].	39
Figure 2.10	Nature of the contact between real surface [122]	42
Figure 3.1	Structure of Nd: YAG solid state laser [1]	44
Figure 3.2	Major components of Nd-YAG laser [Lumonics, MW2000]	45
Figure 3.3	Laser beam path of the 2kW Nd-YAG laser systems.	45
Figure 3.4	Principle for establishing the minimum focus waist position by using a stainless steel plate (a) before beam print; (b) after beam print.	47
Figure 3.5	The phase diagram of Al-Si [129]	51
Figure 3.6	The phase diagram of Al-Mo [129]	51
Figure 3.7	Scanning electron micrograph of as-received tungsten carbide WC particles.	52
Figure 3.8	Scanning electron micrograph of as-received titanium carbide TiC particles.	53
Figure 3.9a	A schematic diagram of Pin-on-disc wear tester	59
Figure 3.9b	Pin-on-disc wear tester.	59
Figure 3.9c	Weight and Pin of the wear tester	60

Figure 4.1a	The surface appearance of successful cladding of specimen WC6.	65
Figure 4.1b	The peel off phenomenon of specimen WC2.	65
Figure 4.2	Cross-section of specimen WC 6, layer clad with 100% WC particles.	66
Figure 4.3	Cross-section of specimen WC2. Porosity at the interface of clad layer and substrate (region a and b).	66
Figure 4.4	Surface condition of the as-received WC particle	67
Figure 4.5	Cross section micrograph of WC particle melted at the edge and with internal cracking after laser cladding	67
Figure 4.6	X-ray diffraction spectra of laser clad specimen WC6.	68
Figure 4.7	Cross-section of specimen TiC 6 , layer clad with 100% TiC pasting powder.	72
Figure 4.8	Relationship between the clad layer thickness versus power . (in the speed of 17 mm/s)	72
Figure 4.9	X-ray diffraction spectra of laser clad specimen TiC6.	73
Figure 4.10	The parameter window for Mo/Al clad layer.	78
Figure 4.11	Dendritic structure formation of specimen Mo4 (100% Mo pasting powder)	78
Figure 4.12	Two different zones in the Mo-Al clad layer specimen Mo4.	79
Figure 4.13	X-ray diffraction spectra of specimen Mo4 (100% Mo pasting power) .	80
Figure 4.14	Compositional variation of specimen Mo4 (100 %Mo) from the top of the clad to the Al alloy substrate.	80
Figure 4.15	The hardness distribution along the specimen Mo4.	81
Figure 4.16a	Al-Mo intermetallic compound formation in specimen Mo4 (100%Mo pasting powder).	81
Figure 4.16b	EDX line scan of specimen Mo4 (100% Mo pasting powder).	82
Figure 4.17a	Schematic diagram of the interrun porosity.	82
Figure 4.17b	Schematic diagram of the porosity occurs in the clad layer interface.	82
Figure 4.18	WC cluster formation in the laser clad layer with 60% Mo and 40% WC powder.	87

Figure 4.19	Columnar dendrites grow epitaxially from the surface of the partially melted WC particles, layer clad with 60% Mo and 40% WC powder.	87
Figure 4.20a	WC particle after laser clad with 60% Mo and 40% WC powder.	88
Figure 4.20b	EDX line scan of figure 4.20a.	88
Figure 4.21	Cross-section of specimen C, layer clad with 60% Mo and 40% WC powder.	89
Figure 4.22	Cross-section of specimen D, layer clad with 40% Mo and 60% WC powder.	89
Figure 4.23	Cross-section of specimen E, layer clad with 20% Mo and 80% WC powder.	90
Figure 4.24	Microhardness versus percentage of tungsten carbide in the pasting powder.	91
Figure 4.25a	X-ray diffraction spectra of Al alloy AA6061-T657.	91
Figure 4.25 b	X-ray diffraction spectra of laser clad specimen B.	92
Figure 4.25c	X-ray diffraction spectra of laser clad specimen C.	92
Figure 4.26a	Cross-section of specimen A, layer clad with 100% Mo pre-placing powder.	96
Figure 4.26b	EDX line scan across the clad layer of specimen A.	96
Figure 4.27a	Cross-section of specimen Bb, layer clad with 50% Mo and 50% TiC powder.	96
Figure 4.27b	EDX line scan across the clad layer of specimen Bb.	96
Figure 4.28a	Cross-section of specimen Cc, layer clad with 40% Mo and 60% TiC powder.	97
Figure 4.28b	EDX line scan across the clad layer of specimen Cc.	97
Figure 4.29a	Cross-section of specimen Dd, layer clad with 30% Mo and 70% TiC powder.	97
Figure 4.29b	EDX line scan across the clad layer of specimen Dd.	97
Figure 4.30a	Cross-section of specimen TiC6, layer clad with 100% TiC pasting powder.	98
Figure 4.30b	EDX line scan across the clad layer of specimen TiC6.	98
Figure 4.3a	X-ray diffraction spectra of laser clad specimen Bb.	98
Figure 4.31b	X-ray diffraction spectra of laser clad specimen Cc.	99

Figure 4.31c	X-ray diffraction spectra of laser clad specimen Dd.	99
Figure 4.32a	Distribution of the Mo/TiC clad layer in specimen Cc.	100
Figure 4.32b	Dissociation behaviors of TiC particles in specimen Cc.	101
Figure 4.32c	EDX line scan of Figure 4.32b.	101
Figure 4.32d	Higher magnification of specimen Cc (zone B of Figure 4.32a).	102
Figure 4.33a-d	Distribution of Mo/TiC particles in the melt pool under SEM mapping examination of specimen Bb.	102-103
Figure 4.34	The surface appearance of 100% Si_3N_4 (pre-placing powder) on Al alloy AA6061.	106
Figure 4.35a	The clad layer of specimen S8 with 100% Si_3N_4 pasting powder.	106
Figure 4.35b	EDX line scan of Figure 4.35a.	107
Figure 4.36a	The microstructure of specimen S8.	107
Figure 4.36b	The cellular structure of zone SS in the 100% pre-placing Si_3N_4 cladding.	108
Figure 4.36c	SEM micrograph of zone S in Figure 4.36a.	109
Figure 4.37	X-ray diffraction spectra of laser clad specimen S8.	109
Figure 4.38	Cross-section of specimen SA10, layer alloyed with 50% Mo and 50% Si_3N_4 powder.	112
Figure 4.39a	EDX composition analysis of specimen SA10.	112
Figure 4.39 b	Black scattered SEM micrograph showing the alloyed layer, in which the white color spots are some un-melted Mo.	113
Figure 4.39c	Black scattered SEM micrograph shows the higher magnification of Figure 4.39b.	113
Figure 4.40	The hardness distribution along the specimen SA10.	114
Figure 4.41 a- b	The optical microscope of gain structure in alloyed zone.	115
Figure 4.42a	The un-melted Mo cluster.	116
Figure 4.42 b	The un-melted Mo and Al-Si-Mo intermetallic compounds in Mo/ Si_3N_4 alloyed layer.	116
Figure 4.43	X-ray diffraction spectra of laser clad specimen SA 10.	117
Figure 4.44	Cross-section of specimen SA6, layer alloyed with 50%TiC and 50% Si_3N_4 powder.	119
Figure 4.45	SEM micrograph of the microstructure of specimen SA6.	120

Figure 5.1	Wear test results of cumulative mass loss on the laser clad specimens and the as-received Al alloy AA6061.	124
Figure 5.2	Results of cumulative mass loss on the laser clad specimens. (note the scale of the vertical axis)	124
Figure 5.3a	Scanning electron micrograph of the worn surface of Al alloy AA6061 surface.	125
Figure 5.3b	Higher magnification of the aluminum alloy AA6061 worn surface.	125
Figure 5.4a	Scanning electron micrograph of the worn surface of specimen Mo4 (100% Mo pasting powder) .	125
Figure 5.4b	Higher magnification of the worn surface of specimen Mo4 (100% Mo pasting powder).	125
Figure 5.5a	Scanning electron micrograph of the worn surface of the specimen E (20%Mo 80%WC in pasting power).	126
Figure 5.5b	WC torn off after the abrasive wear test.	126
Figure 5.6a	Scanning electron micrograph of the worn surface of the specimen WC6 (100%WC in pasting power)	126
Figure 5.6b	Cracking occurred on the worn surface of specimen WC6.	126
Figure 5.7	Wear test results of cumulative mass loss on the laser clad specimens and the as-received Al alloy AA6061.	129
Figure 5.8	Results of cumulative mass loss on the laser clad specimens. (note the scale of the vertical axis)	129
Figure 5.9	Worn surface of the as-received Al alloy AA6061.	130
Figure 5.10	Scanning electron micrograph of the worn surface of specimen D (30%Mo 70% TiC pre- placing powder).	130
Figure 5.11a	Scanning electron micrograph of the worn surface of specimen TiC6 (100% TiC pre-placing powder).	130
Figure 5.11b	Cracking occurred at the overlap track interface.	130
Figure 5.12	Schematic view of a transverse cross-section of the TiC clad layer. (1) clad zone, (2) overlap track interface zone, (3) substrate clad layer interface , (4) heat affected zone in substrate.	131
Figure 5.13	The overlap track interface zone of 100% TiC clad specimen. (Note: the depletion of TiC particles in this zone)	131

Figure 5.14a	The relationship of cumulative mass loss of the as-received Al alloy and laser clad Mo/WC MMC system versus the hardness value.	133
Figure 5.14b	The relationship of cumulative mass loss of the laser clad Mo/WC MMC layers versus the hardness value.	133
Figure 5.15a	The relationship of cumulative mass loss of the as-received Al alloy and laser clad Mo/TiC MMC system versus the hardness value.	134
Figure 5.15b	The relationship of cumulative mass loss of the laser clad Mo/TiC MMC layers versus the hardness value.	134

List of Tables

		Page
Table 2.1	Industrial exploitation of ion implantation. [24]	10
Table 2.2	Manufacturing properties for aluminum alloy series [84].	25
Table 2.3	Summarized most of the published research work on laser cladding or laser surface alloying of Al alloys.	36
Table 3.1	Chemical composition of Al alloy AA6061	48
Table 3.2	Melting point and particles size of powder material	48
Table 3.3	Physical properties of AA6061, Mo, Co, WC, and TiC, Si_3N_4.	49
Table 4.1	Laser parameters for laser clad 100% WC pre-placing powder on AA6061 (beam diameter d =3mm) .	65
Table 4.2	Laser parameters for laser 100% TiC pre-placing powder laser cladding.	71
Table 4.3	Process parameters for laser cladding Mo on aluminum alloy AA6061.	77
Table 4.4	The EDAX weight percentage analysis of region 1 – region 3.	81
Table 4.5	Wt% of Mo and WC in the 0.3 mm thick powder paste and the resulting clad layer hardness and thickness.	86
Table 4.6	% of Mo and %TiC in the 0.25 mm thick powder paste and the clad layer hardness and thickness (carbon was not detected).	95
Table 4.7	Composition of the grey and white phases in Figure 4.32d. (carbon was not detected).	100
Table 4.8	The composition distribution of the clad layer.	107
Table 4.9	The composition analysis of Figure 4.35b.	108
Table 4.10	The composition analysis of the alloyed region in Figure 4.39c.	114
Table 4.11	The composition distribution of the clad layer.	119
Table 5.1	Average mass loss (g) of specimens from the moving pin-on-disc experiment after 1414 m sliding distance (per 5 mins test cycle).	122
Table 5.2	Average mass loss (g) of specimens from the moving pin-on-disc experiment after 1414m sliding distance (per 5 mins test cycle).	128

Chapter 1

Introduction

1.1 BACKGROUND

Aluminum alloys are widely used in many technological fields because of their high specific strength, high specific modulus, high thermal conductivity and good corrosion resistance in atmosphere. Aluminum alloys are increasingly demanded in automobile, robotic and aeronautical industries for the benefits of improved fuel efficiency. In the automobile industry, aluminum alloy 6061 is widely used for the pistons, valves, airplane fittings and many high-temperature service parts.

However, the poor surface properties of Al alloys, such as low hardness, low wear resistance and low corrosion resistance have hindered their application in many other engineering aspects. Aluminum alloys do not have an allotropic transformation as in iron, cobalt, or titanium alloys, so there is no possibility of a martensitic transformation and the hardening effects by conventional solid-state treatments are very limited. A lot of research efforts have been spent on improving these surface properties. Recently, laser surface cladding has been investigated widely as a means to modify the surface of these alloys.

The technique of laser surface cladding has been used to produce some tailor-made surface coatings on a wide range of ferrous and non-ferrous metals. The advantages of this technique over other surfacing technologies are its localized heating, controllable degree of dilution in the clad layer and less distortion to the workpiece. In recent years, studies on laser cladding ceramic-metal composite coating on various alloys have attracted a lot of research interests. Many kinds of ceramic particles, such as WC, TiC and Si_3N_4, SiC etc,

have been clad on titanium and ferrous alloys. Yet cladding of these ceramic particles on aluminum alloys have been scarcely reported. This is mostly due to the difficulty encountered in surface engineering of aluminum alloys. Aluminum alloys have high reflectivity to 10.6 μm laser radiation generated from CO_2 lasers which have been widely used for studies in laser cladding because of its availability of high power. Poor energy absorption of the CO_2 laser beam by the aluminum substrate and made it difficult to clad.

A high power YAG laser was used in this research project for the cladding process. YAG laser light has shorter wavelength than that of carbon dioxide laser. Recent advance in high power YAG laser development has made high power YAG laser available for industrial applications. The shorter wavelength of the YAG laser beam, 1.06 μm, provides a better absorption efficiency to the aluminum alloy and therefore has improved energy coupling efficiency. More efficient energy absorption by the alloy enables a thicker molten pool to be produced which can help the production of a clad layer.

Since the laser cladding process was carried out by pre-placing a layer of clad material on the aluminum alloy substrate, the laser beam may not interact directly with aluminum alloy. Therefore the main difficulty of the process may not be the laser beam reflection by the aluminum, but the large melting point differences between the clad material and the Al substrates as well as the high thermal conductivity of the substrates.

1.2 OBJECTIVES

The present research program aims at improving the wear resistance of aluminum alloy AA6061-T651, which has found wide applications in various industries, by fabricating a metal matrix composite layer on the Al alloy using laser cladding process. The aluminum alloy surface will be coated metallurgically with a layer of ceramic/metal composite.

Objectives of this project are:

- To investigate the process characteristics of laser cladding on aluminum alloys AA6061 by using a high power Nd-YAG laser.
- To laser clad wear resistant MMC layers (WC, TiC, Mo, Si_3N_4, Mo/WC, Mo/TiC, Mo/Si_3N_4 , Si_3N_4/TiC) on aluminum alloys using powder pre-placing method.
- To investigate the microstructure, microhardness and wear resistant properties of the clad layers.

Chapter 2

Literature Review

2.1 SURFACE ENGINEERING

Surface engineering has been defined as " the application of traditional and innovative surface technologies to engineering components and materials in order to produce a composite material with properties unattainable in either the base or surface material [1-9]. One of the main aims of surface engineering is to improve properties such as friction, wear, corrosion, fatigue and bio-compatibility. The basic idea of surface engineering is to use cheaper materials as substrates and rare or strategically important (often expensive) materials as coating, so as to reduce the part cost or weight of the whole part.

Methods of producing a hard surface on metal components are divided into two broad categories in this chapter. They are conventional surface engineering and laser surface engineering techniques.

2.2 CONVENTIONAL SURFACE ENGINEERING TECHNIQUES

The conventional surface coating techniques are electrochemical treatment, thermal spraying, chemical vapour deposition and ion beam implantation (Figure 2.1) . Surface coating processes such as electrochemical treatment, physical vapour deposition and spraying in which the substrate is relatively cold during deposition and can be used on a wide range of substrates. The high temperatures occurring during chemical vapour deposition may make it un-suitable for some substrates and restrict the choice of coating composition.

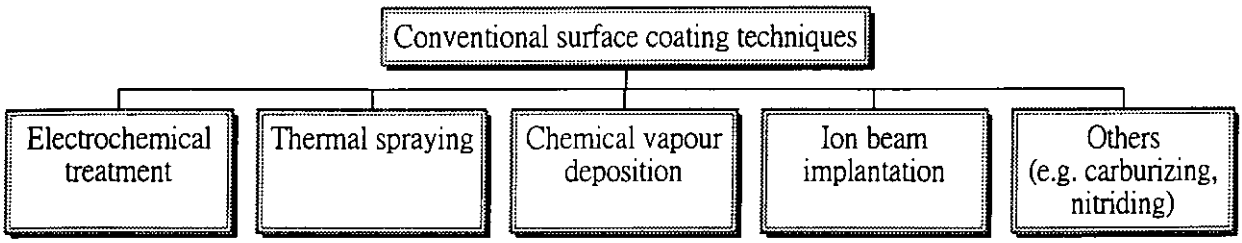

Figure 2.1 Conventional surface engineering techniques

2.2.1 ELECTROCHEMICAL TREATMENT

Electrochemical coatings are produced by electrolysis of an aqueous solution of a salt of the coating metal, the components to be coated being the cathode. For wear resistance, chromium is the coating most widely used as it combines high hardness (~1000 Hv) with corrosion resistance and a low value of friction against steels. Chromium coatings are limited to a thickness of 0.5 mm because of internal stresses. Thicker coatings, up to several millimeters, of nickel can be obtained but as the deposit is relatively soft (~250 Hv), it is seldom used for wear resistant application. Hard particles of carbides (e.g. SiC, Cr_2C_3) and oxides (e.g. Al_2O_3) can be incorporated in electrochemical coatings of nickel and cobalt during plating to give a coating hardness of 600 Hv [10].

2.2.2 THERMAL SPRAYING

Thermal spraying is a technique widely accepted by industry for metal or ceramic powders deposition. The spray materials are in the form of a wire or powder and fed precisely into a heat source and are given sufficient thermal energy to heat the particle to an

advanced plastic state. The resulting molten or nearly molten droplets of materials are accelerated in a gas stream and projected against the surface to be coated. Subsequent particle build-up produces a discrete coating. A lot of work has been done on thermal spraying of some alloys on the metal substrate [10-17].

There are flame powder spraying and plasma spraying processes. Flame powder spraying (Figure 2.2) is a process which sprays the materials in the form of powder (or wire). In the plasma spraying process (Figure 2.3), argon gas, occasionally including nitrogen, hydrogen, or helium, passes through an electric arc and metal or ceramic powder is then introduced into the gas stream. Both are heated and accelerated by high temperature, high-velocity plasma gas stream. The material ranges will be widened with regard to wear applications combined with protection against corrosion, hot gas corrosion, and thermal and electrical insulation, by coating material such as MCrAlY, stabilized ZrO_2, intermetallics, superalloys, refractory metals, and high alloyed steels. The applications of thermal spray coatings are to enhance the wear corrosion resistance of a surface. Other applications include their use for dimensional restoration, as thermal barriers, as thermal conductors, as electromagnetic shielding and to enhance or retard radiation.

A wide variety of materials can be used to make a coating by using thermal spraying. It can re-coat the worn part or damaged coating without changing the properties or dimensions of the part. However, the typical layer porosity, unmelted particles, lower bond strength and narrow working temperature range limit the applications of thermal spraying. This method also prohibits the size of coating and deep cavities coating and the homogeneous coating quality is not guaranteed by using this method [17-18]. Because of these reasons, this process is limited on the applications in both cavitation condition and corrosive environment. Some researchers use plasma spraying and then post-spraying treatment, such as annealing, laser

surface melting / glazing are applied to reduce the porosity and improve the inhomogenized distribution of the particles on the plasma spray deposited layer. At the same time, it improves the wear resistance and heat resistance as well [19-21].

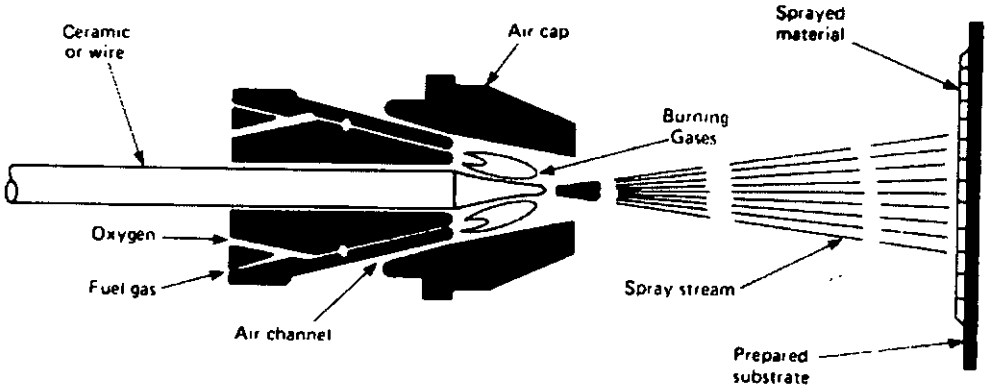

(a)

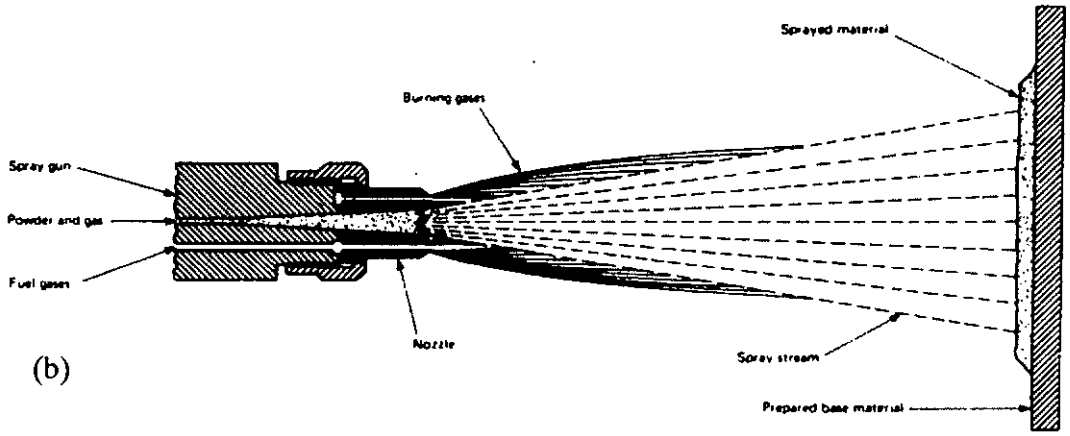

(b)

Figure 2.2 Cross sections of typical flame spray guns. (a) Wire or rod. (b) Powder. [15]

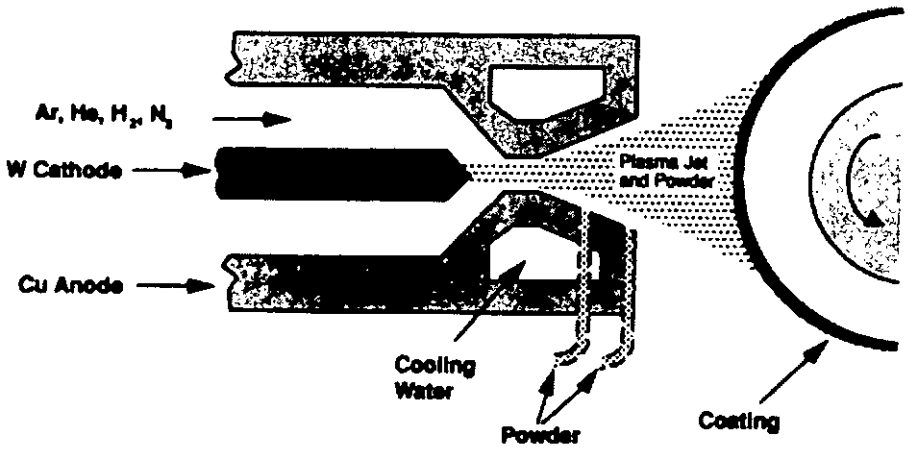

Figure 2.3 Plasma spray process [15].

2.2.3 CHEMICAL VAPOUR DEPOSITION (CVD)

Chemical vapour deposition (CVD) is a process whereby compounds are reacted in the gas phase to form a dense layer on a heated substrate. This is a process where a solid reaction product nucleates and grows on a substrate, due to a gas phase reaction, enhanced by heat, plasma or UV light. The most widely used wear resistant materials deposited by CVD are titanium carbide and titanium nitride and these materials coating thickness are limited to about 10 μm by interfacial stresses. Temperatures in the range 800 – 1000 ℃ are required for deposition and at these temperatures thermal distortion and chemical reaction between coating and substrate limit the choice of substrate. In wear resistant applications, only cemented carbides and some tool steels are used and in these cases the reaction which takes place results in very high bond strengths. Many factors affect a good CVD coating such as gas reactant composition, flow rate, Reynolds number, substrate temperature and total gas pressure.

Many materials can be coated by chemical vapor deposition (CVD). Heavy nickel coatings can be applied from nickel carbonyl to a wide variety of substrate [22]. Chromium

can be applied to high carbon steel to make a hard surface or to soft steel to make a " low cost stainless steel". Silicon carbide can be applied to add durability to optical disks, and diamond or hard diamond-like carbon can be applied to a variety of substrates to impart diamond-like characteristic [22].

2.2.4 ION IMPLANTATION

Ion implantation involves the bombardment of a solid material with medium-to-high-energy ionized atoms and offers the ability to alloy virtually any elemental species into the near surface region of any substrate. Chosen atomic species are ionised and then accelerated in a field of 10 to 1000 keV in a moderate vacuum (1 mPa). The ion source and extraction electrodes are designed so that ions emerge as a beam. Ion penetration is only about 0.2μm but materials properties are greatly altered.

Ion implantation is a low temperature process that have prompted explorations into applications in which the limitations of dimensional changes and possible delamination of conventional coatings are of concern. It has been used extensively in the semi-conductor industry since the 1970s to introduce dopant atoms reproducibly into silicon wafers to modify electrical performance, and it is used routinely in several stages of integrated circuit production. Further, ion implantation was found to play a beneficial effect against decarburization of the alloy. Table 2.1 shows the industrial application of ion implantation.

Pérez *at el* [23] studied the influence of implanted silicon, molybdenum and cerium on the oxidation behaviour of a 18Cr8Ni stainless steel at 1173 K up to 144 h in air under isothermal conditions. The implanted silicon and cerium markedly improved protection against oxidation of the alloy by enhanced chromium transport while molybdenum gave rise

to an accelerated oxidation due to the formation of the volatile MoO_3 species.

Table 2.1 Industrial exploitation of ion implantation. [24]

Material	Application (specific examples)	Typical results
Cemented WC	Drilling (printed circuit board, dental burrs etc.)	Four times normal life, less frequent breakage and better product
Ti-6Al-4V	Orthopaedic implants (artificial hip and knee joints)	Significant (400 times) lifetime increase in laboratory tests
M50,52100 Steel	Bearings (precision bearings for aircraft)	Improved protection against corrosion, sliding wear and rolling contact fatigue.
Various alloys	Extrusion (spinnerets, nozzles and dies)	Four to six times normal performance
D2 steel	Punching and stamping (pellet punches for nuclear fuel, scoring dies for cans)	Three to five times normal life

2.3 COMPARISON BETWEEN LASER AND CONVENTIONAL MATERIAL PROCESSING TECHNIQUE

The principal benefits of laser processing for surface engineering compared with other processing methods are the high processing speeds, low distortion levels and directed heat input that can be achieved in a precise area. Lasers are very good at producing local changes in material properties but are generally not suitable for treating large surface area [25].

The coherent nature of laser light yields the ability for it to be focused to very high power densities. Effective use of a laser requires applications suited to a very localized heat source. The advantages of laser surface engineering processes are (1) Laser energy only heats the substrate to a very shallow layer, so the microstructure can be well controlled to give superior properties as those produced by conventional techniques; (2) Laser energy is chemically clean in that there is no flame and combustion products are not formed; (3) Laser

energy can be shaped using special mirrors and lenses to heat a defined area, so it is particular suitable for treating small area; (4) Magnetic fields do not deflect a laser beam; (5) Laser processing can be carried out at atmospheric pressure with only local shielding.

2.4 LASER SURFACE ENGINEERING

A wide range of laser surface treatment techniques is available today. Lasers have been seen ever increasing the application in a number of ways to modify the properties of surfaces. Laser surface treatment involves using high-power laser beam to heat a material up to a required temperature, followed by rapid cooling by heat conduction to the bulk. By using laser surface engineering techniques, materials may have their surface microstructure and chemical composition modified and affect properties such as wear, friction, corrosion, hardness, abrasion, oxidation resistance and electrical conductivity. At a lower power density, laser energy can be used to change the surface characteristics of a material, such as in laser melting. The thickness of the modified layer covers the range from nanometers (ablation with Excimer lasers) to several millimeters (melting with high power CO_2 lasers). Figure 2.4 and 2.5 show the major types of laser surface engineering, such as laser transformation hardening, laser surface melting, surface alloying, glazing and surface cladding.

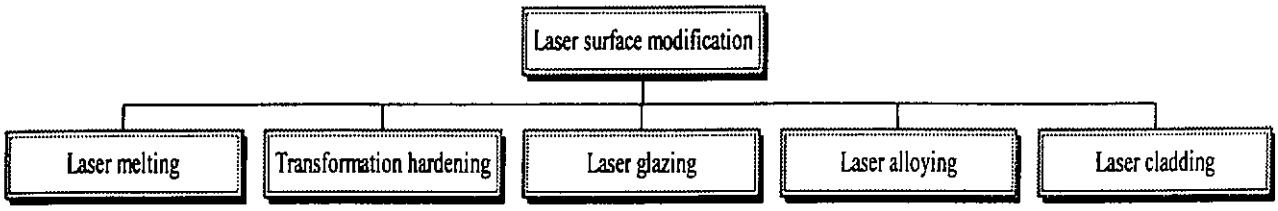

Figure 2.4 Different laser surface modification methods

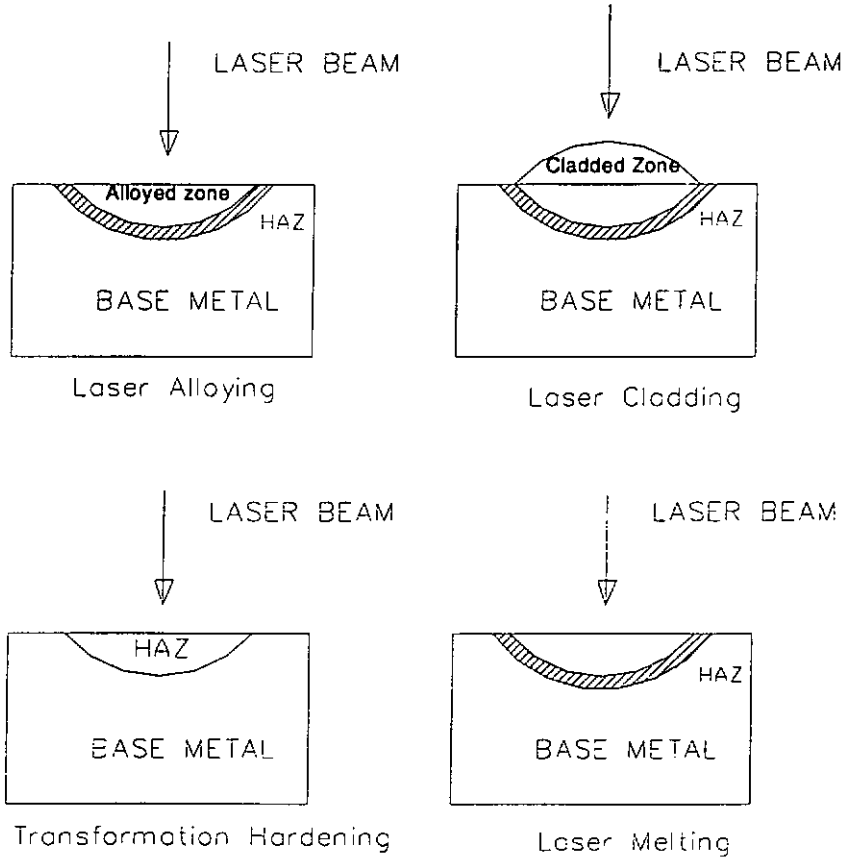

Figure 2.5 Schematic diagram of laser surface treatment process

*Heat-affected zone (HAZ) is built up by previously generated track and then leads to additional heat treatment of the substrate

2.4.1 LASER TRANSFORMATION HARDENING

Laser transformation hardening is the hardening of iron or steel (e.g. carbon steel, cast-iron) by a solid state transformation from austenite to martensite by rapid cooling (Figure 2.6). The laser beam irradiates the metal surface and causes very rapid heating of a thin layer of material near surface. When the beam moves to a different area on the surface, the heat deposited in the thin layer will quickly be conducted away, and the heated area cools rapidly. This is essentially a quenching of the surface region. The basic idea of laser hardening is to freeze a mixture of iron and carbon in a metastable structure called martensite, which is harder than the phases of iron-carbon that are normally present at room temperature. The depth of hardening and the temperature profile are determined by choice of energy density and travel speed.

According to E.V. Locke & R. A. Hella *et al.* [26], they discovered that some changes in grain structure occurred near the surface of the specimen. The CO_2 laser beam was scanned over the surface at a velocity of 10 ft/min, with a coverage of 75 $in.^2$/min. The quenching has produced a finer grain size at the surface and the hardness near the surface is about 20 times more than the base. Zhang and Man [27] studied the laser surface hardened En31 steel by CO_2 laser. The results indicated that laser transformation hardening improved the wear resistance and reduced the coefficient of friction of the En31 steel. The microstructure of the hardened zone was found to be fine martensite.

The advantage of using a laser as hardening tool lies in the possibility of a local treatment with (1) a minimum heat input to the substrate; (2) less thermal distortion, because laser energy is provided a very localized heat sources; (3) the depth of hardening is relatively shallow; thus desirable properties of the substrate metal, such as toughness, are retained.

However, there is also a limitation when larger areas have to be treated because overlapping has to be avoided due to the tempering effect on the previous track.

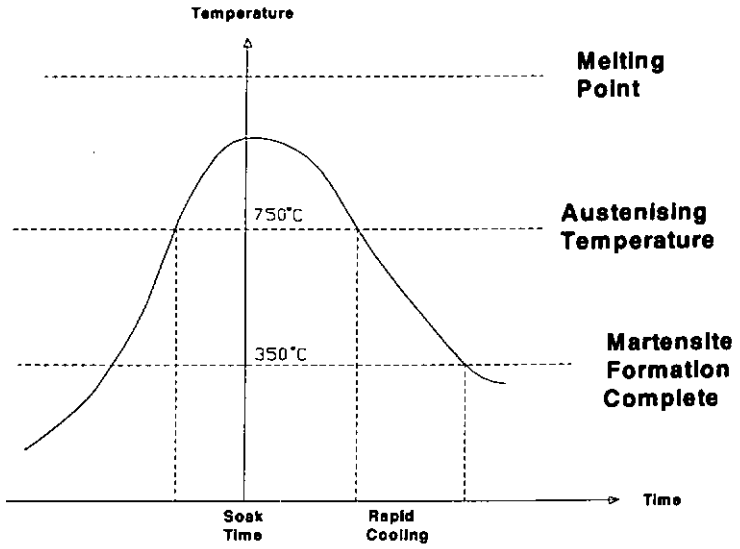

Figure 2.6 Thermal cycle for transformation hardening

2.4.2 LASER SURFACE MELTING

Laser surface melting (LSM) involves the use of high intensity beam to scan the surface of a metal substrate in a shielded gas atmosphere. The laser energy density, wavelength and interaction time control the melting conditions. The heat input from the laser has to be sufficient to promote melting, so that the structure of the surface can be modified. This technique leads to refined microstructures and in certain alloys to the formation of metastable crystalline or non-crystalline phases. Most research efforts were directed to surface melting of the metals whatever in ferrous or non-ferrous alloys, cast irons, tool steels, stainless steels, titanium and aluminum alloys for improving surface hardness, refined structure, corrosion and wear resistant properties [28, 29]. Laser melting of steels lead to the

dissolution of carbides and inclusion. Due to the high solidification rates involved in LSM, microstructures are fine and often contain supersaturated solid solutions. As a result the hardness and wear resistance and corrosion resistance of the material are often improved without degradation of its bulk properties [28]. Melting of grey cast iron leads to a ledeburitic microstructure that has excellent wear and friction properties [29].

Recently, there has been growing interest in improving the corrosion performance of aluminum alloys by laser techniques similar to those used for steel. This is achievable because of the microstructural refinement, reduced segregation, and the production of non-equilibrium phases [30]. A lot of studies on Al-Si alloy laser melting have been carried out [30-36]. The authors investigated its microstructural change by using different laser scanning speeds. The reduction of interdendritic spacing in Al-Si system was obtained. Different microstructural changes would influence its corrosion properities.

Effects of rapid multiple surface remelting by laser on the mechanical properties of Al-Si series aluminum alloys with different alloying elements such as Cu, Ni, Fe have been investigated [37]. It was shown that the homogeneous microstructures of the re-melted zone showed the refining of dendritic arm. Several workers have carried out investigations on pure Al and Al-Cu binary alloys to characterise the modification of the surface microstructure resulting from LSM. Resolidification of the melted layers has been shown to be epitaxial commencing with a very thin layer of planar front growth [37-40]. The surface melting of cast iron camshafts using 6 kW CO_2 laser is being commercialized in the automobile industry. Each cam is melted by a line focus in one step, and gives a smoother surface with same hardness. The technical and economical aspects of this treatment are superior to those of the conventional method (plasma arc melting) [41,42].

2.4.3 LASER GLAZING

Laser glazing [43] involves surface melting at high scanning speed. As the beam from a multi-kilowatt CO_2 laser is scanned over a surface, a thin melt layer is produced under high speed. It heats and cools the surface rapidly, so there is no time for heat to transfer into the interior of the workpiece. After the beam is moved away, resolidification occurs very rapidly. The surface layer is quickly quenched. As a result of this process, one may produce surface microstructures with unusual and possibly useful characteristics. The grain size near the surface is very small, because of the high quench rate. Laser glazing can produce amorphous surfaces or that have glassy, non-crystalline structure. Such surface can have high resistance to corrosion [44]. This technique is applicable both to metals and ceramics. One example of laser glazing is surface melting of cast iron with rapid resolidification. This produces a thin surface layer of very hard material called white cast iron, which can provide excellent wear resistance. Another example that has been demonstrated is the glazing of aluminum bronze, which leads to surface structures with enhanced corrosion resistance [44].

2.4.4 LASER SURFACE ALLOYING AND LASER SURFACE CLADDING

The objective of laser-surface alloying (LSA) is the complete mixing of the added material within the molten substrate surface. A lot of research work of LSA to produce hardfacing layer or improved corrosion resistant layer have been carried out [23,45-63]. The structure of the laser-alloyed layer often contains supersaturated solid solutions and sometimes intermetallic compounds. Refractory and carbide-stabilizing elements melted into the substrate and the hardness of alloyed region is increased as a result.

Laser cladding is a hardfacing process that uses a high-powered laser beam to melt the coating material and a thin layer of the substrate to form porosity-free coating of 50 μ m –2 mm thick with low dilution and perfectly bonded to the substrate [64]. The advantages of laser cladding are substantial and can include improvements in wear and corrosion resistance, reclamation of worn parts, and improved electrical and thermal conductivity. At most time, only the particular parts of surfaces that are vulnerable to corrosion or wear are treated so that it can save material and part cost, and offer the appropriate physical and mechanical properties at the same time [65]. Laser cladding with powder injection is superior to alternative processes and is the only one that has found practical use, because it is more energy efficient and allows for better process and reproducibility [66].

2.4.4.1 DIFFERENCE BETWEEN LASER ALLOYING AND LASER CLADDING

Both laser alloying and cladding processes involve adding alloying elements to the melt pool, either as a pre-deposited layer, or by feeding powder or wire into the melt pool. The major difference between LSA and LSC is the dilution ratio of the material and the substrate. Compared with the laser cladding process, lower scanning speed is normally used in laser surface alloying, and this causes higher dilution ratio of the alloying region. In laser cladding, the addition material feed rate is increased so as to build up an overlay layer that coats the substrate and with very low dilution ratio.

2.4.4.2 *DILUTION RATIO BETWEEN OF LSA AND LSC*

Dilution ratio (DR) can be determined based on the geometric volume or characteristic thickness as illustrated in Figure 2.7. Isamu Miyamoto *et al* [36] studied the mechanism of dilution ratio by using powder feeding method. In practice, a laser modified surface is achieved by overlapping of a number of single tracks. Assume the composition of the clad layer is uniform, the dilution ratio (DR) is defined as

$$DR = \frac{V_1}{V_1 + V_2} x100\%$$

$$DR = \frac{t}{d} x100\%$$

When the dilution ratio of the solidified surface is less than 10% (i.e. degree of dilution is minimized), it is termed LSC. When it is higher than 10% (i.e. higher degree of dilution), it is considered as LSA.

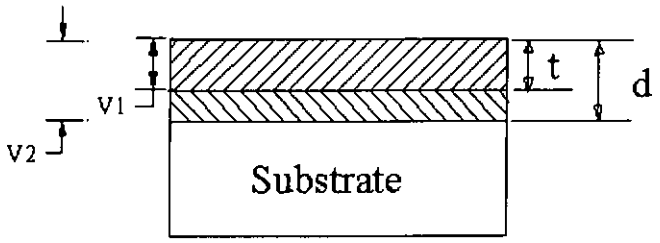

V_1 : Volume of the deposit above the interface

V_2 : Volume of the fused zone beneath the workpiece surface

t : Thickness of the coating

d : Melt depth (clad)

Figure 2.7 Schematic diagram of cross section through a melted layer showing calculation of dilution ratio.

Also, Other researchers [Pro. Lin Li] define if the properties of the clad is maintained, it is called laser cladding; and if a new alloy is formed involving the substrate, it is called laser alloying.

2.4.4.3 MICROSTRUCTURE FORMATION IN LASER ALLOYING AND LASER CLADDING

Solidification mechanism influences the microstructure formation and material properties of the clad layer. Under laser radiation, the high temperature gradients within the melt pool cause intense convection by the Marangoni effect, leading to rapid homogenization of the melt [63]. Mazumder et al. [67-68] studied the mass transport in laser melt pools and observed extremely fast homogenization in laser alloying and concluded that convection must play an important role.

Their research suggested that surface tension is an important data to influence the convection on liquid homogenization, given by

$$S=\frac{(d\sigma/dT)qd}{\mu\mu_0 k}$$

where $(d\sigma/dT)$ is the temperature derivative of the surface tension

q is the net heat flow from the laser beam

d is the diameter of the laser beam

μ is the viscosity

μ_0 is the scanning speed of the laser beam

k is the thermal conductivity

When S is low, convection is negligible, and mass transport in the melting pool is predominantly diffusive. Due to the short lifetime of the melt pool, homogenization will be insufficient. When S is high, convection plays a dominant role in the heat and mass transfer in the melt pool. It is difficult to obtain homogenization from alloying or cladding aluminum with other elements because the melting point of the alloying elements is higher than the melting temperature of the substrate material. The alloying elements react with the melt pool material to form insoluble high melting temperature intermetallic phases. Different materials melt at different temperatures. So, the layer has a higher tendency to form high melting intermetallic compounds.

The cooling rates found in laser alloying and laser cladding are very high (in the range 5 x 10^3 to 10^6 K/s, depending on the processing parameters) and solid state diffusive transformations are usually suppressed. The solidification of laser processed materials has been studied in detail by Kurz and co-workers [69]. The solidification microstructure depends essentially on the local solidification conditions (solidification rate R, temperature gradient at the solid-liquid interface G), which in turn depends on heat and mass transfer in the system.

A simple relation exists between the local solidification rate and the scanning speed V.

$$R = V \cos\theta \quad [70],$$

where θ is the angle between the normal to the S/L interface and the scanning speed vector. Since $\cos\theta = 0$ at the bottom of the melt pool, R=0. The solidification rate increases as the surface is approached, but stays lower than the scanning speed. R increases rapidly from 0 at the bottom to a constant value during most of the solidification time. The thermal gradient, G, is the highest at the bottom of the melt pool and decreases progressively towards the surface. If R and G are known, two other important solidification parameters can be calculated: the

ratio (G/R) and the cooling rate (dT/dt = G*R) present an infinite value at the bottom of the melt pool and decreases as solidification proceeds. The cooling rate is zero at maximum depth and increases as solidification proceeds.

Different cooling rates affect the formation of different microstructures. Different microstructure will cause different mechanical properties of the alloying / cladding layer. Also, alloy homogenization is a critical factor for the performance of the coating. In order to obtain the appropriate microstructure and material properties of the clad layer, it is essential to understand and control the solidification microstructure.

2.4.4.4 METHODS OF FEEDING THE CLADDING MATERIALS

Laser surface cladding processes differ in the rate of coating material supplied [64]. In the two-step laser cladding, the coating material is pre-deposited on the substrate by thermal spray process, electroplating, paste bound powder, etc. Then the coating layer is melted by a scanning laser beam. In one-step laser cladding, the cladding material is injected directly into the melt pool created by the laser beam and then forming a coating layer. Followings are different kind of powder-placing methods.

1. Laser Cladding with pre-placed powder by thermal sprayed coating or electroplating

Some studies have been made by using plasma-sprayed or electroplating process the composite coating first and then with laser post-treatment [19-20,65-66, 71]. The imperfect properties of plasma-sprayed composite coatings can be modified by laser post-treatment which increases the density and bond strength, and improves the microstructure [70-71]. The

process presents some drawbacks. The application of the powder slurry is time consuming. It is difficult to deposit a uniform layer of slurry on a complex-shaped component.

2. Laser Cladding with paste bound powders

Laser cladding with pre-placed powder is performed by scanning the laser beam over a bed of the hardfacing powder previously mixed with a binder to form a slurry and overlaid on the substrate surface [72-74]. This method is very simple and is suitable to research a lot of materials but is not suitable for actual production. As it is difficult to preplace the powder exactly at the same thickness and density, which results in the quality of alloyed layer becoming unstable [26]. Usually, the binder does not evaporate completely in the short time under laser beam and this may cause pore formation.

3. Laser Cladding by wire feeding

In this process, the clad material is supplied to the melt pool as a wire. It is a one-step process and material use efficiency should be high, but extremely good beam alignment with the wire is required to get a good result. When energy transfer is enhanced by heating the wire or by using a higher energy density, dilution becomes excessively high and the process is difficult to control. Stern *et al.* [75] suggested to pre-heat the wire up to 1000 ℃ before the process. Hensel and Binroth [76] directed the wire and the laser beam at an oblique angle to the surface and increased the laser radiation absorption efficiency.

4. Laser Cladding by powder injection

The clad powder is delivered to the melt pool by using a powder feeding system [18,49,55,77-80]. This method can provide good metallurgically bonding to the substrate surface and form a clad layer with low dilution rate. The process is traditionally done with a

side blown powder feed. Powder particles injected laterally into the interaction region through an injection tube. The particles are transported by a steam of inert gas, which protects the melt from oxidation. By scanning the laser beam, the incoming powder striking the melt pool is melted and the molten powder then adheres to the hot surfaces.

The main limitation of lateral powder feeding systems is that they are not axially symmetric since the powder must be brought to the melt pool in the plane defined by the laser beam and the scanning direction and directed towards the melt pool surface. A nozzle for coaxial laser cladding was designed to overcome this problem [81-83]. Recently, Lin and Steen [81,82] designed a coaxial laser cladding system to increase powder catchment efficiency up to 40% with a 1kW CO_2 laser. Probably, powder injection laser cladding will become the dominant method to be researched for actual application.

2.5 *LASER ALLOYING OR CLADDING ON ALUMINUM ALLOYS*

2.5.1 SURFACE ENGINEERING OF ALUMINUM ALLOYS

Aluminum is one of the most important materials in the world. It can be strong or weak, hard or soft depending upon the application. Traditionally aluminum has been and always said to be a " soft metal". That is only true of the pure metal. By alloying, and then either by rolling to a fully-hard condition or by appropriate heat treatment, the strength of aluminum can be increased by up to a factor of 10 times. Heat treatable wrought aluminum alloys of 2xxx, 6xxx and 7xxx groups are all can be precipitation-strengthened [84]. Table 2.2 showed that the general properties for aluminum alloy series.

Aluminum alloys have been used extensively in auto-motive and aircraft industries

because of their low strength, low density, low hardness, poor friction and low wear resistance. Aluminum alloys do not have an allotropic transformation as iron, cobalt, or titanium alloys, so there is no possibility of a martensitic transformation and the hardening effects by conventional solid-state treatments are very limited.

Because of the limitations, there have been a lot of research interest in the surface treatment of aluminum alloys. Ion implantation, chemical or physical vapor deposition are methods to modify the surface properties of aluminum alloys. However, the depth of coating offered by these methods are only restricted into few micrometers. This is not suitable for some stress-intensity applications. Electron beam, deposition arc welding and thermal spraying are high-energy beam treatment. Because of the high energy input of these methods, they may cause distortion of workpiece and have the limitation of coating of small and depth cavities. Moreover, thermal spraying usually produces porous coating and does not provide sufficient bonding to the substrate in many applications.

In the past two decades, laser alloying, laser cladding, laser melting and laser nitriding of Al alloys have received immense interest because of the strength, hardness and wear resistance of the coating were improved greatly. In laser surface melting of Al-Cu or Al-Fe system led to an extended solubility of the alloying elements in the matrix and these two factors contribute to the hardness enhancement [30]. However, laser melting and laser nitriding only provided very thin layer of coating and have little improvement on its hardness when compared with laser cladding.

CO_2 laser has been utilized for surface engineering of steel, titanium and stellite. The application of this gas laser for laser surface treatment of aluminum alloys has been limited. This is because aluminum alloys have high reflectivity to the 10.6 μm radiation of CO_2 laser. However, Nd-YAG laser with shorter wavelength (1.06 μm) is more suitable for laser

treatment of metallic materials than the CO_2 laser. On the other hand, the relatively high thermal conductivity of Al (226.5 W/mK), compared with stainless steel 304 is 65.3 W/mK, create difficulties in producing continuous tracks on its surface. Research study on laser cladding on aluminum is much lesser then steel.

There are many studies that have demonstrated WC and TiC could be clad on Al alloys successfully. These two ceramics were chosen as the reinforced material at the initial stage. H. C. Man [73] found the cavitation erosion resistance of specimens laser clad Si_3N_4 on Al alloy AA6061 was increased by 3 times. So, Si_3N_4 was also tried in the later stage. Those ceramic particles are used as a strengthening phase. From the study of Almeida [53] and McMahon [87], the results confirmed that Mo can mix well with Al alloy and forms homogenized structure with high hardness and defect free coating layer. So, Mo has be chosen as the matrix material in this work. Because of the above reasons, Mo/WC, Mo/TiC Mo/Si_3N_4 and TiC/ Si_3N_4 systems were studied in this work.

Table 2.2 Manufacturing properties for aluminum alloy series [84].

Al alloy series	Main element	Properties
1XXX	Aluminum (99% minimum)	Excellent corrosion resistance, high electrical and thermal conductivity, good work ability, low strength, not heat treatable.
2XXX	Copper	High strength-to-weight ratio, low resistance to corrosion, heat treatable.
3XXX	Magnesium	Good weldability, moderate strength, generally not heat treatable
4XXX	Silicon	Lower melting point, forms dark-gray to charcoal oxide film, generally not heat-treatable.
5XXX	Magnesium	Good corrosion resistance and weldability, moderate to high strength, not heat-treatable.
6XXX	Magnesium and silicon	Medium strength; good formability, machinability, weldability, and corrosion resistance; heat treatable.
7XXX	Zinc	Moderate to very high strength, heat treatable.
8XXX	Other elements	-

2.5.2 LASER ALLOYING / CLADDING OF ALUMINUM ALLOYS WITH METALLIC MATERIAL

Laser cladding or alloying has been used to improve the wear resistance and hardness of aluminum alloys. The alloying elements and compounds commonly used including Co, Fe, Cu , Ni, Ti, W, Cr, Mo, Zr-Ni, TiN, Co-Cu, Al-Ti-Ni ferrovanadium, Ni-Cr-Al and other systems [20,46-57, 59-60, 85, 87-89]. Liang *et al.* [20] clad Ni-Cr-Al into Al-Si alloy and found that amorphous structure and crystallites exist in the laser-clad Ni-Cr-Al coating. It confirmed that the amorphous and ultra-fine crystalline structure can increase the hardness and wear resistance.

Tomlinson & Bransden [50] studied the effect of laser surface alloying of Al-Si alloy

using various amounts of Ni, Fe, Cu, Mn, Cr, Co, Mo and Ti and assessed for the integrity, uniformity, hardness, and response to age hardening. Addition of copper, manganese and chromium showed a significant degree of hardness improvement, and these elements were used to improve the properties of nickel and iron based coating. Vilar *et al.* [53,87] carried out an extensive work on laser surface alloying Al alloy with Mo and found a significant increase in the critical pitting potential after the laser alloying process. Vilar identified a series of Mo-Al compounds on the alloyed layer. Mo is a particular interesting element to produce high strength alloys because it presents a low coefficient and solid solubility in Al [53].

Liu *et. al.* [57] using a mixed excimer laser and CO_2 laser beam processing to generate a Cr alloyed layer on Al alloy 2014. By using dual wavelength laser beam method, the homogeneity of the alloying region, hardness of the chromium melted layer and corrosion resistance were greatly improved. Liu also showed that by laser alloying of Al-Ti-Ni alloy onto Al alloy 2014, an amorphous layer could be formed. This kind of structure has no grain boundaries, so it can enhance corrosion properties of aluminum alloy [51].

2.5.3 LASER ALLOYING / CLADDING OF ALUMINUM ALLOYS WITH CERAMICS MATERIAL

Most studies pre-mixed metal powder with the reinforced ceramic particle phase to form the aluminum matrix composite MMC on the surface of Al alloys. This soft and low melting point matrix is unable to bound the hard ceramic phase when the surface was subjected to shear stress and high temperature, such as in the case of wear. Various ceramic or ceramic-alloy systems, such as Si, Al_2O_3/TiO_2, TiC, WC, SiC, ZrO_2/Y_2O_3, SiC/Si_3N_4 and SiC/Al_2O_3

synthesized on aluminum or aluminum alloys have been studied [18,58,66,73-74,80].

Laser surface alloying of silicon into aluminum casting alloys 319 and 320 to improve the wear resistance of these low silicon content alloy and for automobile industry application [58]. Hu and Baker [74] were laser clad Al alloy 8090 surface by producing an in-situ Al-SiCp metal matrix composite layer on the surface. They found that SiCp partially dissolved in the liquid and reprecipitated during the solidification. The precipitated material was proved as Al_4SiC_4.MMC layer limited to 30-50 μm. Roósz *et al.* [80] found that TiC particles did not penetrate deep into the substrate and agglomerate at the surface of the samples while WC sinks into the bottom of the melt pool.

Man *et al.* clad SiC/Si_3N_4 on Al alloy AA6061 to improve the cavitation erosion of Al alloys [73]. Under high energy density, SiC and Si_3N_4 were partially dissolved in the melt. Al_4C_3 , Al_4SiC_4 and AlN were identified by XRD. The results showed that the hardness of the surface was increased by 4 times. They also found that Si_3N_4 decomposed during the irradiation of laser beam and the cavitation erosion resistance was increased by 3 times as compared with the as-received Al alloy AA6061. Nowotny *et al.* [18] laser clad powders Al_2O_3, TiO_2 and ZrO_2 into aluminum and titanium alloys. The best results were achieved with an Al_2O_3/TiO_2 powder composite. Layers in this material have a compact and nonporous cast structure and a high adhesive strength with respect to the substrate material. The coating thickness is up to 1mm.

2.5.4 LASER ALLOYING / CLADDING OF ALUMINUM ALLOYS WITH MMC OR CMC

G. Y. Liang *et al.* [45] laser clad Ni-WC layer on Al-Si alloy and the results showed that the chemical composition of the coating is not uniform. Composition segregation in the laser-melted zone was found. In the nickel-rich region, the microhardness was up to 1027Hv. The difference in density between the particulate and the matrix will affect the homogenization and the distribution of the clad layer. Chong & Man [92] studied Mo-WC laser cladding, and found that the density of particles has greatly influenced the homogenization and particle distribution. Density of tungsten carbide (WC) is about 1.5 times of Molybdenum (Mo) and 6 times of Aluminum alloy.

2.5.5 PROBLEMS ASSOCIATED WITH LSA/LSC OF ALUMINUM ALLOYS

The major concern for laser alloying is to avoid defects such as cracking, porosity, and unacceptable roughness in the clad surface. Because of the different thermal expansion coefficients of the substrate and coating and in addition with the high cooling rate in laser processing, cracking is the most important problem associated with laser treatment. Preheating the substrate is usually used to eliminate the formation of cracking. Some research studies found that adding some chemical element into the coating may decrease the residual stress in the coating and prevent the cracking formation, such as adding Nickel [59,93-95] as the alloying material. Other researchers found that it is difficult to alloy Fe and Ni onto aluminum alloy without cracking [93]. To improve the cracking problem, some researchers tried to premix the alloyed powder with Al [94-96]. According to Taeda *et al* [45],

Fe based alloyed powder was premixed with pure Al powder so as to "dilute" with the substrate material in advance and cracks could be prevented at slower processing speed using this premixed powder. J. L. Sun *et al* [97] found that direct laser alloying of Al-Sn alloy on mild steel produces continuous brittle intermetallic Fe_xAl_y layers at the interface resulting in weak bonding between the clad and the substrate. To overcome this problem, both pure Ni and Al were used as intermediate coatings. Pure Al coating was found to be a better barrier layer to prevent continuous formation of such embrittlement.

2.6 LASER CLADDING OF WC ON VARIOUS ALLOYS

Tungsten carbide (WC) holds a leading position on surface engineering among other carbides since it combines favorable properties, such as high hardness, good strength and stable at high temperature. It does not dissociate significantly during the laser melting process as in the case of SiC. SiC dissociates and reacts with Al substrate to form Al_4SiC_4 or Al_4C and Si [36, 72-74, 91].

WC mixed with metallic ductile binders (Ni and Co base powder) is a very effective method for producing protection layer on highly stressed components, to withstand abrasive wear, impact or fatigue. A lot of works have done on Ni-WC cladding on steel or aluminum alloy [19,77,98-100]. Wang *et al* [98] shows the Ni60+60%WC coating on cast iron has the great improvement under abrasive wear test. Brandt *et al.* [100] studied cladding WC/Ni on H13 tool steel and produced 1 mm thick, fully dense and crack-free clad layer.

In addition, tungsten carbide has appropriate amount of plasticity and good wettability by molten cobalt. Laser cladding of tungsten carbide/cobalt has gained a lot of research interested recently [102,103-108]. Gassmann [102] produced coatings with up to 40 vol%

unmelted carbides on mild steel with excellent bonding and no cracks for enhanced abrasive wear resistance. He confirmed that in the area of applying composite materials, laser powder cladding is technologically superior to conventional deposition welding using filler wire. Yang [103] clad WC/Co-base alloy powder onto low carbon steel and showed that the microstructures of the coating varied considerably with different processing conditions. Coating thickness of 2mm and hardness 1725 Hv were achieved and the wear resistance increased by a factor of 5. Grunenwald *et al* [104] also clad WC/Co onto low carbon steel and found similar characteristics in the clad. Cadenas *et al.* [106] analyzed the wear behavior in laser clad and plasma sprayed 83% WC-17%Co coatings on AISI 1043 and found that the wear rate of the laser clad sample was 34% lower than that of the plasma sprayed WC-Co coating. By comparing two processes, laser clad specimen had fewer porosity, higher hardness and better adherence between coating and substrate.

2.7 LASER CLADDING OF TiC ON VARIOUS ALLOYS

Compared with WC, TiC has a wide solubility range and is much more stable than WC. The free formation enthalpy of TiC and WC are $-184\ kJmol^{-1}$ and $-38.5\ kJmol^{-1}$ [109] Ayers [110] injected TiC powder into 304 Stainless Steel. Partial dissolution of the carbide particles increased the microhardness of the austenitic matrix to 200 – 250Hv. The dissolved TiC will recrystallize back to TiC particulate and does not lead to matrix embrittlement [108-112].

Some researchers found that TiC would partially dissolve and recrystallize back to TiC or other intermetallic after laser cladding [110-113]. Other researches also studied in-situ TiC formation during laser cladding. TiC formed at the SiC-matrix interfaces [36,72,91,114-116]. SiC is un-stable at high temperatures. SiC has high tendency to partial dissociation and led to

matrix enrichment with Si and C. A wear resistant surface metal matrix composites in both aluminum alloys and titanium alloys were created by using Ti/SiC_p [72]. The precipitation of TiC, by the partial dissolution of SiC_p , is then agglomered into a hard layer (1400 HV). Man *et al.* [115] in situ synthesized TiC on the surface of aluminum alloy substrate by laser cladding of Ti and SiC. The hardness of clad layer has 4 times improvement. In situ reacted TiC particles with Ni on 5CrMnMo steel substrate was studied by Xiaolei Wu [116]. TiC particles were distributed uniformly. TiC-γ-Ni interfaces were free from any deleterious surface reaction.

TiC and Stellite 6 powders were premixed by Lugscheider and Bolender in a single hopper and clad onto mild-steel and produced high-grade wear and erosion resistant coatings [111]. The TiC particles dissolved in the melting but precipitated on cooling producing a very hard coating. Li *et al.* [112] studied the microstructural characterization of laser cladding self-fluxing Ni-Cr-B-Si-C alloy and TiC composite coatings on AISI 1045 steel. The result showed that the partially dissolution of TiC was occurred on melting and the epitaxial growth of the remaining particles took place by the precipitation of TiC upon cooling. Lei and Quyang [117-118] laser clad TiC-Ni to 1045 steel and studied its tribological behaviour by using pin-on-ring friction and adhesive wear test. The results showed that the degree of wear depended mainly on the extend of debonding and removal of TiC.

2.8 LASER CLADDING OF Si_3N_4 ON VARIOUS ALLOYS

There is seldom research in the laser cladding of Si_3N_4 on steel or aluminum. Man *et al.* clad SiC/Si_3N_4 on Al alloy AA6061 to improve the cavitation erosion mechanism [73]. A research study found that by using laser irradiation of pre-mixed Fe/Cr/Mo, Fe/Cr/Si_3N_4 and

Fe/Cr/Mo/ Si_3N_4 powders on the surface of carbon steel, Fe-Cr-Mo, Fe-Cr-Si-N and Fe-Cr-Mo-Si-N stainless surface layers can be formed [119]. The addition of molybdenum is to increase the resistance of stainless steels to localized corrosion. This research [119] focused on incorporating a Fe/Cr/Mo/Si_3N_4 layer on the surface of carbon steel. Its corrosion resistance was enhanced by forming a stainless steel protective surface layer on carbon steel. The polarization resistance of the laser clad Fe-Cr-Mo-Si-N layer was proven to be higher than the other layers. Huang [120] also studied laser surface alloying with Fe-Cr- Si_3N_4 on AISI 1020 carbon steel. He mentioned that the decomposition of Si_3N_4 can help to lower the oxygen content in surface alloyed layer, because of the formation of N_2 after the alloying process. Moreover, a large portion of the laser energy for melting Si_3N_4 led to little energy penetration into the alloying layer and caused low dilution rate.

2.9 SUMMARY OF LASER CLADDING ON ALUMINUM ALLOYS

Table 2.3 summarizes most of the published research work on laser cladding or laser surface alloying of Al alloys.

Author	Substrate	Coating/ adding material	Year	Finding	Remarks	Ref.
				Laser cladding on aluminum alloy		
Toshihide Taeda	Aluminum alloy (Japanese standard: AC2B)	Fe, Ni, Cu	1992	Fe and Ni were used powder feeding system and Cu wire was embedded in the substrate. Pure Al powder was used to pre-mixed with the powders mentioned above, so as to "dilute" with the substrate material in advance. Also, Cracking was prevented by using low processing speed.	5 kW CO_2 laser, powder feeding system	45
P. Vanhille	Aluminum alloy	Ni	1992	The region with fine dendritic structure had higher hardness. Sometimes, cracking was owing to the brittleness of this hard surface alloy.	CO_2 laser and electron beam	46
Kreutz	Aluminum (A1 99.99) and AlSi10Mg	Cr and Ni	1992	Laser radiation generated a fine grain size microstructure with an improvement of hardness of nearly 100%.	CO_2 laser	47
P. Sallamand	Al-7at%Si	Ni, TiC	1993	Clad layer thickness was up to 1 mm, and without crack and porosity. Microstructure of the clad layer consisted mainly of dendritic structures, which were intermetallic compound, such as Al_3Ni, and Al_3Ni_3.Layer with TiC particles had high hardness value 800Hv.	CO_2 laser, powder injection	48
A. Almeida	Aluminum alloy ANSI 7175	Cr	1993	The concentration of Cr influenced the quality of alloyed layer.	Powder injection	49
T.N. Baker	Pure aluminum (CP Al), 6061 and 8090 Al alloys	SiCp, Ti	1994	A wear resistant surface metal matrix composites in both aluminum alloys and titanium alloys were created by using Ti/SiC_p	CO_2 laser, pre-placed powder by using chemical binder	72

D. Pantelis	Al alloy A-S7G0.3	SiC	1995	SiC particles had partially reacted with the matrix. Wear test showed that extremely high wear resistance of the clad layer (90 times higher)	3.4 kW CO_2 laser, powder injection, pin-on-disc wear test	79
W. J. Tomlinson	Al-12Si alloy	Si, Ni, fe, Cu, Mn, Cr, Co, Mo and Ti	1995	Cracking was occurred in alloy layer with more than 30% Fe. Mo and Ti were difficult to melt completely even under high laser irradation. Additions of Cu, Mn and Cr considerably increased the hardness of the Ni base coatings.	CO_2 laser	50
Z. Liu	Aluminum alloy 2014	Al-Ti-Ni	1995	Amorphous layer was formed. This kind of structure had no grain boundaries, so it could enhance corrosion properties of aluminum alloy.	CO_2 laser	51
C. Hu, T.N. Baker	Aluminum alloy 8090	SiCp	1995	SiCp partially dissolved in the liquid and reprecipitated during the solidification. The precipitated material was proved as Al_4SiC_4. MMC layer thickness was limited to 30-50 μ m.	CO_2 laser, pre-placed powder by using chemical binder	74
Liu and Mazumder	Aluminum silicon alloys AA333	Ni-Al	1995	In the θ and γ_1 phase region, cracking was observed. There were 2 features that differ from the equilibrium Cu-Al phase diagram. The authors suggested that this was due to the high cooling rate after laser irradiation.	10kW CO_2 laser, pneumatic powder feed system with a screw feed	52
A. Almeida	Aluminum alloy	Mo	1996	By using the 2 step processes to improve the alloying quality, high hardness Al-Mo surface alloy was found.	CO_2 laser	53
Z. Liu	Aluminum alloy 2014	Cr, W, Zr-Ni, Ti-Ni	1996	Pitting resistance of CO_2 laser melted 2014 alloys was increased.	CO_2 laser	54
Miyamoto	Aluminum alloy (AC2A)	Cu alloy powder	1997	The mechanism of clad layer formation was studied and analyzed the dilution by using surface tension theory.	CO_2 laser, powder injection	55
K. G. Watkins	Different series of Al alloy		1997	LSM of Al-Cu, Al-Si, Al-Zn, Al-Fe, Al-transitional element: LSA of Al-Ni, Al-Cr, and Al-Mo.	A review	23
M. Ignatiev	Al substrate	Fe and Sn	1997	By using different surface modification methods, CO_2 laser, Nd:YAG laser and Electron Beam, to compare with their feasibility on Al substrate .	CO_2 laser, Nd:YAG laser and Electron Beam	56

Z. Liu	2014 -T6 Al alloy	Cr	1997	Using dual laser beams to generate a Cr alloyed layer, micohardness of the chromium melted layer and corrosion resistance were greatly improved.	Mixed excimer laser and CO_2 laser, powder feeding system is used	57
G. Y. Liang	Al-Si cast alloy surface	Ni-WC	1997	The highest microhardness 1027 Hv was found in the high nickel-region.	Plasma spraying with CO_2 laser post-treatment	19
Y. Q. Fu	Aluminum alloy AA6061	Ni and Cr	1998	Cracking can be prevented by addition of Ni and Cr and the hardness was increased too.		59
N. Pirch	Al and AlSi10Mg	Ni, Ti	1998	Mathematical modeling of LSA.	CO_2 laser	60
András Roósz	Al alloy	TiC, WC	1998	Result showed that WC with much higher density, WC had higher tendency to sink into the bottom of the clad. TiC was agglomerated at the surface of the sample. Because TiC particles did not penetrate the oxide layer of Al alloy.	CO_2 laser, powder injection	80
Kelly and Mazumder	Aluminum silicon alloys AA333	Mn-Al bronze	1998	The coating was mechanically sound, relatively free of small cracks and porosity, with a strong, tough metallurgical bond. The coatings were 3 to 4 time harder than the substrate.	6 kW CO_2 laser, a "two pin on ring" geometry was used.	61
S. Nowotny	Aluminum and titanium alloys.	Al_2O_3, TiO_2 and ZrO_2	1999	The best results were achieved with an Al_2O_3/TiO_2 composite powder. Layers in this material had a compact, nonporous cast structure and a high adhesive strength with respect to the substrate material. The coating thickness was up to 1mm.	6 kW CO_2 laser, powder injection	18
A. H. Wang	Al-Si eutectic alloy	Fe based alloy	1999	Three regions were found in the clad layer, the clad layer, the transitional region and the post-molten region.	62 kW CO_2 laser, powder injection	62
H. C. Man	Alumimum Alloy AA6061	SiC/Si_3N_4	2000	The cavitation erosion resistance of 100% Si_3N_4 was improved by 3 times than that of monolithic AA6061, whereas no significant improvement in specimen cladded with 100% SiC.	2kW Nd-YAG laser, pre-placed with PVA paster	73

P.H. Chong	Aluminum Alloy AA6061	Mo/WC	2001	Different ratios of Mo and WC powders were investigated. The surface hardness of the Al specimens cladded with Mo/WC was increased by 7 times.	2kW Nd:YAG laser, pre-placed powder	92
G.Y. Liang	Al-Si alloy	Ni-Cr-Al	2000	Amorphous structure and crystallites existed in the laser-clad Ni-Cr-Al coating. It proved that the higher the amorphous content, the smaller the wear amount.	Plasma spray coating and post-treatment by 5kW CO_2 laser, Block-on-ring wear tester was used	20
T. T. Wong	$AlSi_8Cu_1Mg$	Ni-Cr-B-Si and Ni-Cr-B-Si+WC	2000	Laser-clad plasma-sprayed specimen had higher hardness and better abrasion wear resistance than plasma sprayed specimen. The author proved that the Ni-Cr-B-Si+WC laser clad specimen without significant in improvement of wear resistance when compared with laser-clad Ni-Cr-B-Si sample.	Plasma spray coating and post laser treatment by 5 kW CO_2 laser, Pin-on-disc abrasion wear tester	21
Xu & Leong	Aluminum casting alloy 319 & 320	Si	2000	The silicon content was enhanced and a very fine silicon-rich phase produced. Crack free and porosity free with fine microstructure layer were formed.	Nd:YAG laser	58
H.C. Man	Aluminum Alloy AA6061	In situ Ti SiC synthesize	2001	The hardness of clad layer reached 650 Hv.	2kW Nd:YAG laser, pre-placed powder by using chemical binder	115

2.10 SURFACE ENGINEERING AND WEAR

Surface engineering is a multidiscipline activity aimed at tailoring the properties or surfaces of engineering materials to improve their function or service life. Wear is a major industrial problem. The cost of replacing worn parts is a major expense in many processes. Wear is the loss of material from a surface caused by interaction with another surface or material. The main interactions are loads and motions producing adhesion, abrasion or fatigue, all of which can lead to the loss of wear fragments. Figure 2.8 gives the classification of wear processes. All of the abrasive forms of wear involve the contact of a solid with a hard particles or sharp protuberance. The erosion forms of wear all involve at least a component of damage due to the mechanical action of a fluid in motion. Adhesive wear processes often occur in systems involving a solid sliding on another solid. Figure 2.9 Illustrations of the three general ways by which materials wear.

Wear resistant coatings of nickel-base hardfacing alloys using various techniques such as laser cladding, plasma transferred arc welding, atmospheric plasma spraying have been studied [52]. This study showed that laser cladding is best suited for production of very localised small coating areas with a moderate thickness and track width. This offers the possibility that does not exist with most other surface engineering methods. The extended area coverage may be achieved by overlapping treated areas. Sometimes, overlapping may not be necessary for wear resistance improvement. Zhang *et al* [121] investigated the wear properties of steel that contains a single laser hardened track on the surface and found that the wear properties of the steel concerned could be improved.

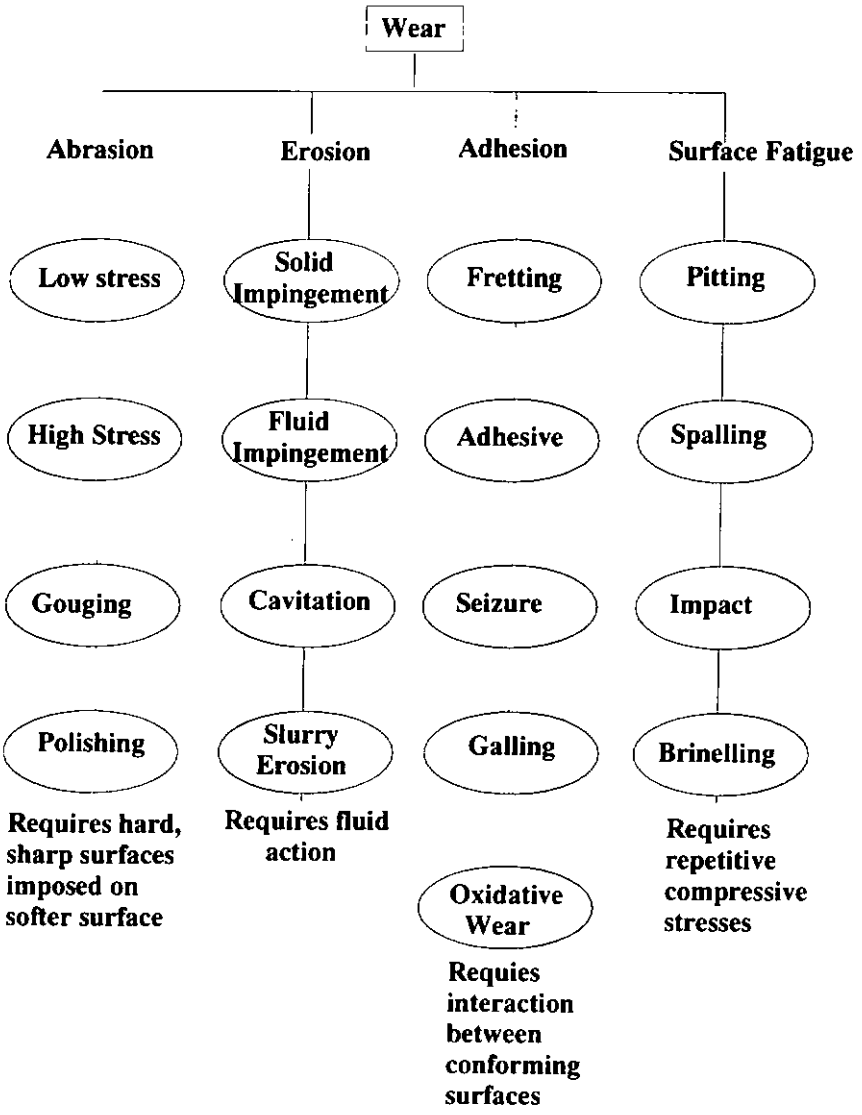

Figure 2.8 Basic categories of wear and specific wear modes [22]

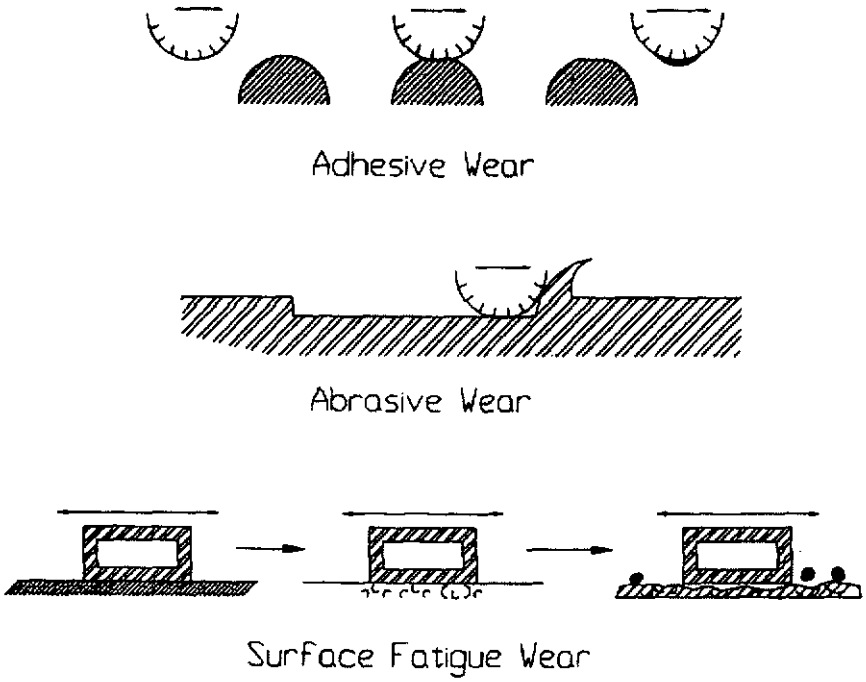

Figure 2.9 Illustrations of the three general ways by which materials wear [122].

2.10.1 ABRASIVE WEAR

Abrasive wear arises from the cutting action of hard surfaces sliding on softer materials, such as hard protuberance silicon carbide sandblasting paper on surface or a hard particles trapped between two surface. The resistance of a material to abrasive wear is basically governed by its hardness. In general, the hardness increases the abrasive wear resistance increase. However, sometimes this may influence by the size of reinforcement particles and the bonding strength between the reinforcement and soft matrix. The hard abrasive material indents the surface, the material removal rate depends on various mechanism, e.g. cutting, ploughing, clipping or by fatigue cracking. In most case, the best abrasive wear performance is achieved with ceramic carbide or some MMC material.

Cobalt and nickel are good wetting material for tungsten carbide to form MMC. Wang [92] suggested that nickel-based alloy containing WC carbides has selected as one of the

wear-protective coating material for piston ring and cylinder liner. Wang *et al* [98] produced Ni-WC composite coatings with varied contents of WC particles. He shows that coating composition with Ni60+60%WC has 5-10% improvement in wear resistance in comparsion with the Ni45+40%WC coating. He suggested that the load carrying capacity of the hard-phases structure is an important factor form wear resistance improvement. Brandt *et al.* [98] studied cladding WC/Ni on H13 tool steel and produced 1 mm thick, fully dense and crack-free clad layer. The average microhardness of the coating was 650Hv and abrasive wear resistance was up to 10 times higher than the heat-treated H13 steel. Nowotny and Techel [105] showed that unliked sintered hard metals, clad layers had maximum abrasive wear resistance at contents of nondissolved WC particles as low as 40 vol%. Thus, the layers were ductile, which gave higher resistance to fatigue, impact and thermal shock. Nickel base powder and WC-Co ceramic particles using CO_2 laser to perform laser cladding process [107]. Block-on-ring dry sliding wear test and rubber wheel slurry erosive abrasive wear test had been conducted to study wear properties. The WC-CO cladded samples were showed to have superior wear and corrosion resistance.

Lee and Lu [123] studied the abrasive wear of powder metallurgy Al alloy 6061-SiC particle composites and showed that the number and size of SiCp particles were affected the wear rate. The wear rates of composites decreased as the amount of SiCp increased. For the same amount of SiCp particles, the wear rates decreased with increasing SiCp size. For elevated temperature service, when the matrix has an insufficient strength, the detachment of hard carbide particles in the wear debris enhanced wear. Moreover, increasing the volume fraction of carbide (from 0.3 to 0.5) leads to increase in the wear resistance for low stress abrasion [124]. Kagawa *et al.* [124] showed that carbide layers containing more than 60wt% Cr had superior wear resistance than other wear resistant alloys. Xiaolei Wu [114] also

showed that the in-situ TiC reinforced composite with strong interface bond and enhanced its wear resistance significantly.

2.10.2 ADHESIVE WEAR

When two surfaces move relative to one another, wear occurs by steel pulling the material out of the clad surface. The area of contact of two surfaces must be considered first before study the adhesive wear. When two bodies are loaded together, the opposing asperities make contact, deform and many weld together due to inter-atomic forces. With sliding motion present, and if the bond is stronger than the underlying material, the material shears or flows and work-hardening take place. Material which is transferred from one surface to the other may later be removed as wear debris. Figure 2.10 shows the nature of the contact between real surface. Quyang [117-118] studied its tribological behavior by using pin-on-ring friction and wear test. The results showed that the incorporation of TiC particles enhances the resistance to plastic deformation and delays the occurrence of delamination.

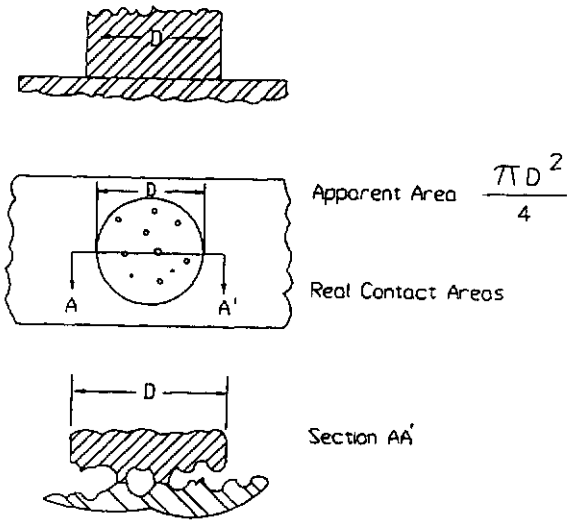

Figure 2.10 Nature of the contact between real surface [122]

Chapter 3

Experimental Details

3.1 NEODYMIUM: YAG LASER

The neodymium-doped yttrium aluminum garnet laser, denoted as Nd: YAG (Figure 3.1), has been by far the most commonly employed solid state laser for many years. It is available in a wide variety of forms including continuous, normal pulsed, and Q-switched. Neodymiumn lasers can be excited by intense broad-spectrum light sources, by continuous tungsten lamps or flashlamps.

In this project, laser surface cladding was carried out using a high power Nd-YAG laser (Lumonics, MW2000). The laser can achieve a maximum mean output power of 2 kW in continuous wave (CW) mode. The laser system comprises of a single enclosure housing of top-mount laser head, with control and power electronics modules and cooling system below. Laser output is delivered by a single fibre optic cable through an output connector on the laser head lid. Figure 3.2 shows the major components of the laser system.

The laser path is shown in Figure 3.3. Laser radiation is generated essentially by four pumping chambers, which form a single oscillator, and rear and front mirrors M1 and M2. Each pumping chamber houses a cylinder of crystalline Nd-YAG laser rod and two quartz tubes (flashlamp). Cooling water is pumped through the chamber to dissipate the heat generated during excitation of the laser rod. The rear and front mirrors, M1 and M2, form the resonator. M1 is totally reflective and is fitted with tilt controls. Mounted in a machined cell, there is a partially reflective mirror through which the laser output beam passes. A silicon photodiode power monitor PM1, which is mounted adjacent to M2, monitors the laser output

houses a shutter/beam turning mechanism M3, a motor, a beam turning mirror M4 and lens assembly L1. A water-cooled beam dump is secured to the outside of the enclose. When no output is required, the resonator output beam is directed into the beam dump which absorbs the generated power. When an output is required, M3 is driven into the beam path to turn the beam through 90° and direct the oscillator output beam onto M4. The beam is turned through 90° by M4 and directed via lens assembly L1. From the lens assembly the beam enters the fiber input connector which houses a focusing lens L2 to focus the beam into the end of the fibre-optical. From the fibre input connector, the fibre-optic cable, carrying the output beam, exists the laser head via an output connector.

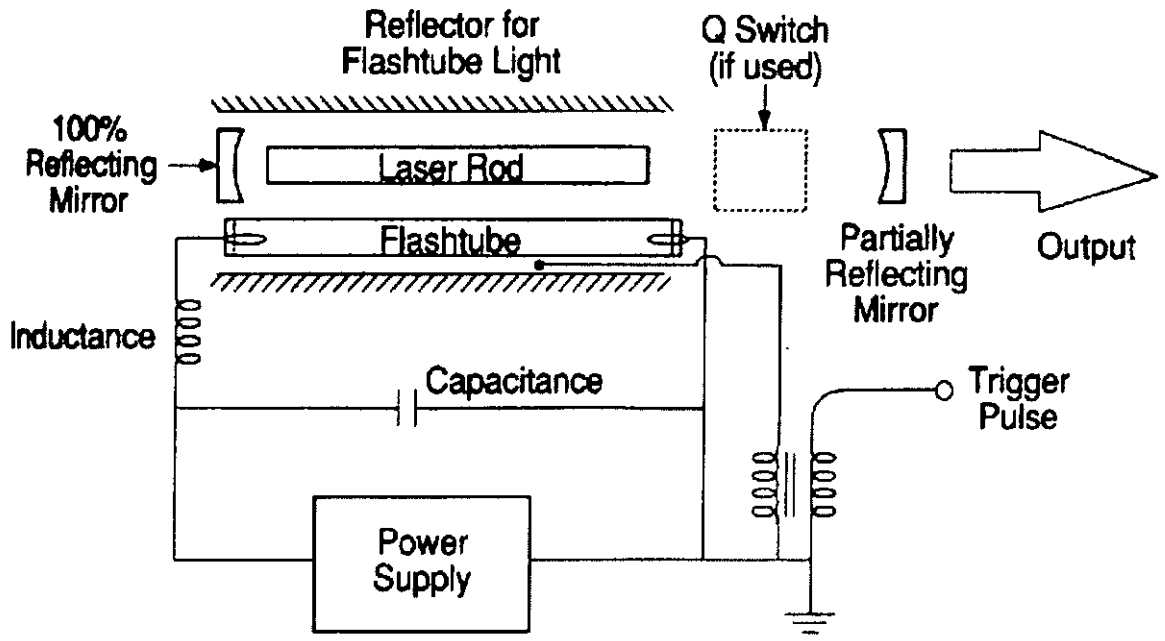

Figure 3.1 Structure of Nd: YAG solid state laser [1]

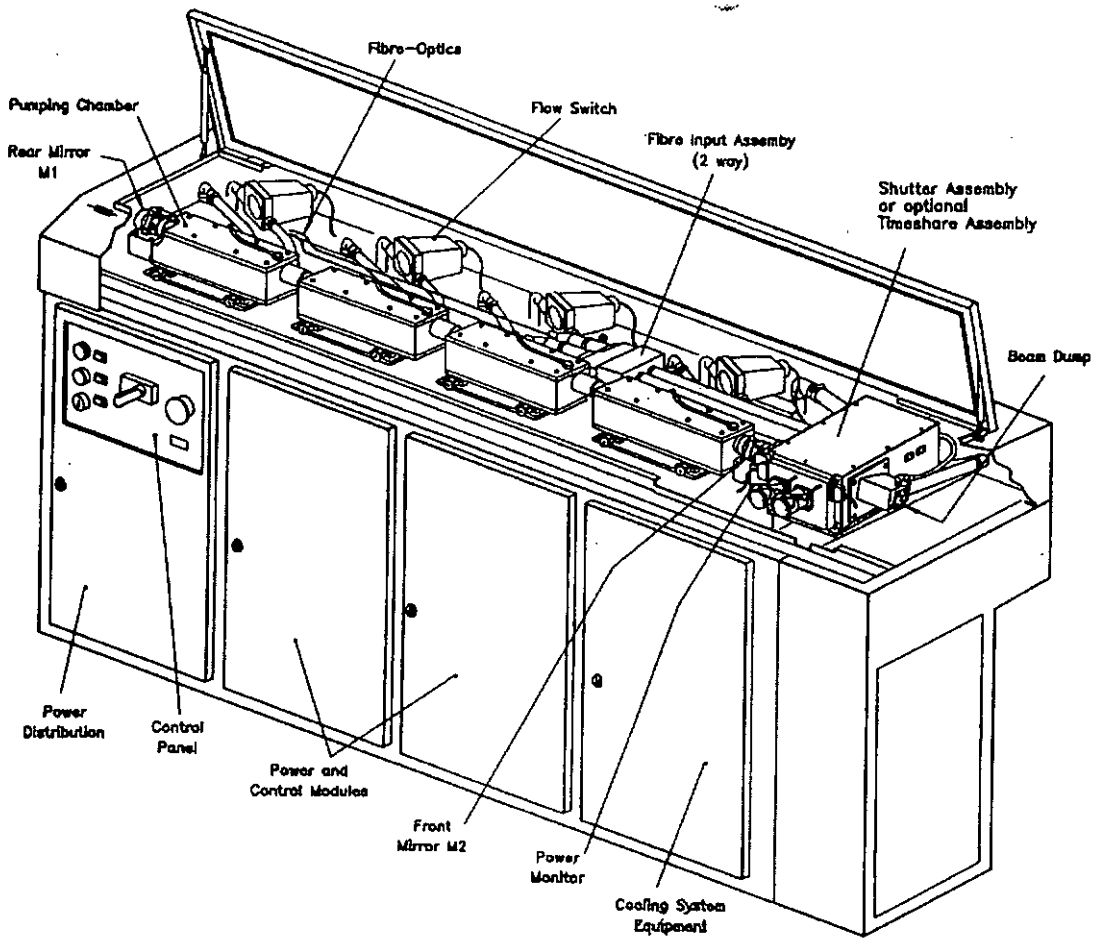

Figure 3.2 Major components of Nd-YAG laser [Lumonics, MW2000]

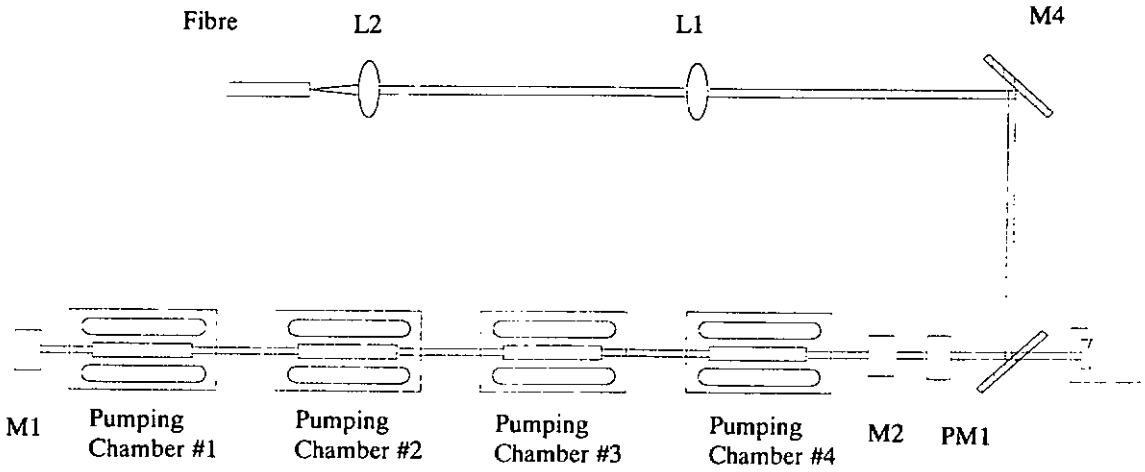

Figure 3.3 Laser beam path of the 2kW Nd-YAG laser systems.

3.1.1 FOCUSING HEAD

The laser beam was transmitted by optical fibre and focussed onto the specimen by a Zinc Selenide (ZnSe) lens. The focusing head was equipped with a recollimating lens of 200 mm focal length and a focus lens of 100mm focal length. In order to prevent back reflections from the workpiece (may damage the optics and fibre end), the focusing head was titled by 13° relative to the workpiece normal. The movement of the focusing head was controlled by a computerized X-Y-Z table.

3.1.2 FOCUSING POSITION

A simple visual examination on laser beam alignment could be made by the helium-neon (HeNe) laser, with 0.5mW output. The focused YAG laser beam was aligned with this red spot of the HeNe laser, which is then used for alignment on the clad track. The minimum waist position of focus point was checked by blue flash techniques. A focus beam print was made on a small stainless plate which was tilted with an angle 45° as shown in Figure 3.4. The power and scanning speed of laser used was 1.1 kW and 25 mm/s respectively.

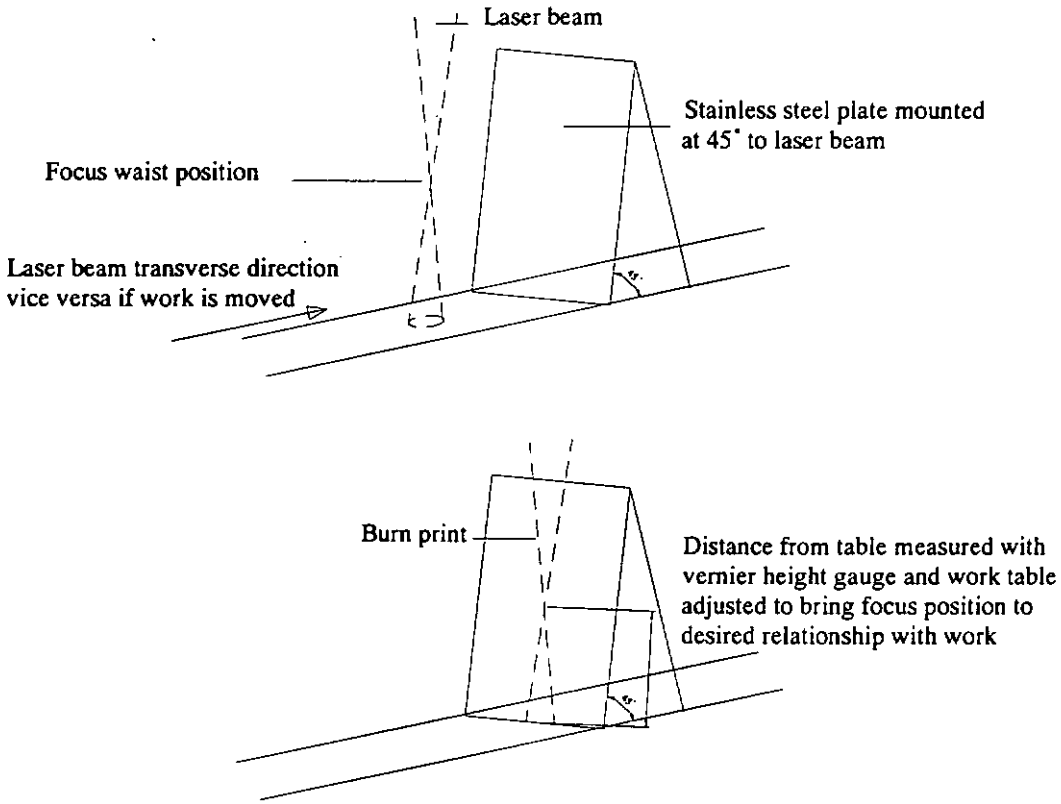

Figure 3.4 Principle for establishing the minimum focus waist position by using a stainless steel plate (a) before beam print; (b) after beam print.

3.1.3 GAS SHIELDING

During the experiment, shielding gas (Argon) was blown coaxially and through a lens protection and melt pool shielding from surface oxidation during laser cladding. The gas flow rate was controlled by using two separated flow meters, one was connected to the coaxial gas shielding and the other to the side jet tube. A 4 mm internal diameter pipe was used as the side jet shielding pipe and clamped tightly and positioned with an angle of 45°. The gas flow rate of the coaxial gas shielding and side jet were 40 liter/min and 15 liter/min respectively.

3.2 MATERIAL SELECTION

The 10 mm thick aluminum alloy AA6061 plate was used for this project. The nominal composition of aluminum alloy AA6061 is shown in Table 3.1. The reagent grade powder materials for LSC are shown in Table 3.2. Table 3.3 shows the physical properties of Al, Mo, WC, TiC and Si_3N_4.

Table 3.1 Chemical composition of Al alloy AA6061

Chemical composition limits of Al alloy 6061									
Base alloy (Wt %)	Si	Mn	Zn	Fe	Mg	Ti	Cu	Cr	Al
Al alloy 6061	0.4 - 0.8	Max 0.15	Max 0.25	Max 0.7	0.8-1.2	Max 0.15	0.15-0.4	0.04 - 0.35	Balance

Table 3.2 Melting point and particle size of powder material

Powder material	Formula	Melting point (℃)	Particle size
Molybdenum	Mo	2617	> 325 mesh (< 43 micron)
Tungsten Carbide	WC	2835	~ 230 mesh (~ 62 micron)
Titanium Carbide	TiC	3060	> 400 mesh (< 38 micron)
Silicon Nitride	Si_3N_4	2000	> 400 mesh (< 38 micron)

Table 3.3 Physical properties of AA6061, Mo, Co, WC, and TiC, Si_3N_4.

Typical Physical Properties of Al alloy, Mo, Co, WC, and TiC, Si_3N_4							
	Material	**Al alloy**	**Mo**	**Co**	**WC**	**TiC**	**Si_3N_4**
1	Nominal density kg/ m^3	2680	10220	8800	15529	4904	3200
2	Hardness, Brinell (500kg load with 10mm ball)	95	225	125	-	-	-
3	Hardness, Knoop	120	-	-	-	3900	2200
4	Hardness, Rockwell A	40	60	-	90	93	-
5	Hardness, Rockwell B	60	98	-	-	-	-
6	Hardness, Vickers	107	230	253	2200	3200	2000
7	Melting point ℃	582	2617	1493	2835	3060	2000
8	Solidus temperature ℃	582	-	-	-	3050	-
9	Liquidus temperature ℃	652	-	-	-	3080	-
10	Heat capacity Cp (at 298K) J/mol	24.28	23.96	24.79	35.38	33.79	99.09
11	Heat capacity Cp (at 2000K) J/mol	31.75	36.06	40.50	56.33	59.09	185.92
12	Free formation enthalpy (-ΔH) (at 298K) kJ/mol	0	0	0	38.5	184	744.75
13	Thermal conductivity W/m-K	167	138	69.21	-	-	15
14	Electrical resistivity, Ohm-cm	0.000004	0.0000057	0.000006 24	0.000067	$6.8x10^{-7}$	-
15	Tensile strength ultimate, MPa	310	324	-	344	258	-
16	Tensile strength yield, MPa	275	-	225	-	-	-
17	Elongation %, break	12	-	-	-	-	-

(Items 10-12 came from reference [109])

3.2.1 GENERAL CHARACTERISTICS OF ALUMINUM ALLOY

Aluminum alloys are characterized by their low strength, low density, low hardness, poor friction and low wear resistance. Research in many areas of aluminum technology, such as advanced alloys, rapid solidification, composites, and corrosion resistance, is aimed at keeping aluminum competitive in traditional as well as new applications.

Recently, the processing flexibility of the laser cladding provides the potential to improve its properties and the cost-effective competitive alloy coatings with better quality. Laser surface modification of Al-Si alloy components has developed for used in automotive application [61]. Figure 3.5 shows the binary phase diagram of Al-Si. In this project, aluminum alloy 6061 was used. The principal alloying elements of this alloy are magnesium and silicon which combine together to form an intermetallic compound, Mg_2Si, which in precipitate form strengthens this Al alloy.

3.2.2 GENERAL CHARACTERISTICS OF MOLYBDENUM

Mo is a particularly interesting cladding element to produce stable high-strength alloys because it presents a low diffusion coefficient and solid solubility in Al. Figure 3.6 shows the phase diagram of binary Al-Mo phase. The work carried out so far on rapid solidification (RS) of Al-Mo alloys has concentrated mainly on the study of their phases structure and precipitation behaviour [125-126] and on extending the solid solubility of Mo in Al [127-128]. Polesya *et al* [126] reported that it is possible to retain up to 2.5 at. % Mo in solution in Al by melt spinning, as compared to a maximum equilibrium solid solubility of about 0.1 at % Mo. It was found that melt-spun supersaturated Al-Mo solid solutions are stable for many

hours at temperatures up to 450℃ and that once precipitation occurs, $Al_{12}Mo$ forms at grain boundaries, without any significant hardening effect.

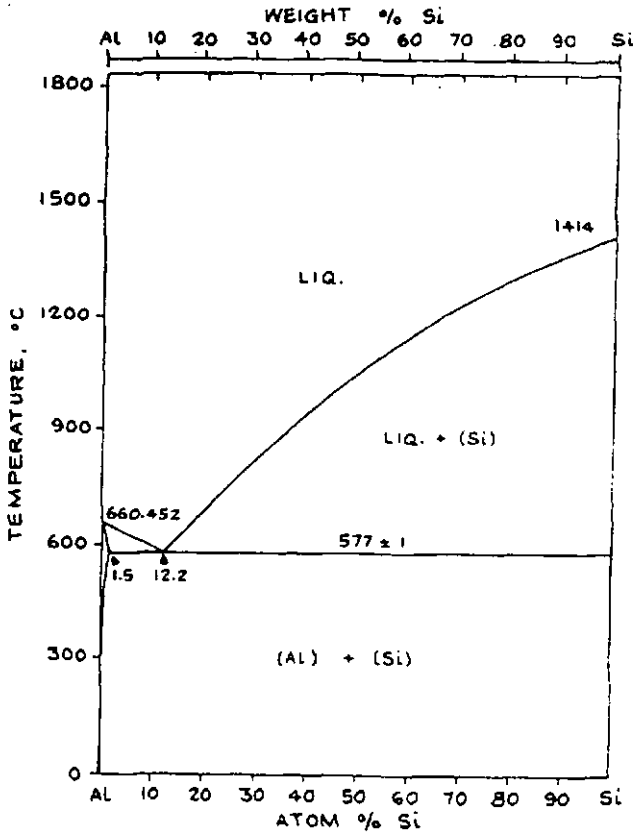

Figure 3.5 The phase diagram of Al-Si [129]

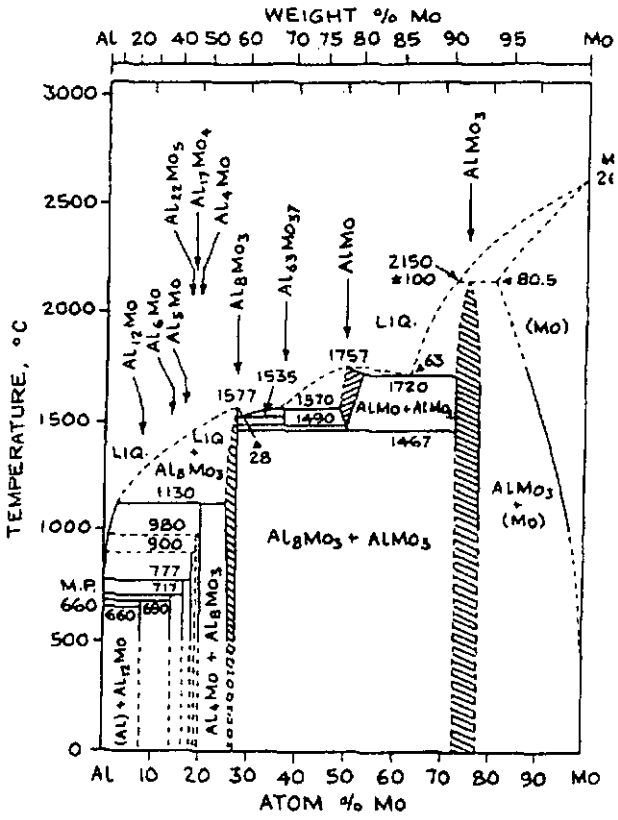

Figure 3.6 The phase diagram of Al-Mo [129]

3.2.3 GENERAL CHARACTERISTICS OF CERAMICS PARTICLES

It is well known that ceramics particle played an important role for improving wear resistance. Tungsten carbide, titanium carbide and silicon nitrite holds a leading position in industrial applications. Because of their high hardness, good abrasive wear resistance, low coefficient if thermal expansion. In this research project, tungsten carbide WC, titanium carbide TiC and silicon nitride Si_3N_4 were selected to use as the cladding material. Figure 3.7 & 3.8 show the tungsten carbide and titanium carbide particles. Tungsten carbide is about 230 mesh (62 micron) and the size of titanium carbide is less than 400 mesh (<38 micron).

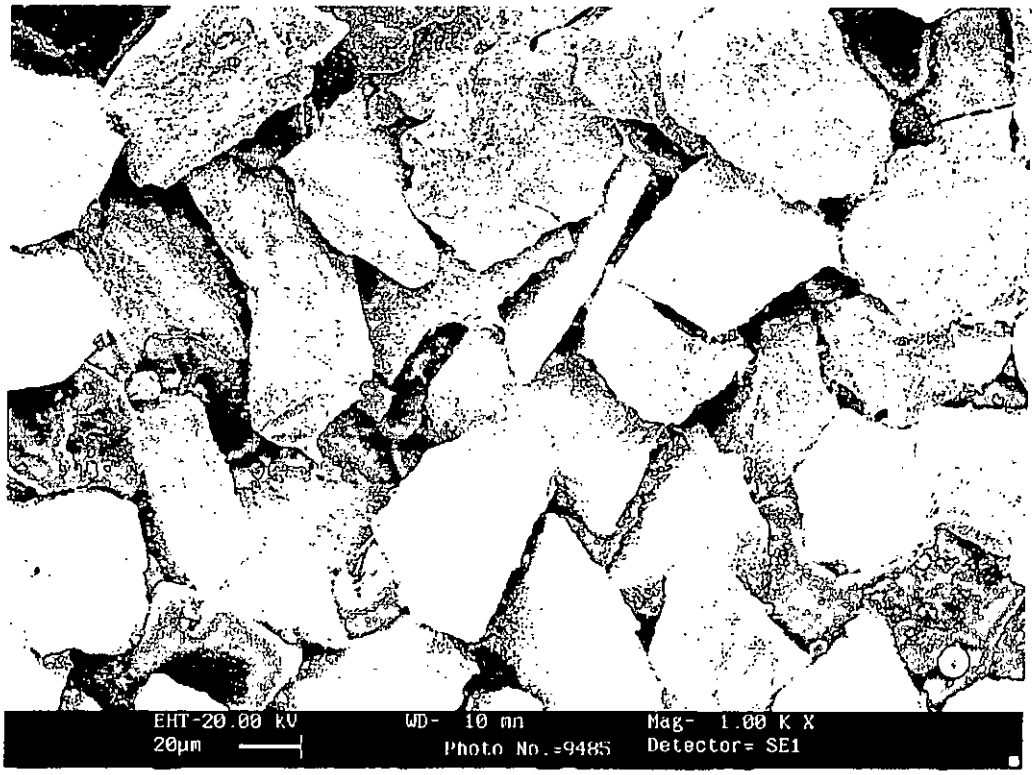

Figure 3.7 Scanning electron micrograph of as-received tungsten carbide WC particles.

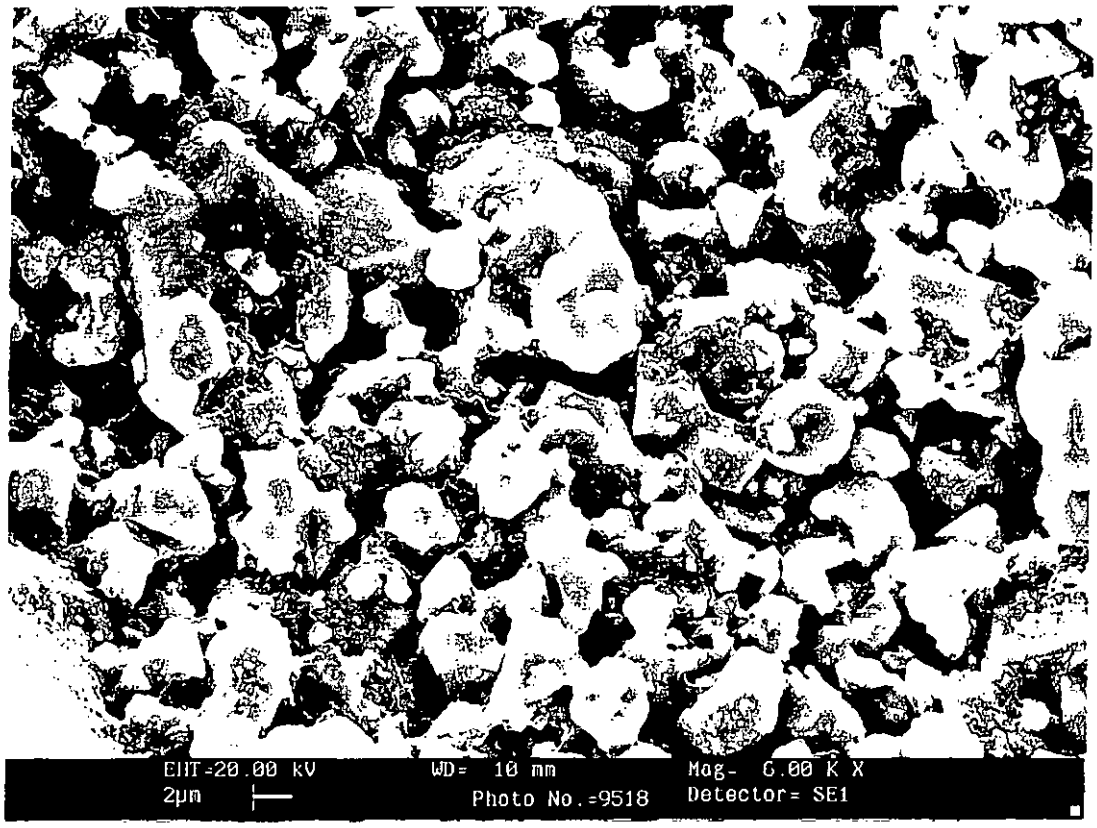

Figure 3.8 Scanning electron micrograph of as-received titanium carbide TiC particles.

3.3 SPECIMEN PREPARATION

Under natural conditions, the surface of the aluminum alloy is covered by an oxide layer which consists of water crystallization in the form of Al_2O_3+ nH_2O. This oxide film has a high melting point (2025 ℃) and directly affects the metallurgical bonding between the clad layer and the substrate. Moreover, the water crystallization may react with the molten Al in the melt pool according to:

$$Al(l) + 3/2\ H_2O(g) \rightarrow 1/2\ \gamma - Al_2O_3 + 3[H] \qquad [115]$$

The hydrogen produced might dissolve in the molten alloy but on solidification, forms hydrogen gas and results in porosity in the clad layer. The Al alloy specimens were sand blasted to achieve a consistent rough surface (Ra=0.2 μm) and then ultrasonic cleaned in

water and alcohol respectively.

Different ratio of powder mixtures were preplaced into the surface of Al alloy by using 4 wt% polyvinyl alcohol as pasting binder. The specimens were dried in an oven for 24 hours at 50 ℃. Finally the pasted specimens were polished by a 1000 grit silicon carbide paper to make a uniform layer of ~ 0.25- 0.3mm thick, as measured by a micrometer.

3.4 LASER CLADDING PROCEDURE

The specimen was placed at the top of a 20 mm steel plate. A range of spot can be achieved by adjusting the distance from the focus. Then, the specimen was aligned with laser beam using the Helium Neon laser spot. The processing parameters were 10 - 25 mm/s beam scanning speed and 1 kW – 1.6 kW laser power at workpiece. By using 50-70% overlap on each track was practiced to make up a surface. A coaxial jet and a side jet of argon gas were used to protect the melt pool from contamination and oxidation. Good cladding surfaces were obtained by varying the scanning speed, power and spot size. During the experiment, shielding gas (Argon) and side jet system were used for blowing away the vapor and prevent surface oxidation of the molten pool.

3.5 CALCULATION OF LASER DENSITY

During laser irradiation, the specific density (E) supplied by the laser source is given by

$$E = P / dv \qquad \text{---------- (1)}$$

Where P is the laser power (W), d is the laser spot diameter (mm) and v is the laser scanning speed (mm/s). The processing laser power used in this project was between 1 kW – 1.6 kW

and beam scanning speed was between 10 - 25mm/s. The spot diameter used was 3 mm beam size.

3.6 MICROSTRUCTURE AND SURFACE MORPHOLOGY INVESTIGATION

After laser treatment, the clad samples were sectioned, mounted and polished for metallographic examination. Optical microscopy, scanning electron microscopy (SEM) with EDAX were used to determine the microstructure and compositions of the clad surfaces.

3.6.1 METALLOGRAPHY AND STRUCTURAL EXAMINATION

The laser treated specimens were mounted, sectioned, polished for microstructural investigation. After the mounting process, the mounted specimens were ground by different grade of silicon carbide paper, from lower grade (400) to higher grade (2400). In order to obtain good grinding surface, the abrasion direction of specimen should be perpendicular to the pre-existing scratches. The specimen was polished with 6 μ m and 1 μ m gamma diamond until scratch free surface was obtained. A light pressure should be applied to specimen and oil acts as the lubricant.

The cross-section of the specimen was etched slightly with a solution of 15 ml HCl, 10 ml acetic acid and 5 ml glycerol or acidic ferric chloride solution (25g $FeCl_3$, 25ml and 100 ml H_2O) for 30 seconds [87].

3.6.1.1 OPTICAL MICROSCOPY (OM)

Optical microscopy can give magnification from 50 to 1000 times (Nikon, Microphot-FXA). It was used to study the microstructures of laser treated specimens and to measure their melt depth.

3.6.1.2 SCANNING ELECTRON MICROSCOPY (SEM)

Scanning electron microscopy (Cambridge, Model S250) from Leica is used as the supplement to OM for microstructural analysis of the laser treated specimens. It can provide magnification up to 300,000 times. The morphology of the intermetallic compound was studied by using SEM backscattered electron images. Quantitative characterization of the microstructure was performed using SEM backscattered electron images and an image analysis computer program.

In order to determine the wear mechanism of the aluminum alloy and its composites, the worn surfaces and debris were examined by scanning electron microscopy. The worn samples were gold coated prior to SEM examination.

3.6.1.3 ENERGY DISPERSIVE X-RAY SPECTROSCOPY (EDX)

The compositional analysis of selected samples was performed using Energy Dispersive Analysis by X-rays (EDAX). When high energy electrons produced with SEM interact with the atoms within the top few μm of the specimen surface, X-rays are generated with an energy characteristic of the atom that produced them. The intensity of such X-ray is

proportional to the atom that produced them. The intensity of such X-ray is proportional to the mass fraction of that element in the specimen, so the chemical compositions of the laser treated specimens can be found by EDX accompanied with SEM. Also, EDX line scan was used to detect the distribution of the metal/ceramic composite.

3.6.1.4 X-RAY DIFFRACTOMETRY (XRD)

The basic idea of x-ray phases analysis is based on the fact that monochromatic X-rays with wavelength λ strikes a polycrystalline specimen at an angle θ, grains with interplanar spacing d diffracts the radiation at the same angle, according to Bragg 's law [118]. When x-ray fall on an atoms of all the planes in a crystal, each atom scatters a small fraction of the incident beam. The reflected beams from all the planes involved interfere and the resultant reflected beam is only strong if the path difference between successive plane is a whole number of wavelengths of the incident x-radiation. Thus reinforcement only occurs for planes x and y when

$$AB + BC = n\lambda$$

Where n is an integer and λ is the wavelength of the x-rays. If d is the distance between planes of atoms and θ is the angle between the x-ray beam and the crystal surface, called the glancing angle, then AB-BC =2 d sin θ and the angle reflected beam has maximum intensity

By using Bragg equation

$$n\lambda = 2\, d_A \sin\theta$$

Phase of the laser cladded materials were studied by X-ray diffractometry (XRD, Philips, Model PW3710). In this work, the radiation sources used was Cu Kα, generated at 1.2 kV and the scan rate was 1.5 °/min. The unique diffraction pattern of particular substrate

was identified by the Powder Diffraction File (PDF) from Joint Committee on Powder Diffraction Standards (JCPDS) [130].

3.7 ABRASIVE PIN-ON-DISC WEAR TEST

A pin-on-disc wear testing machine was built for the wear test. It is similar to the pin-on-disc wear test machine mentioned by Kagawa [123,124]. The machine is based on the conventional pin-on-disc testing technique. The pin is held stationary on the top of a ground rotating disc, with the required load applied through the pin [131]. The specimen for wear test was cut into 10mm x 10mm square and then insert in the slot of the pin. Grade 200 and 220 grits abrasive papers were selected to use in the test. The abrasive paper was stuck on disc. The disc was rotated at 150 rpm and a load of 300 g was applied on the specimen. The total sliding distance was 1414 m. For every 5 minutes, the specimen was taken out and ultra-sonic machine was used to remove the worn out debris and abrasive particles. After 5 minutes, the specimen was dried and its weight loss was measured by an electronic balance with ± 0.001mg accuracy. A fresh paper was used after every 5 minutes measurement. Water is used in the test for washing out the ploughing abrasive particles. The linear speed of the disc at the point where the pin is located is :

$$v_{disc} = 2\ \pi\ RN \quad \text{---------- (2)}$$

Where v_{disc} is the linear speed of the rotating disc (mm/s), R is the distance from the center of the pin to the center of the disc (mm). N is the rotational speed of the disc (rev/s). Figure 3.9 (a-c) show the Pin-on-disc wear tester.

The pin-on-disc wear test is usually conducted with a fixed R value taken into account during the design of the equipment. At this test, R is equal to 150 mm.

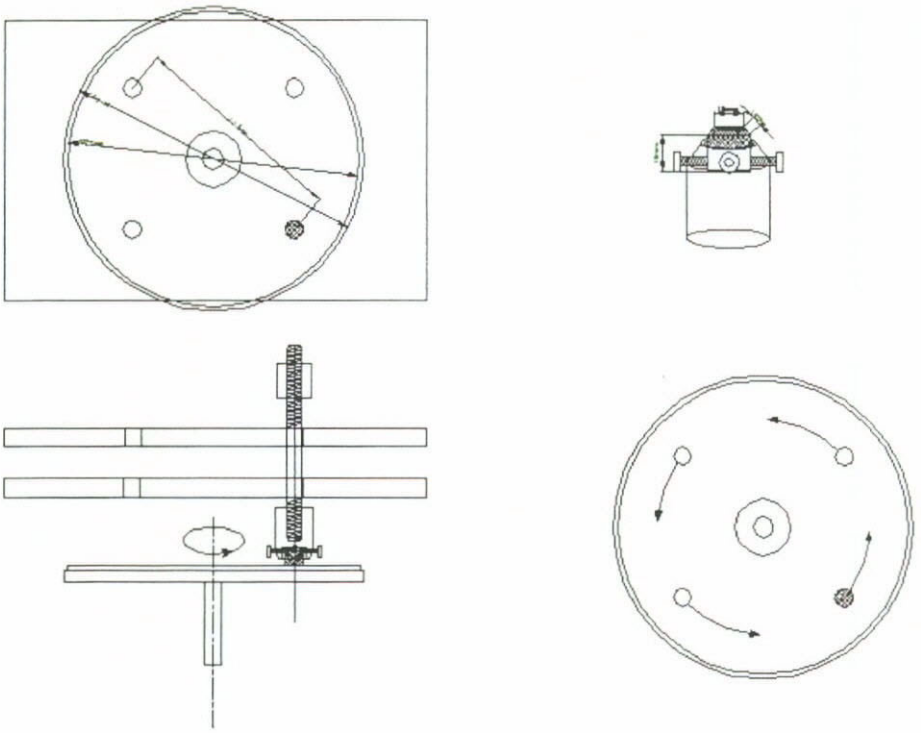

Figure 3.9a A schematic diagram of Pin-on-disc wear tester

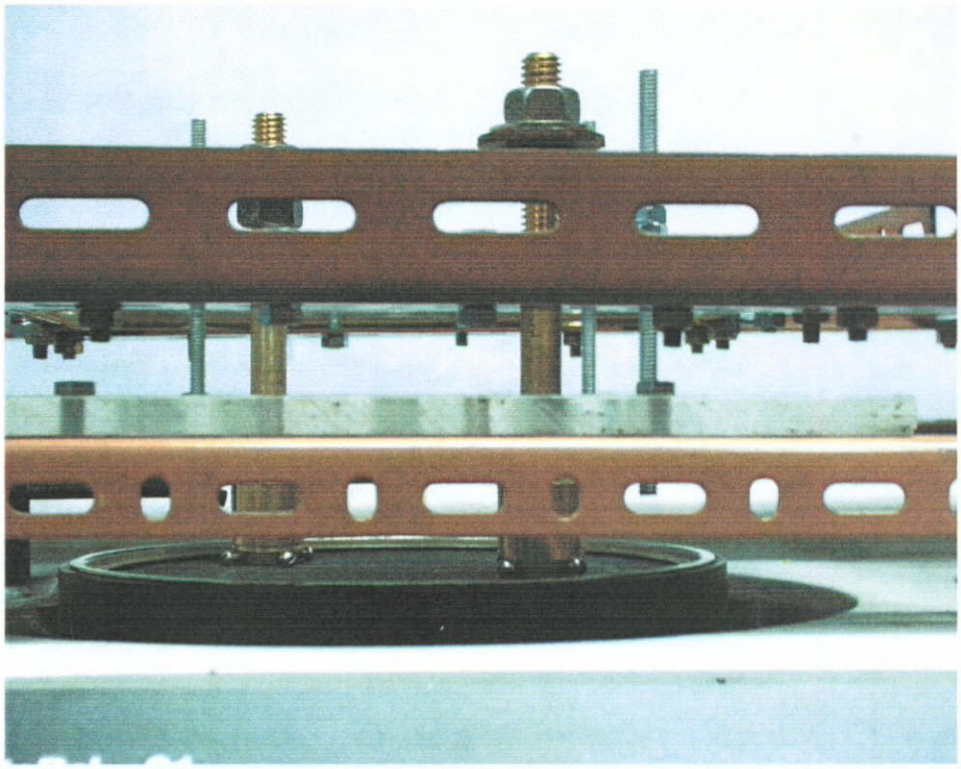

Figure 3.9b Pin-on-disc wear tester.

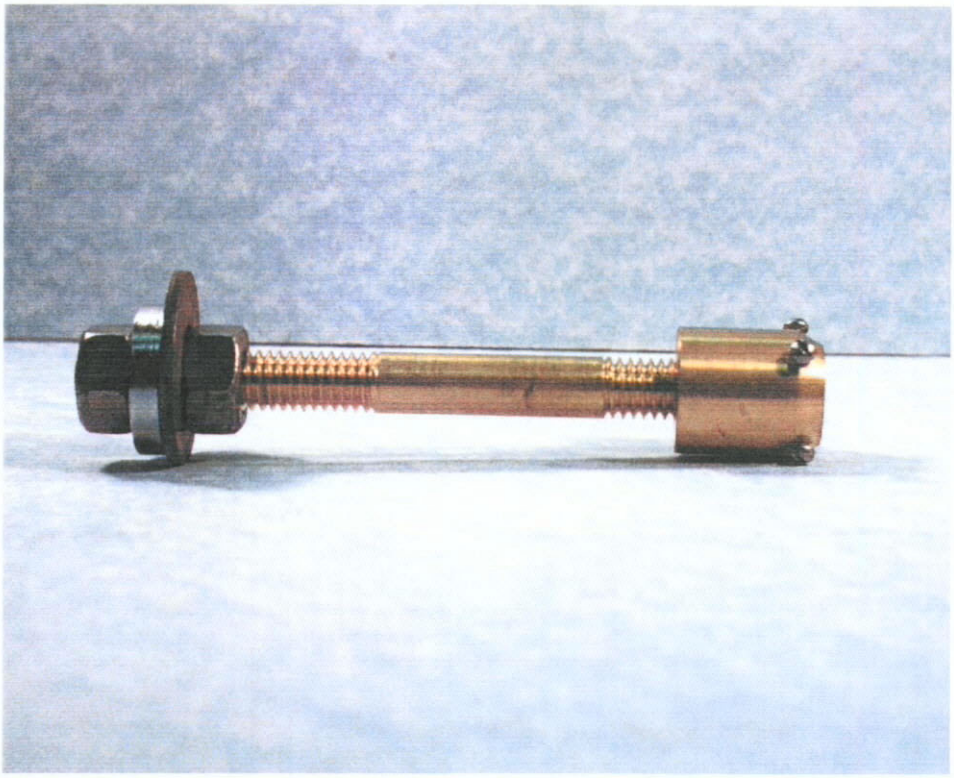

Figure 3.9c Weight and Pin of the wear tester

3.8 MICROHARNESS OF VICKERS MICROHARDNESS

The microhardness test was performed to investigate the hardness value of the alloyed zone and the parent metal. In order to measure a more precise result, the surface of specimen must be well polished and at least 5 points were taken for each specimen. The optical microscope was used to investigate the effect of laser parameters on the surface and cross-section morphology. The measurement was performed using a Shimadzu Vicker's microhardness testing machine that forced a diamond indenter of specific geometry into the surface of the testing material. The microscope was located on the top of the testing region and the stage was moved under 200g indenter weight. The time for indentation was taken as 15 seconds. Optical equipment used in microhardness testing must focus on both ends (or on

diagonally opposite corners) of the indentation at the same time and must be rigid and free from effects of vibration. With the Vickers indenter, both diagonals were measured and the average was taken. Then, the microhardness value was transformed by the diagonal measurement table.

Hv = test load (kg) / surface area of the indentation (mm^2)

$$H_v = \frac{2\,F\sin\left(\frac{\theta}{2}\right)}{d^2} \times 1000$$

$$H_v = 1854 \times \frac{F}{d^2}$$

where Hv is Vickers hardness, F is test load (g), d is the arithmetic mean of two diagonals of the indentation d1 and d2 (mm) and θ is the angle between the opposite faces at the vertex of pyramidal indentor (136°).

Chapter 4

Results and Discussions -

Laser Cladding of MMC on Al Alloy AA6061

4.1 INTRODUCTION

Aluminum alloys are characterized by their low strength, low density, low hardness, poor friction and low wear resistance. Al-based discontinuous fiber reinforced metal matrix composites (MMCs) have received immense research interest in the last 30 years because of their improved strength, hardness and wear resistance over traditional Al alloys. A mixture of the hard ceramic or fibre phase with tough alloy matrix in the MMC contribute to the improvement of these properties [72,77,107,132].

For most of studies, aluminum as the substrate was used to mix with the reinforced ceramic particle phase to form the aluminum matrix composite MMC. This soft and low melting point matrix is unable to bound the hard ceramic phase when the surface was subjected to shear stress and high temperature, such as in the case of wear. The strength of the matrix and the interfacial strength between the two phases of a composite play critical roles in the performance of the composite. In the case of producing a surface MMC on Al alloy by laser cladding, the interface bonding between the surface layer and the Al alloy substrate is also a critical factor for the performance of the surface MMC.

In this section, results of laser cladding of the WC, TiC, Mo, Mo/WC, Mo/TiC, Mo/Si_3N_4 and Si_3N_4/TiC are discussed.

4.2 LASER CLADDING OF WC ON ALUMINUM ALLOY AA6061

Tungsten carbide (WC) holds a leading position on surface engineering among other carbides since it combines favorable properties, such as high hardness, good strength and stable at high temperature. It does not dissociate significantly as other ceramics during the laser processing.

In this study, WC was pre-placed by PVA binder on aluminum alloy. 1.4 kW laser power was used as processing parameters and the pre-placed layer was about 0.3 mm thick. Table 4.1 shows the parameters for the laser cladding of WC onto aluminum alloy AA6061. From equation 1, it was found that the high quality clad layer could be formed when the energy density was in the optimum range of 21-39 J/mm^2. Figure 4.1a shows the appearance of successful WC cladding on the Al alloy AA6061. Figure 4.2 shows the WC was well distributed in a smooth surface layer and well embedded in the Al alloy substrate.

Certain defects such as cracks, porosity, surface roughness, compositional inhomogeneity and excessive dilution have been observed when the specific energy density is out of the optimum range. Laser processing speed and power density are two of the most important factors on the success of laser cladding. In addition, these two factors can influence the thickness of the clad layer. When the energy density is below 20 J/mm^2 , cracking occurred on the surface of the clad layer. This is due to the difference in solidification rate between the clad layer and substrate. The laser energy is sufficient to melt the top layer of the pre-placed powder but only with little fusion with the substrate. During the solidification process, the contraction of the layer causes cracking due to high residual stresses on the layer and results in peeling (Figure 4.1b).

The high energy density of a laser melting process creates good mixing within the

molten pool, while the short interaction time produces a small HAZ and little diffusion of the cladding material into the substrate surface. However, the density of WC is almost 6 times of Al alloy substrate, the WC particles have high tendency to sink into the bottom of the clad and lead to inhomogenized distribution of the clad layer (figure 4.3). On the other hand, when the energy is higher than 40 J/mm^2, excessive melting and evaporation of aluminum alloy caused perforation and porosity in the molten zone (figure 4.3). This phenomenon was also observed by other authors, such as Mazunder and Goswami [77, 131]. In this case, the layer is not smooth, and there is a significant degree of porosity at the interface between the MMC layer and the substrate.

Figure 3.7 & 4.4 shows the surface condition of the as-received WC particle. The as-received WC particles are irregular shape. After laser irradiation, the large WC particle were broken down into small ones, probably due to the thermal shock, and partly dissociated by this high-energy source. Figure 4.5 shows the cross section of a cracked WC particle in the melted track. The residual stresses formation after laser irradiation may lead to the cracking of WC particle. The residual stress causing the cladding layer to crack is also related to some extent to the difference in physical properties between the cladding layer and the substrate. The great difference in ductility between the ceramic clad layer and aluminum alloy substrate also contributes to the residual stress.

According to the experimental observations, a large number of phases have formed. Their formation depends upon the nucleation and growth properties of each phase, the wettability of the contact surface, chemical reactions between the interacting phases, and the rates of diffusion of the reacting species through the interlayer. Typical X-ray diffractograms of the specimen WC6 (100% WC pasting powder) are presented in Figure 4.6. The major phases are WC, $(Al_5W)12H$, Al_4C_3 and WAl_{12}.

Table 4.1 Laser parameters for laser clad 100% WC pre-placing powder on AA6061 (beam diameter d = 3mm) .

Specimen No.	Power (kW)	Speed v (mm/s)	Specific Energy Density (E=P/dv)	Ar_2 Shielding gas (l/mm)	Overlapping (%)	Thickness (μm)	Remarks
WC1	1.2	15	26.7	50	50	167	Successful cladding
WC2	1.4	10	46.6	50	50	240	Rough surface, crack and porosity
WC3	1.4	12	38.9	50	50	203	Successful cladding
WC4	1.4	14	33.3	50	50	180	Successful cladding
WC5	1.4	16	29.2	50	50	168	Successful cladding
WC6	1.4	17	27.5	50	50	150	Successful cladding
WC7	1.4	18	26	50	50	164	Successful cladding
WC8	1.4	20	23.3	50	50	155	Successful cladding
WC9	1.4	22	21.2	50	50	140	Successful cladding
WC10	1.4	24	19.4	50	50	135	Crack and porosity
WC11	1.4	26	17.9	50	50	105	Crack and porosity

- Successful cladding = only have few or without porosity and without crack on the surface or cross-section.

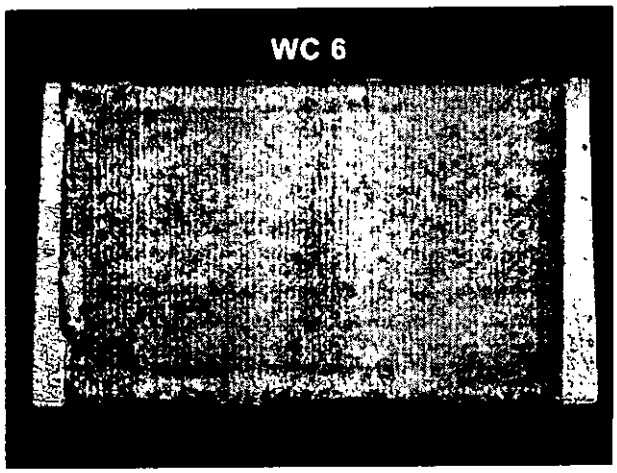

Figure 4.1a The surface appearance of successful cladding of specimen WC6.

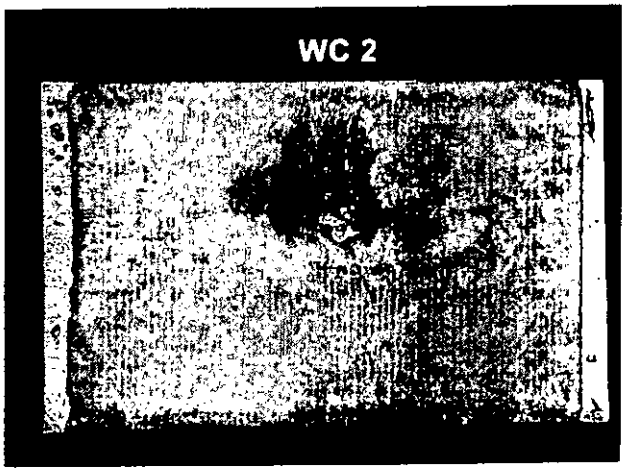

Figure 4.1b The peel off phenomenon of specimen WC2.

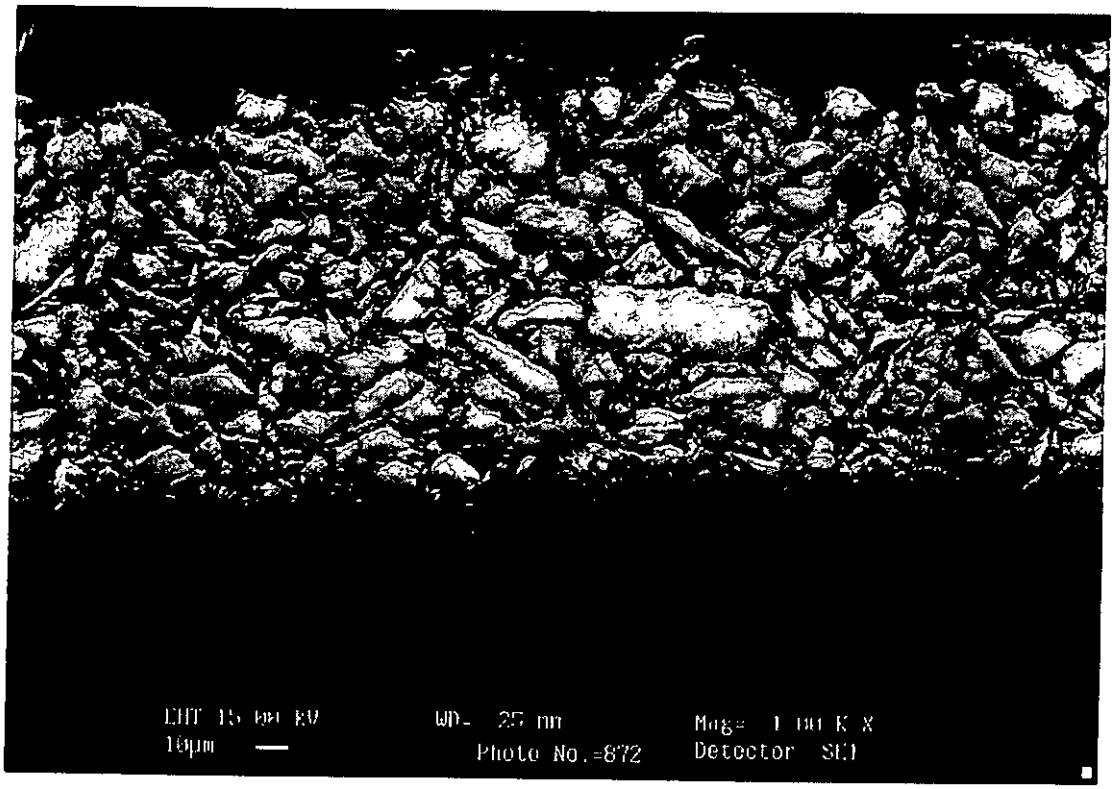

Figure 4.2 Cross-section of specimen WC 6, layer clad with 100% WC particles.

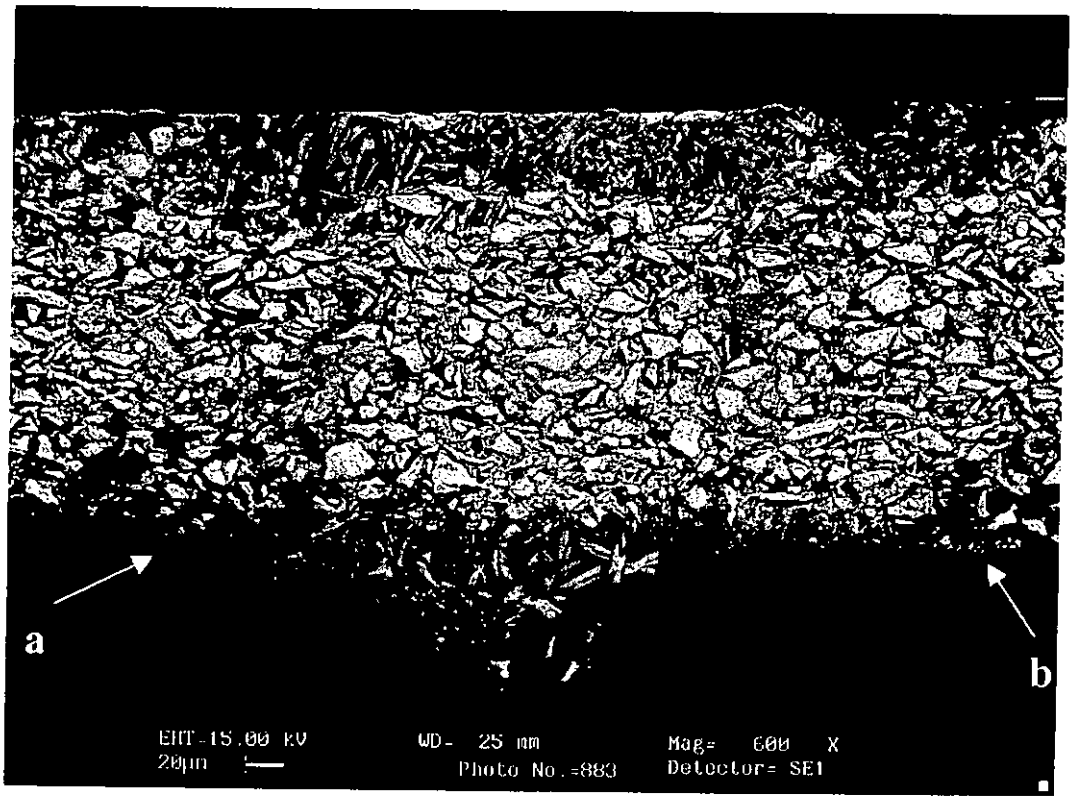

Figure 4.3 Cross-section of specimen WC2. Porosity and crack occur at the interface of clad layer and substrate (region a and b).

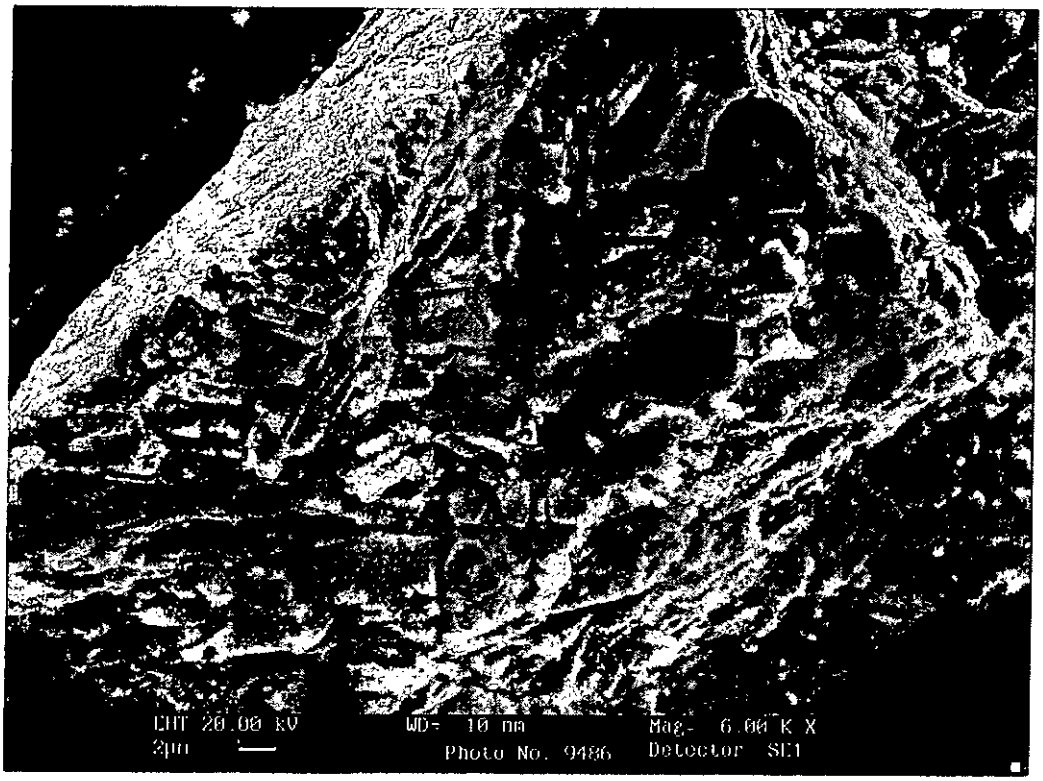

Figure 4.4 Surface condition of the as-received WC particle

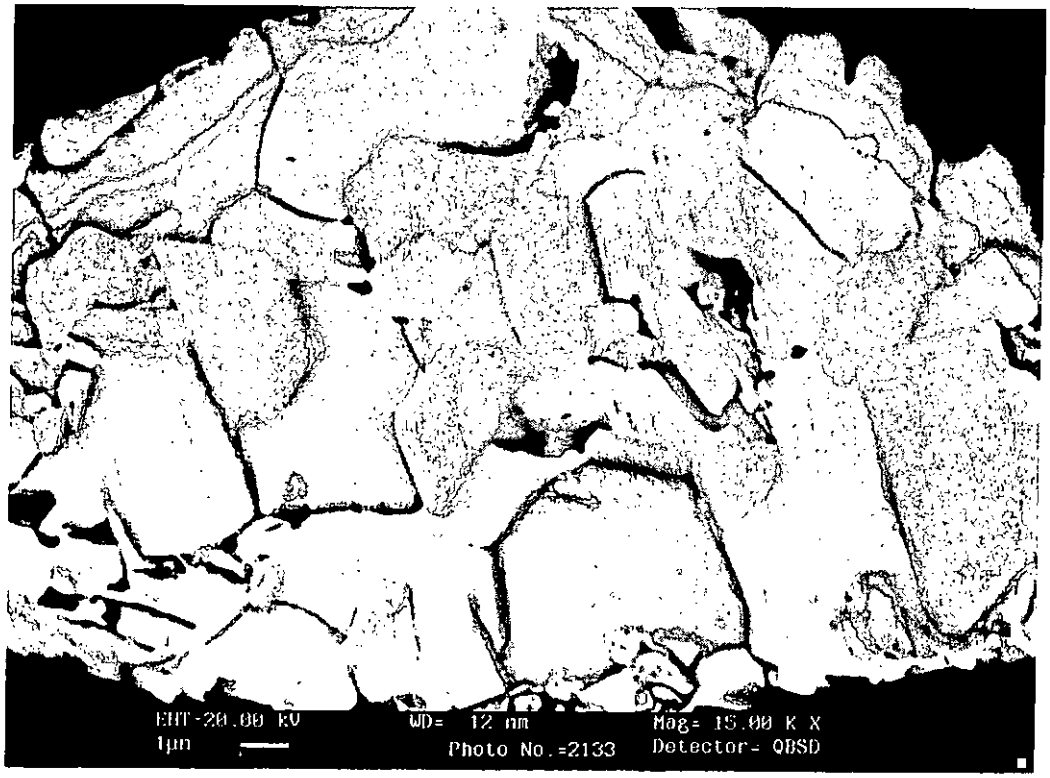

Figure 4.5 Cross section micrograph of WC particle melted at the edge and with internal cracking after laser cladding.

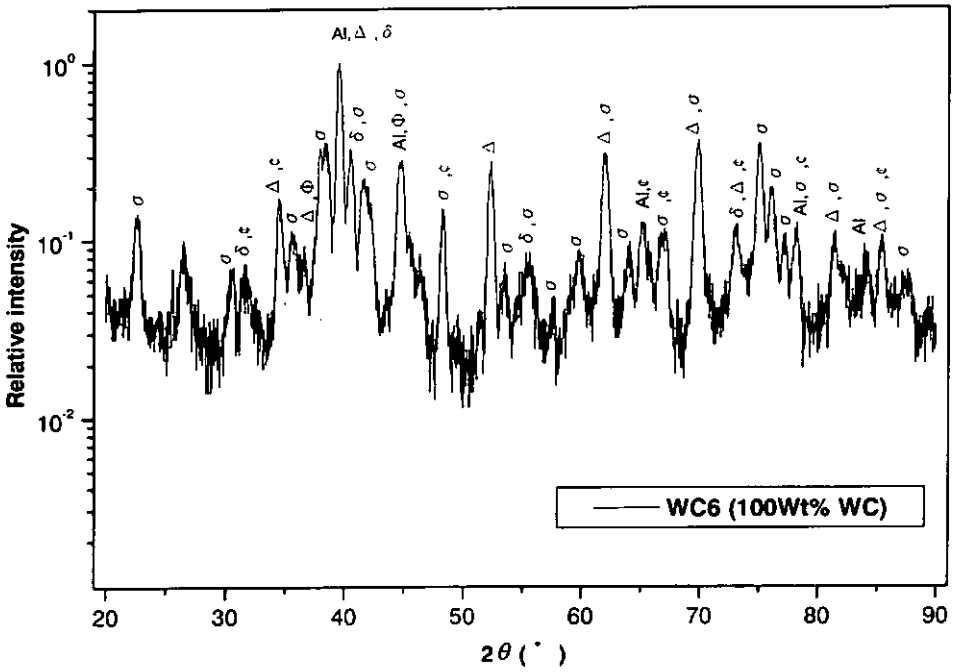

Al=Al, ¢ = WC ; o =Al_5Mo ; x = $Al_{17}Mo_4$; # = $Al_{22}Mo_5$; σ = $(Al_5W)12H$; δ = Al_4C_3 ; Δ = α-Mo_2C ; Φ = WAl_{12}

Figure 4.6 X-ray diffraction spectra of laser clad specimen WC6.

4.3 LASER CLADDING OF TiC ON ALUMINUM ALLOY AA6061

The addition of titanium carbide particles (TiCp) into a matrix alloy results in changes of the energy, momentum and mass transport in the laser melt pool, and hence in the solidified microstructure. The distribution of TiCp in the coating is controlled by the flow and velocity field, melt viscosity, the difference in density between the particulate and the matrix, and interaction of the remaining particles with the solid/ liquid solidification fronts in the laser melt pool.

During the laser cladding process, MMC requires a sufficient volume of liquid filling into the pre-placed TiC layer and forms a perfect clad layer with well-embedded TiC

particles. During laser irradiation, the molten liquid was dragged upward to the pre-placed layer by capillary force and the TiC particles were mixed well by the convection flow. Based on this reason, the thickness of the pre-placed layer is limited for successive surface cladding process. In this study, TiC was pre-placed by PVA binder on aluminum alloy AA6061. By experimental results, the maximum pre-placed layer thickness was 0.25 mm. When the thickness of pre-placed layer was less than 0.25 mm, the clad layer was too thin to perform its function. When the thickness of pre-placed layer was larger than 0.25 mm, the clad layer could not be successfully. The thicker the pre-placed layer, the larger volume of liquid is required from the restricted source. If the pre-placed layer thickness is increased, most of the energy will be absorbed by the pre-placed powders and less energy will reach the substrate. This implies that insufficient volume of molten liquid can be dragged by the capillary force and inter-filtrate into the pre-placed layer. In most cases, the clad layer was separated from the substrate and with very rough surface.

Table 4.2 shows the parameters for the laser cladding of TiC onto aluminum alloy AA6061. Using equation 1, it is found that high quality TiC clad layers could be formed when the energy density is in the range of 19-30 J/mm^2. When the energy density is below 19 J/mm^2 , the energy is only sufficient to melt the top layer of the pre-placed powder and solidification occurred before the heat was conducted to melt the substrate. Once it solidified and contracted, the layer peels off. Outside this range of the optimum processing parameters, the MMC layer was poorly incorporated with the Al alloy substrate surface. Figure 4.7 shows a good TiC clad layer.

Figure 4.8 shows the clad layer thickness versus power (in the speed of 17 mm/s). At processing speed of 17 mm/s, the thickness of clad layer reaches a maximum when laser power is 1400 W. For 20 mm/s processing speed, the clad layer thickness has a trend to

increase to 225 μ m. From the study of Baker [74], capillary force and Marangoni convection are the important issues for the successful clad layer. Large volume of molten substrate material is needed from the restricted source during the laser cladding process. The capillary force drags the liquid upwards to fill in the pre-placed layer. The molten substrate surface has the highest temperature and lowest viscosity, and therefore it has the highest potential capillary. This implies that the liquid in the molten zone infiltrates into the pre-placed layer by capillary action. The convective flow due to the high surface tension gradient in the liquid may promote this molten fluid movement. Therefore, it is suggested that the energy distribution of the laser processing determines the thickness limit of using pre-placed TiC and the formation of cavities if the preplaced TiC thickness limit is exceeded.

TiC was partially dissolved in the melt and precipitated during solidification. From the X-ray diffractograms of specimen TiC6 (100% TiC pre-placing powder), different phases of TiC occurred, such as TiC, Ti_8C_5, $Ti_6C_{5.75}$, $Ti_{5.75}C_{3.72}$. TiC decomposed into Ti and C during the irradiation of the laser beam. Ti combines with Al to form $TiAl_3$, Ti_3Al. TiC combines with Si from Al Alloy substrate to form Ti_3SiC_2 .

Table 4.2 Laser parameters for laser 100% TiC pre-placing powder laser cladding.

Specimen No.	Power (kW)	Speed v (mm/s)	Specific Energy Density (E=P/dv)	Ar_2 Shielding gas (l/mm)	Overlapping (%)	Thickness (μm)	Remarks
TiC1	1.1	17	21.7	50	50	156	good surface
TiC2	1.1	20	18.3	50	50	150	Poor surface and surface peel off
TiC3	1.1	22	16.67	50	50	135	Poor surface and surface peel off
TiC4	1.2	17	23.5	50	50	179	good surface
TiC5	1.3	15	28.9	50	50	247	good surface
TiC6	1.3	17	25.5	50	50	252	good surface
TiC7	1.3	20	21.7	50	50	168	good surface
TiC8	1.4	16	29.2	50	50	250	good surface
TiC9	1.4	17	27.5	50	50	256	good surface
TiC10	1.4	18	26	50	50	190	good surface
TiC11	1.4	20	23.3	50	50	189	good surface
TiC12	1.4	22	21.2	50	50	190	good surface
TiC13	1.4	24	19.4	50	50	179	good surface
TiC14	1.5	17	29	50	50	240	good surface
TiC15	1.5	20	25	50	50	225	good surface
TiC16	1.5	23	21.7	50	50	209	good surface

*Good surface = only have few or without porosity and without crack on the surface or cross-section.

*Poor surface = with unacceptable amount of porosity, crack and with rough surface.

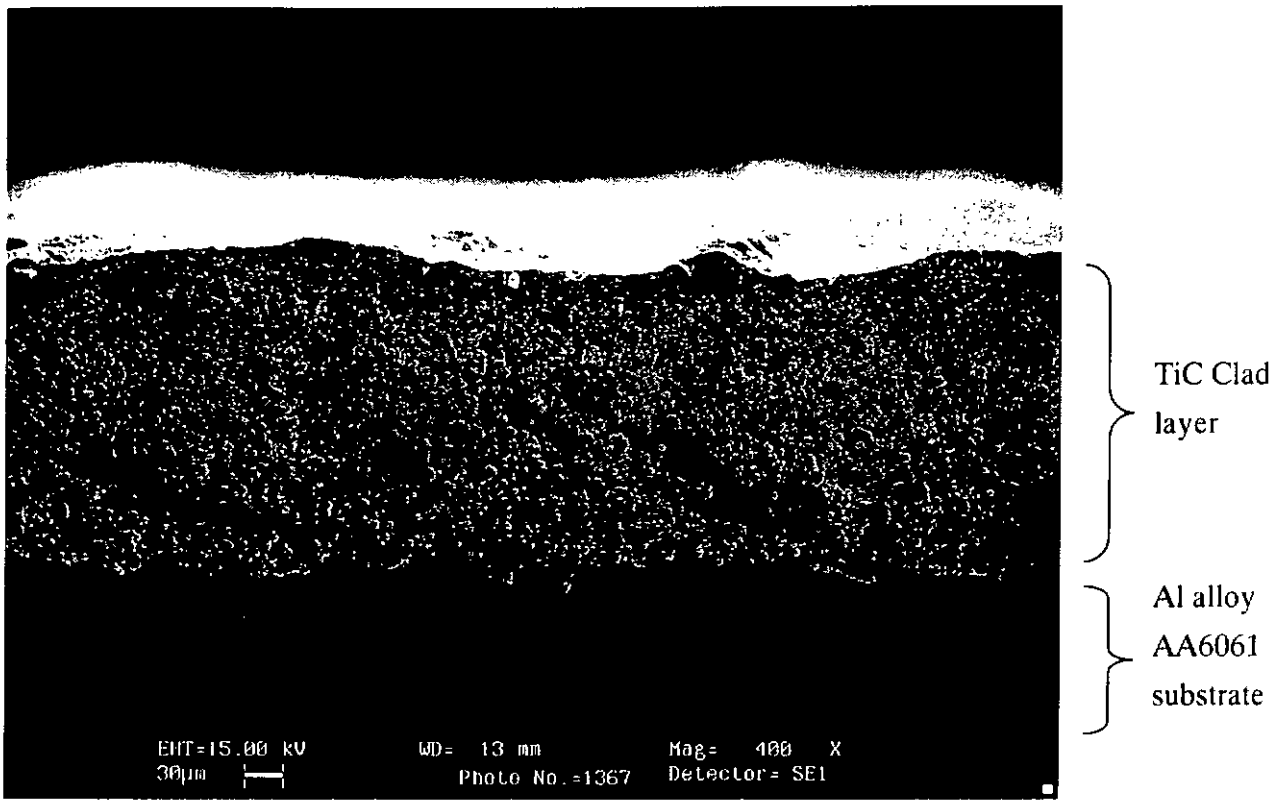

Figure 4.7 Cross-section of specimen TiC 6 , layer clad with 100% TiC pasting powder.

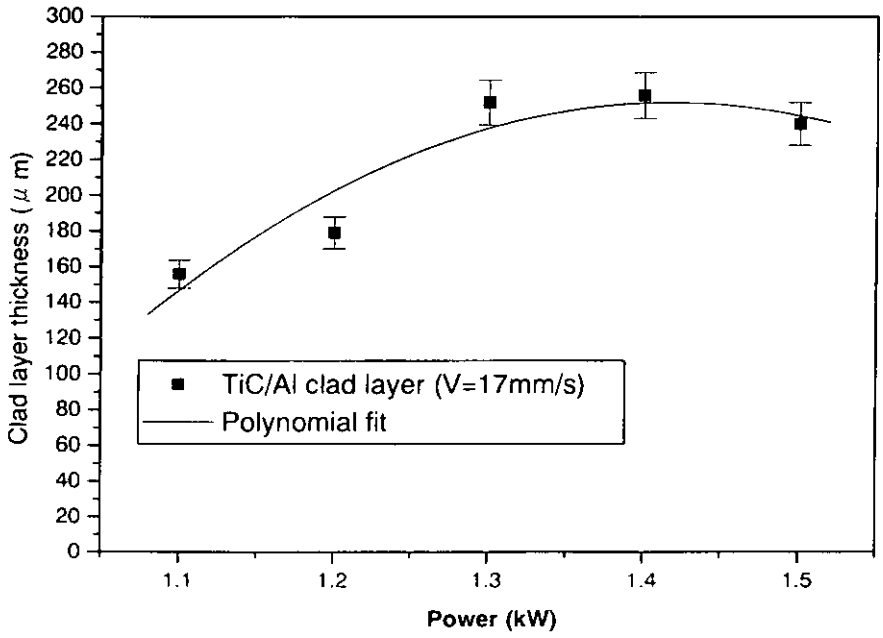

Figure 4.8 Relationship between the clad layer thickness versus power .
(scan speed 17 mm/s)

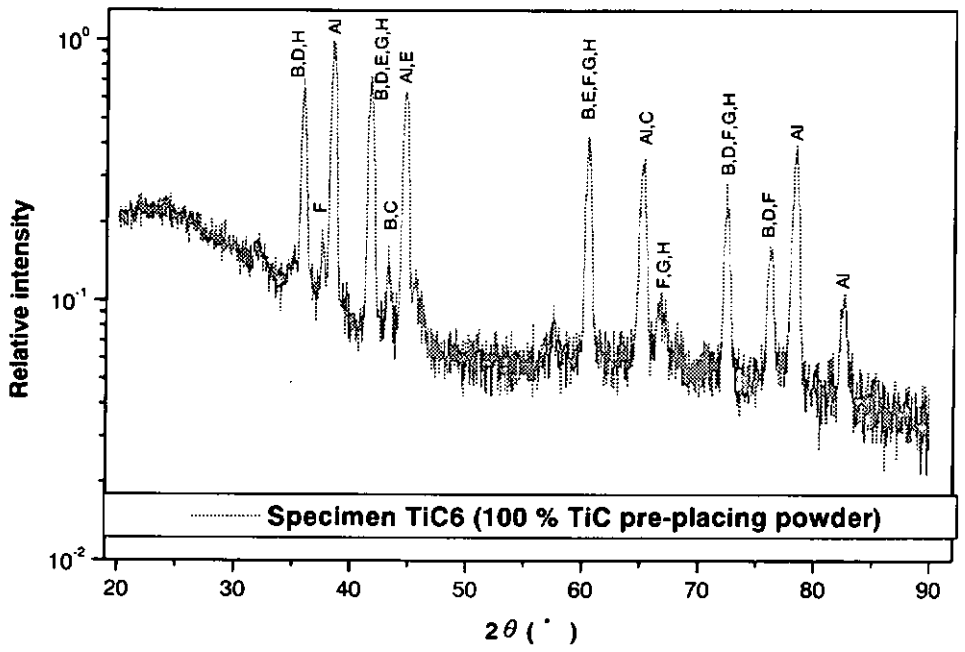

Al=Al, B = TiC, C = $TiAl_3$, D = Ti_3Al, E = Ti_8C_5, F = Ti_3SiC_2, G = $Ti_6C_{5.75}$, H = $Ti_{5.75}C_{3.72}$

Figure 4.9 X-ray diffraction spectra of laser clad specimen TiC6.

4.4 LASER CLADDING OF Mo ON ALUMINUM ALLOY AA6061

Molybdenum is a particularly interesting element to produce high strength matrix alloy because it has high solubility with Al [53]. Tomlinson *et al* [50] carried out a preliminary study of laser alloying of Mo on Al alloy substrate and found that it was difficult to melt and form un-dissolved particles of molybdenum. Then, Almeida and Vilar [53] carried out an extensive work on laser surface alloying Al alloy with Mo and identified a series of Mo-Al compounds on the alloyed layer.

In this work, the processing parameters were 10 - 28 mm/s beam scanning speed, 3 mm beam diameter, 1.3 – 1.5 kW laser power at work and the thickness of Mo coating is 0.3 mm. Table 4.3 shows results of laser cladding Mo on aluminum alloy AA6061. Figure 4.10 shows the parameter window for a good clad layer. The successfully performed laser

cladding layers were without cracks, porosity and have perfect adherence to the substrate. The optimum specific energy density range was found to be 26-42 J/mm^2 .

(a) General characteristic of Mo clad layer

The microstructure of the good quality laser-clad layer consists of mainly two kinds of different structure and a heat-affected zone adjacent to the fusion line (Figure 4.11). Figure 4.12 shows the higher magnification of Figure 4.11. The strong orientated dendrites in the upper zone are dispersed in the matrix of á-Al. Dendritic microstructure is produced during rapid solidification after laser melting. The lower zone is formed by some equiaxed morphologies and dendritic structure with secondary arming . The spacing between the dendritic arms are depended on the solidification rate [133]. Owing to cross-sectional effect of three-dimensional growth network, the dendrites appear to be randomly oriented at the lower part.

(b) Characteristic study of specimen Mo4

Figure 4.11 shows the cross-section of the successfully laser-clad specimen Mo4 which contains 100%wt Mo in the pasting powder. Mo reacts with molten aluminum to produce high melting point intermetallic phases, i.e. Al_{22} Mo_5, Al_5 Mo and $Al_{17}Mo_4$ (Figure 4.13), as found by XRD. Figure 4.14 shows the concentration profile of Al. Si and Mo along the depth of the clad layer of specimen Mo4. The clad layer reaches 430 μm for the Mo-Al laser cladding. The almost homogenized distribution of the elements in the layer indicates that the Marangoni Flow is effective in mixing the molten alloy. The

dendrites and matrix consist of various types of intermetallic compounds which have been studied by Almeida and Vilar [53]. Figure 4.14 shows a slight decrease of Mo and a slightly increase of Al concentration along the depth of the clad layer.

Figure 4.15 is the hardness distribution along the clad layer. Hardness of the clad surface is much higher than that of the substrate, i.e. 300-350Hv for the former as compared with 60 Hv of the latter. A sharp transition occurs between the surface layer and the bulk owing to absence of diffusion of the molybdenum in the aluminum solid state matrix. From the gradual decrease of Mo along the depth of the clad layer, as shown in the concentration profile of Figure 4.14, and the less amount of dendrites at the lower portion of the clad layer as shown in Figure 4.11- 4.12, the gradual decrease of hardness along the depth of the clad layer of Figure 4.15 can be explained by the decreasing amount of Al-Mo intermetallic dendrites along the depth of the clad layer. As the top portion of the clad layer solidified last, growth of Al-Mo intermetallic dendrites is from the bottom of the melt pool toward the direction of cooling.

In order to dissolve the particles, the temperature of the melt pool must be higher than the melting point of these particles. Compared with the melting point of Al alloy, the melting point of Mo is very high which is about 2617℃. Mo particles may not be molten totally in the melt pool and some of them may form intermetallic compounds. Because of this reason, laser cladding of aluminum is difficult to obtain homogenization. Although the EDAX analysis of the composition distribution of Mo is quite even in the clad layer, islands of non-uniformity of composition were also found (figure 4.16a). Figure 4.16b is a line scan of this intermetallic compound. Table 4.4 shows the EDX study on the 3 different regions of this intermetallic compound which contain 84-89 wt. % Mo , 10–14.5 wt. % Al and little amount of Si. So, this suggested that the intermetallic compound may be Al_8Mo_3

+ $AlMo_3$, as identified from the phase diagram in Figure 3.6. At point 2 and 3 of Table 4.4, the concentration of Al is much higher than point 1. Because the local temperature is lower than the melting point of this newly form intermetallic compound, molybdenum particles rapidly surrounded by a layer of aluminum compound.

(c) Defects on un-successful Mo laser clad specimens

Specimens Mo2, Mo3, Mo7- Mo9, Mo11- Mo14 have high surface roughness. Surface roughness is also influenced by other factors, such as porosity and cracking, as in Mo8-Mo9, Mo11-Mo14. When the specific energy density is lower than 26 J/mm^2 or higher than 42 J/mm^2 , the surface roughness is increased. Also, a lot of porosity appeared in the cross-section and sometimes occurred at the bottom of the track. During the melting process, gases were released from the binding agent, oxides of Al alloy and water moisture in the powder. During cooling, these gases appear in the form of bubbles because of the surface tension effect and escape by the floating to the top. When the scanning speed is very high (i.e. the interaction time is very low), these bubbles do not have the chance to reach the surface before solidification and are trapped within the clad layer in the form of porosity. This kind of porosity always trapped between successive overlapping passes or formed at the interface between the clad layer and the substrate, as depicted in Figure 4.17a and 4.17b.

Table 4.3 Process parameters for laser cladding Mo on aluminum alloy AA6061.

Specimen No.	Power (kW)	Speed *v* (mm/s)	Specific Energy density (E=P/dv)	Ar_2 Shielding gas (l/mm)	Overlapping (%)	Thickness (μm)	Remarks
Mo1	1.3	14	31	50	50	375	good surface
Mo2	1.3	17	25.5	50	50	355	rough surface
Mo3	1.3	20	21.7	50	50	310	rough surface
Mo4	1.4	12	39	50	50	430	good surface
Mo5	1.4	15	31	50	50	389	good surface
Mo6	1.4	17	26	50	50	335	good surface
Mo7	1.4	20	23.3	50	50	330	rough surface
Mo8	1.5	10	50	50	50	450	good surface appearance, porosity at the cross-section
Mo9	1.5	12	41.7	50	50	435	good surface appearance, porosity at the cross-section
Mo10	1.5	15	33.3	50	50	415	good surface
Mo11	1.5	18	27.8	50	50	365	rough surface, a lot of porosity at the cross-section
Mo12	1.5	20	25	50	50	355	rough surface, a lot of porosity at the cross-section
Mo13	1.5	25	20	50	50	310	rough surface and porosity occurred on the surface
Mo14	1.5	28	17.8	50	70	275	rough surface, a lot of porosity at the cross-section

*Good surface = only have few or without porosity and without crack on the surface or cross-section.

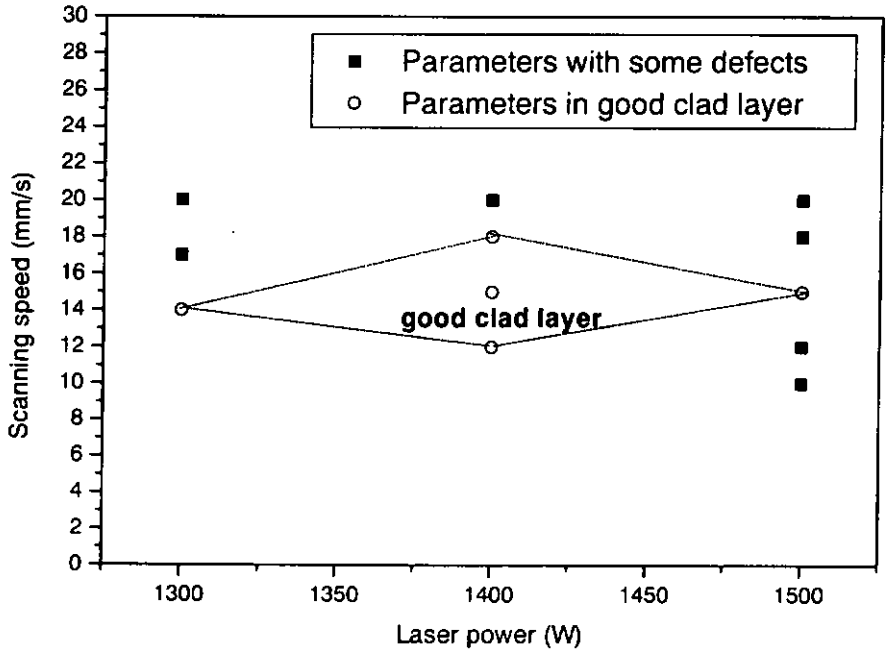

Figure 4.10 The parameter window for Mo/Al clad layer.

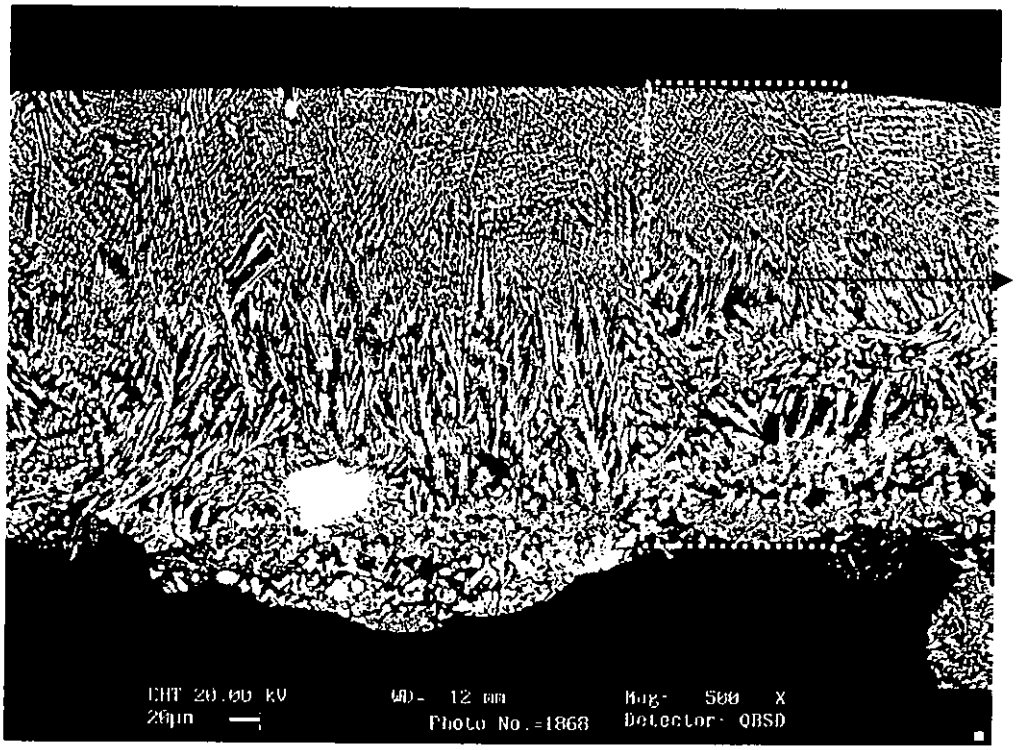

Figure 4.12

Figure 4.11 Dendritic structure formation of specimen Mo4 (100% Mo pasting powder)

Oriented dendritic structure at the upper zone

Coarse dendritic structure with secondary arm due to the lower cooling rate.

Figure 4.12
Two different zones in the Mo-Al clad layer specimen Mo4.

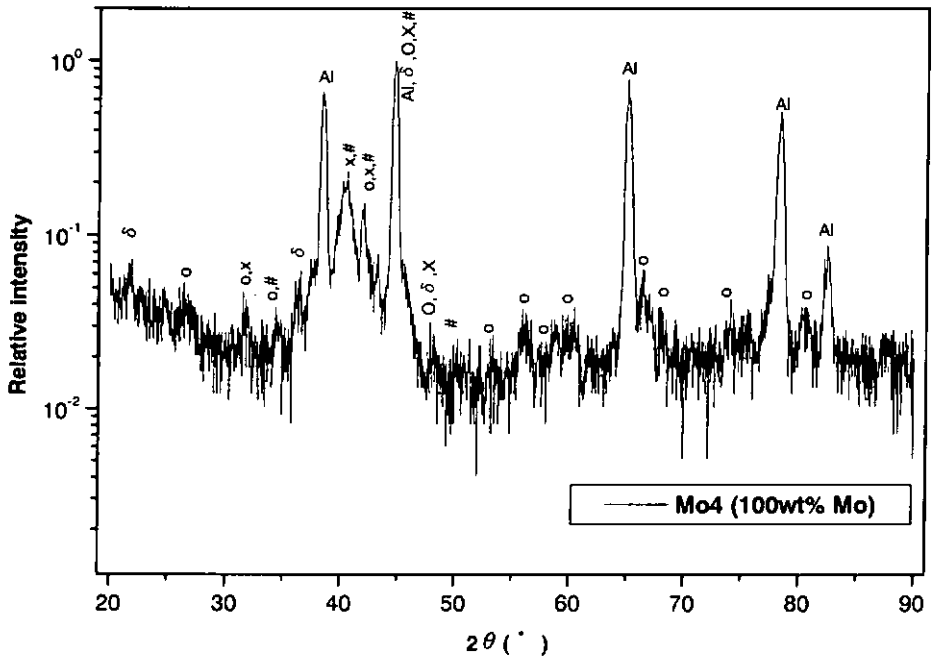

Al=Al, o =Al_5Mo ; x = $Al_{17}Mo_4$; # = $Al_{22}Mo_5$; δ = $Al_{22}Mo$

Figure 4.13 X-ray diffraction spectra of specimen Mo4 (100% Mo pasting power) .

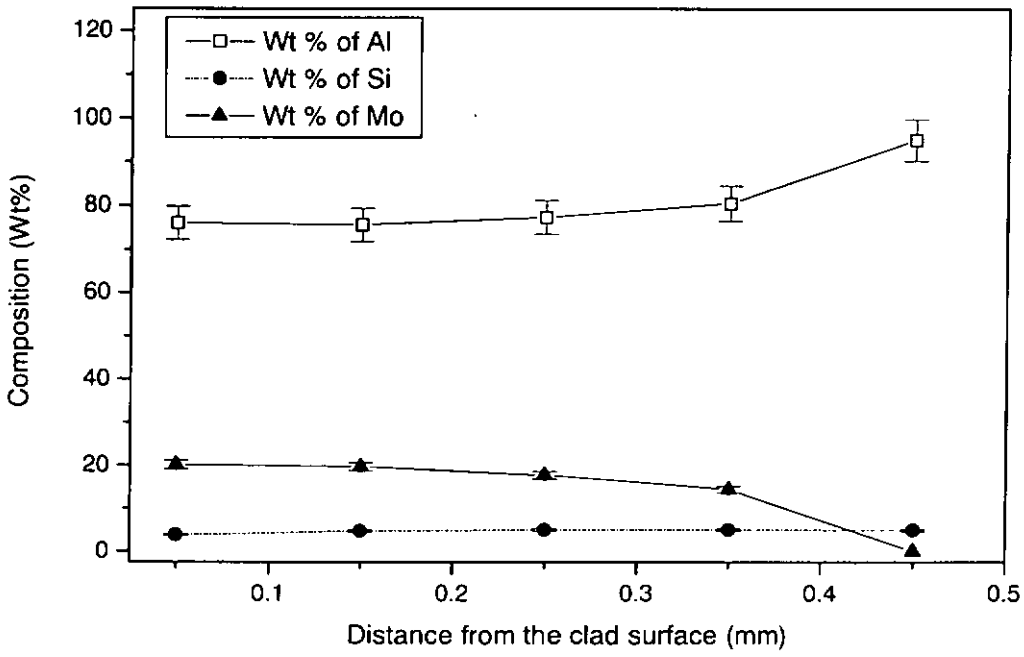

Figure 4.14 Compositional variation of specimen Mo4 (100 %Mo) from the top of the clad to the Al alloy substrate.

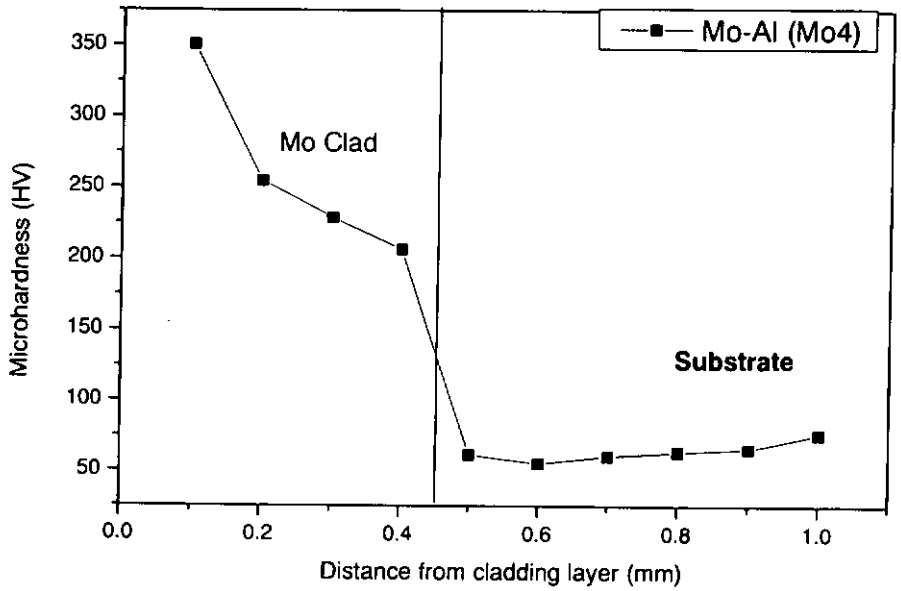

Figure 4.15 The hardness distribution along the specimen Mo4.

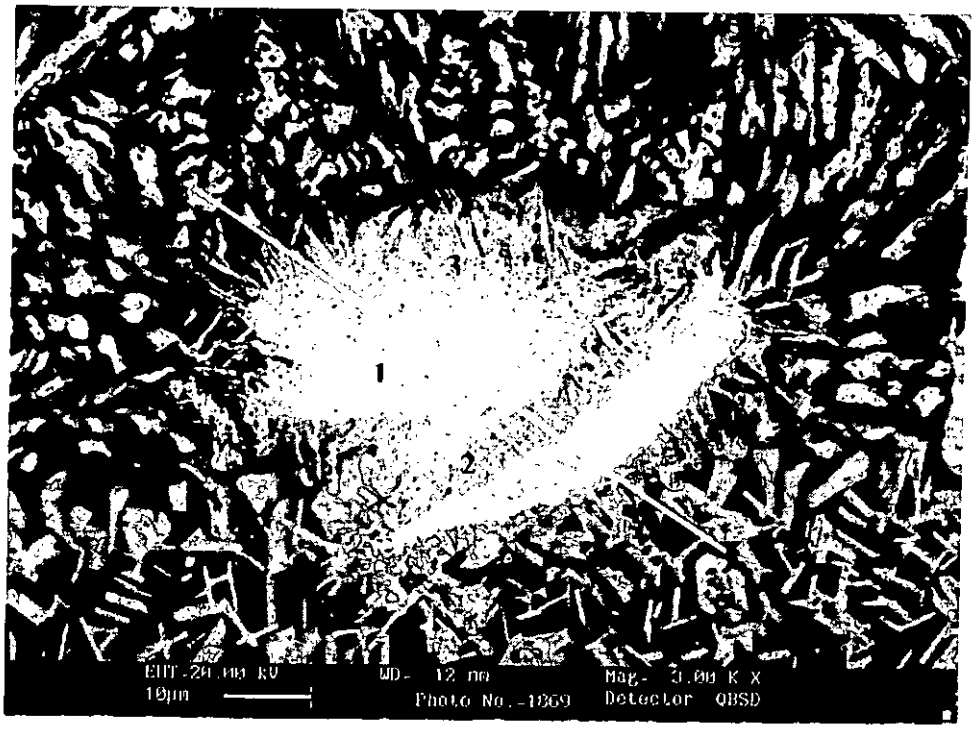

Figure 4.16a Al-Mo intermetallic compound formation in specimen Mo4 (100%Mo pasting powder).

Table 4.4 The EDAX weight percentage analysis of region 1 – region 3.

	Al wt %	Si wt%	Mo wt%
Region 1	9.84	0.34	89.81
Region 2	14.49	0.27	85.25
Region 3	14.43	0.72	84.85

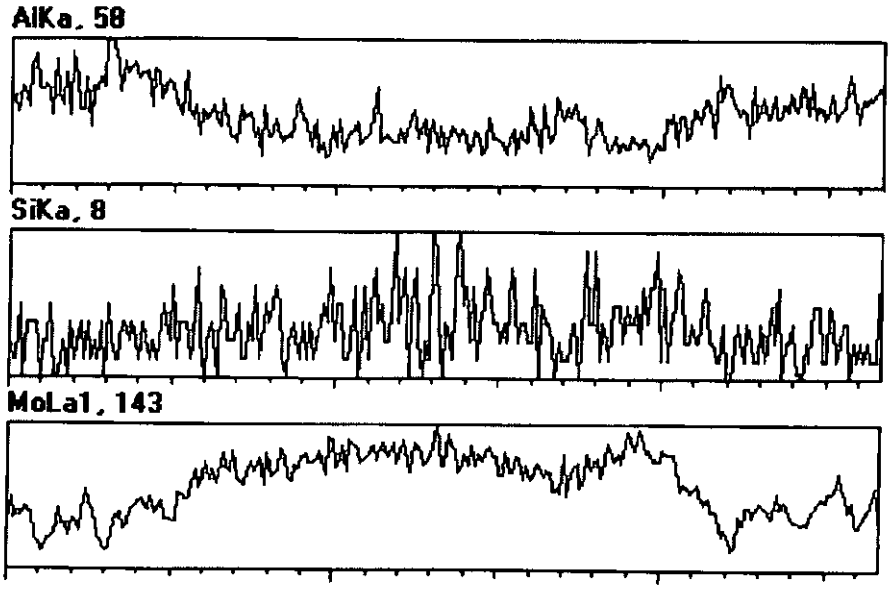

Figure 4.16b EDX line scan of specimen Mo4 (100% Mo pasting powder).

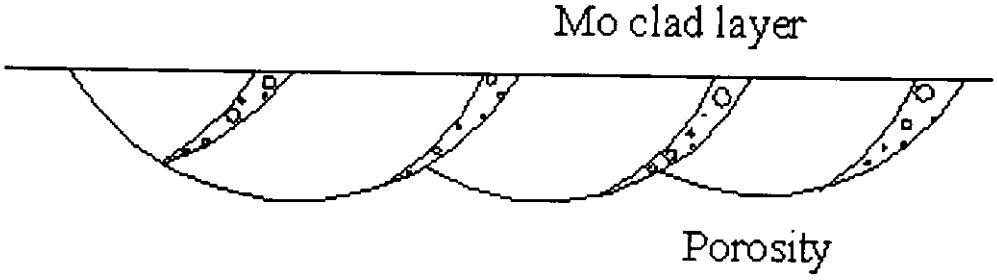

Figure 4.17a Schematic diagram of the interrun porosity.

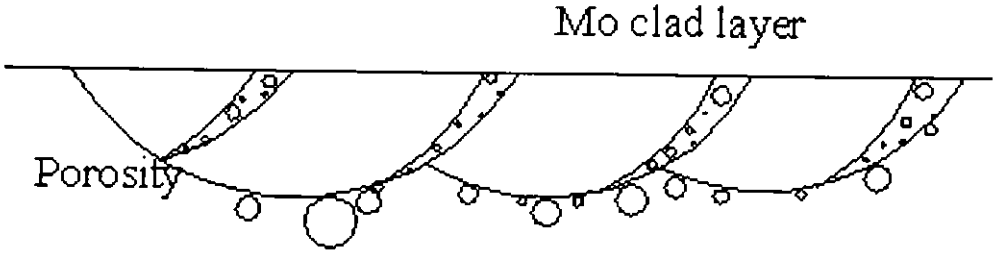

Figure 4.17b Schematic diagram of the porosity occurring in the clad layer interface.

4.4 LASER CLADDING OF Mo /WC ON ALUMINUM ALLOY AA6061

In this part, laser cladding Mo-WC system on AA6061 alloy was investigated. The results in section 4.3 confirmed that Mo was suitable to be used to produce a high strength matrix alloy with Al alloy AA6061 because it has high solubility with Al [53]. Based on the results of Section 4.3, it is postulated that the interface between the MMC layer of Mo-WC on Al alloy would be a continuous metallurgical bond. Section 4.3 also indicated that the hardness of Mo-Al clad layer is not very high. In order to obtain a layer with appropriate thickness and with higher wear resistance, WC is added into the system. WC has high hardness, good strength and stable at high temperature. The results in section 4.1 indicated that it does not dissociate significantly during the laser melting. Binding this particle phase to the matrix is an important issue to the strength of the MMC. If the surface of the ceramic particles is melted and forms some sorts of bonding with the matrix, the interfacial strength between the reinforced ceramic phase and the Mo-Al matrix will be enhanced.

During the cladding process, only a very thin layer of powder-pasted aluminum alloy substrate were melted and solidified to form a clad layer. The processing parameters were 17 mms^{-1} beam scanning speed, 3 mm beam diameter and 1400 W laser power at work. Surface oxidation was prevented using a coaxial jet and a side jet of argon gas. The clad surface was built up by 50% overlapped single tracks. A good surface finish and porosity-free surface layer were produced using the optimised processing parameters as quoted. The thickness and shape of the clad track were carefully controlled by laser power, scanning speed and focusing distance. Using the same laser processing conditions, the typical clad thickness was in the range of 200-250 μm for the Mo/WC clad layer with different mixing

ratio. The thickness of each clad layer is shown in Table 4.5.

The different layer thickness achieved is probably due to the different heat transfer effectiveness between Mo and WC powders. There are great differences in the heat capacity (Cp) between Mo and WC at the high temperature condition (at 2000K) considered [117], as shown in Table 3.3. The results indicated that the existence of WC powders affect the heat transfer of the laser energy towards the aluminum alloy substrate. The clad layers are free of crack and porosity. High integrity laser surface cladding of Mo-WC on aluminum alloy could therefore be produced successfully.

For the Mo/WC-Al system, specimen B to E, the heat input of the laser beam was enough to melt the matrix metal, Mo, in the composite but not quite sufficient to melt the WC reinforced particles. Some partially melted WC particles were observed in the clad layer. Other researchers also observed that the WC particles were partially dissolved in different alloy matrixs [45,99,107]. The layer thus consisted of melted, unmelted and partially melted WC particles embedded in Mo-Al-Si matrix. Good interfacial bonding between the particle phase and the matrix was observed and no cracking occurred. Figure 4.18 shows that a cluster of WC particles were surrounded by the matrix and partial melting of some of the WC particles was obvious. This agrees with the result of other authors that WC particles can be melted in the matrix [45, 97, 107]. Roósz *et al.* [107] reported that WC particles partially dissolved in the melt and W_2C particles solidified from the melt and mostly deposited on the original WC particles. It is clearly shown in Figure 4.19 that WC particles partially dissociated at the edge, and some of the columnar dendrites grew epitaxially from the surface of the partially melted WC particles. This enhances the interfacial strength between the reinforcing phase and the matrix alloy significantly. Figure 4.20b is the EDX line scan of Figure 4.20a. It shows that certain amount of Mo and

Al surrounding the edge of the large WC particle combine with the dissolved WC and some form of Al-Mo-W compounds are formed.

Figures 4.21-4.23 show the different distributions of WC particles in the clad layer. With different powder composition, the difference in powder densities, melting points of the phases in the melt pools, viscosity of the melt and solidification rates of the phases all play a role in the distribution of the ceramic particles. In specimen C (Figure 4.21), WC particles tend to sink in the bottom of the melt pool. This is due to the great difference in the powder density between WC and Mo, i.e. the density of WC is 1.5 times that of Mo. The lower melting points and slower solidification rates of the Al and Mo solid solutions and their intermetallic compounds allow time for the WC particles to sink towards the bottom of the melt pool. The Marangoni convection for mixing the particles was not effective in this case. This uneven distribution of the hard particles could be advantageous. The clad surface, in real industrial application, needs to be machined and polished before it can be used. The slightly softer top portion of the layer is ideal for the post-cladding machining process. Once the slightly softer top portion is removed, the portion with high concentration of WC particles is exposed for wear resistant application. The higher the percentage of WC particles present, the less effective the Marangoni flow will be in the mixing of the carbide particles. But on the other hand, the higher the content of the WC particles, the less the amount of the substrate metal is melted and the higher the solidification rate the layer will experience. Hence, the degree of uneven distribution of the WC particles in the clad layer diminishes with the increase in the content of WC particles. The matrix is mainly Al-Si alloy which is relatively soft as compared with the Al-Mo-Si compounds. Figure 4.24 shows the increase of microhardness of the clad layer against the percentage of WC in the pasting powder. The hardness reading was taken at the mid-point

of the layer depth. The higher the WC content, the higher hardness of the clad layer results, as expected.

Typical X-ray diffractograms of the as-received Al alloy AA6061 and Mo/WC clad specimens, B to E, are presented in Figure 4.25 a-c. For Specimen Mo/WC specimens, the phases were WC, Al, Al_5Mo, $Al_{22}Mo_5$, $Al_{17}Mo_4$, $(Al_5W)12H$, α-Mo_2C, Al_4C_3 and WAl_{12}. The exact amount of each phase is difficult to estimate.

Table 4.5 Wt% of Mo and WC in the 0.3 mm thick powder paste and the resulting clad layer hardness and thickness.

Specimens	Wt% of Mo (paste composition)	Wt% of WC (paste composition)	Average microhardness $VHN_{(200g)}$	Thickness (μm)
Mo4	100	-	225	430
B	80	20	302	250
C	60	40	473	200
D	40	60	508	200
E	20	80	643	200
WC6	-	100	766	150

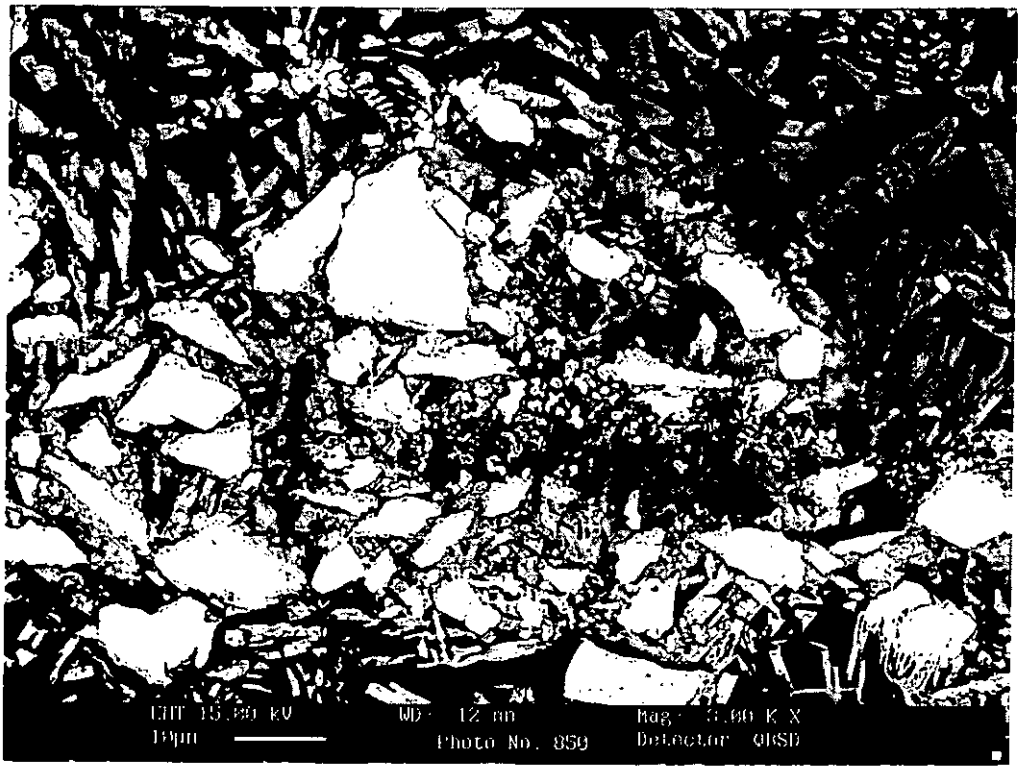

Figure 4.18 WC cluster formation in the laser clad layer with 60% Mo and 40% WC powder.

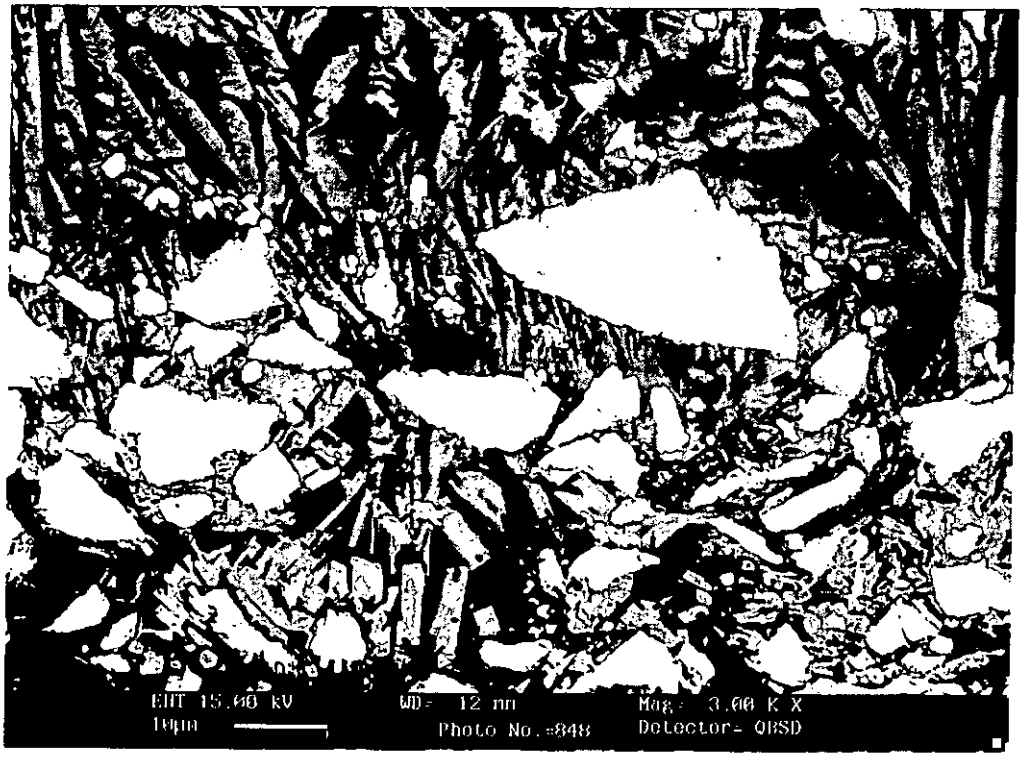

Figure 4.19 Columnar dendrites grow epitaxially from the surface of the partially melted WC particles, layer clad with 60% Mo and 40% WC powder.

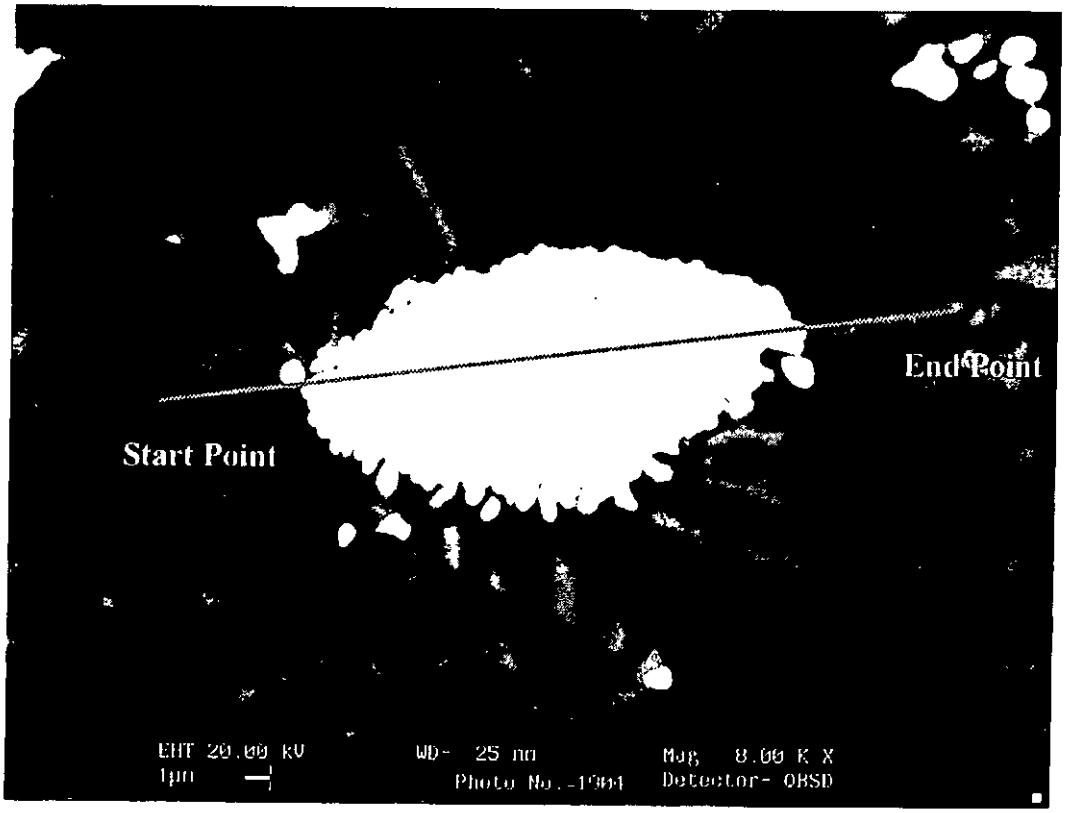

Figure 4.20a WC particle after laser clad with 60% Mo and 40% WC powder.

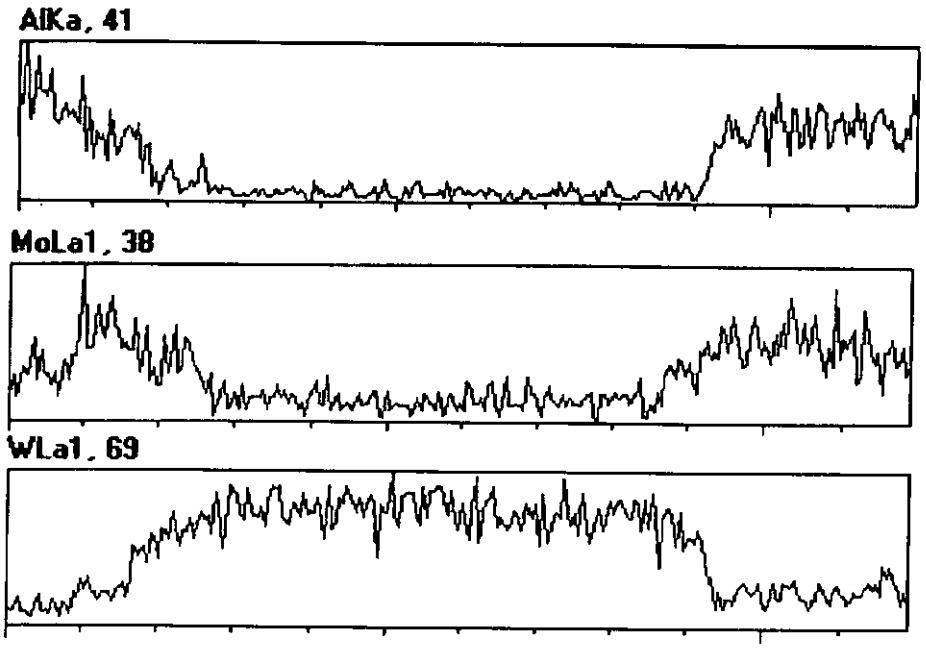

Figure 4.20b EDX line scan of figure 4.20a.

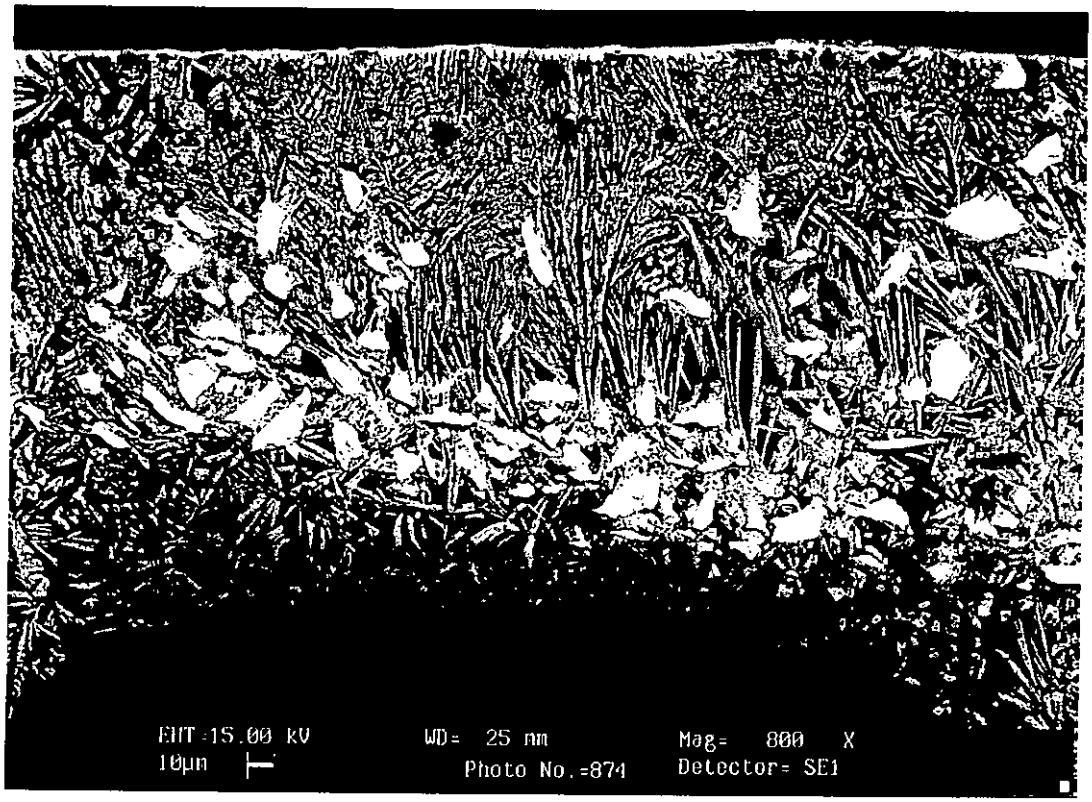

Figure 4.21 Cross-section of specimen C, layer clad with 60% Mo and 40% WC powder.

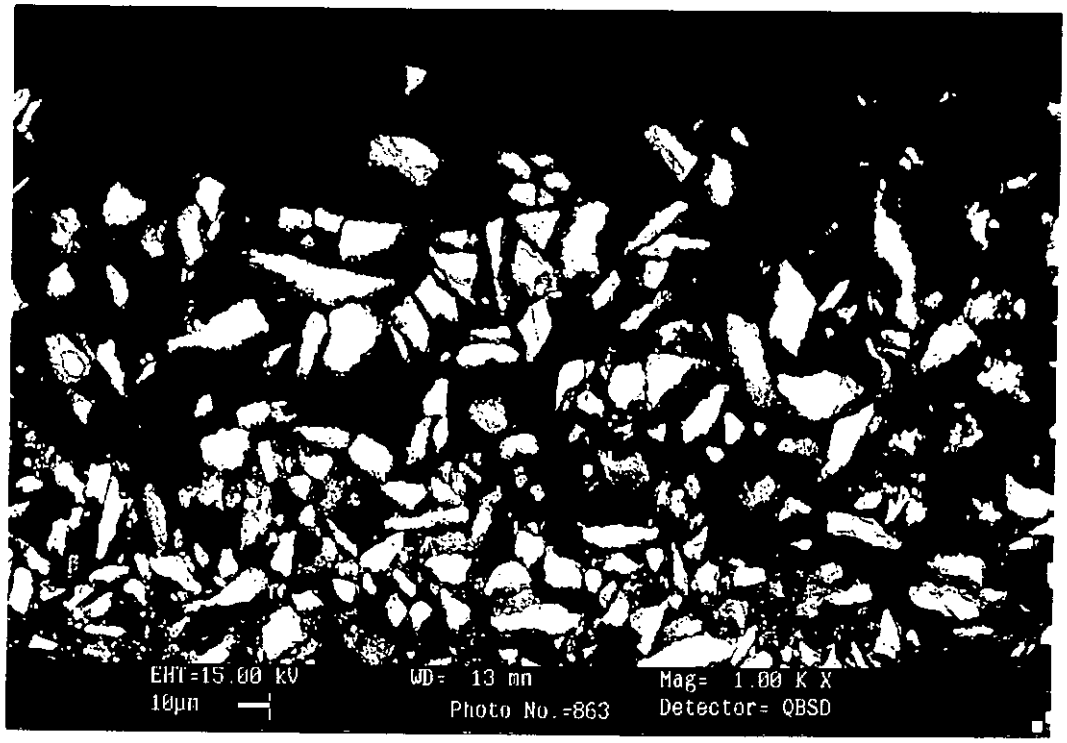

Figure 4.22 Cross-section of specimen D, layer clad with 40% Mo and 60% WC powder.

Figure 4.23 Cross-section of specimen E, layer clad with 20% Mo and 80% WC powder.

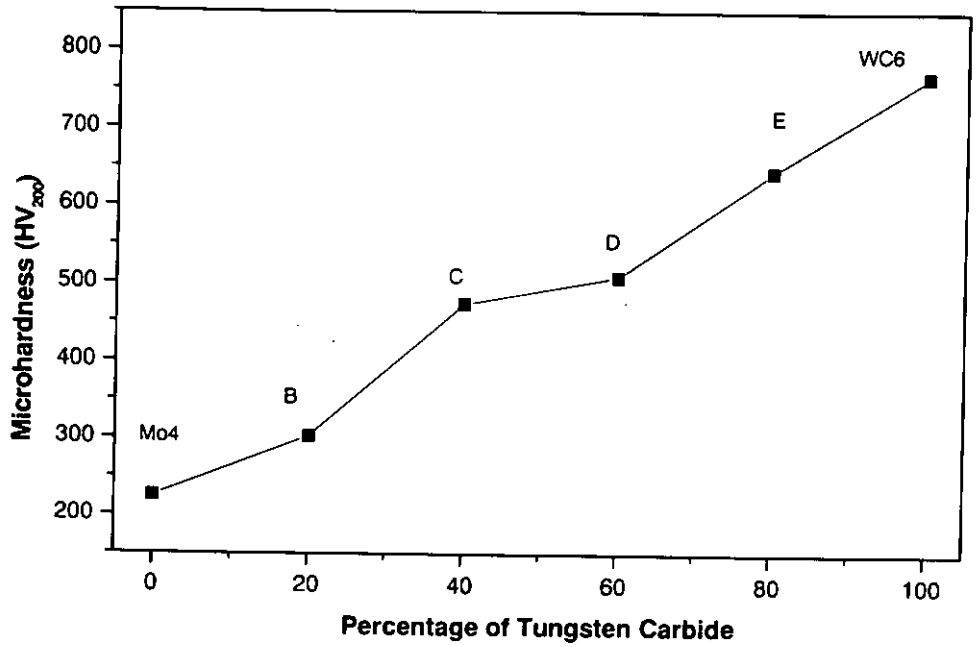

Figure 4.24 Microhardness versus percentage of tungsten carbide in the pasting powder.

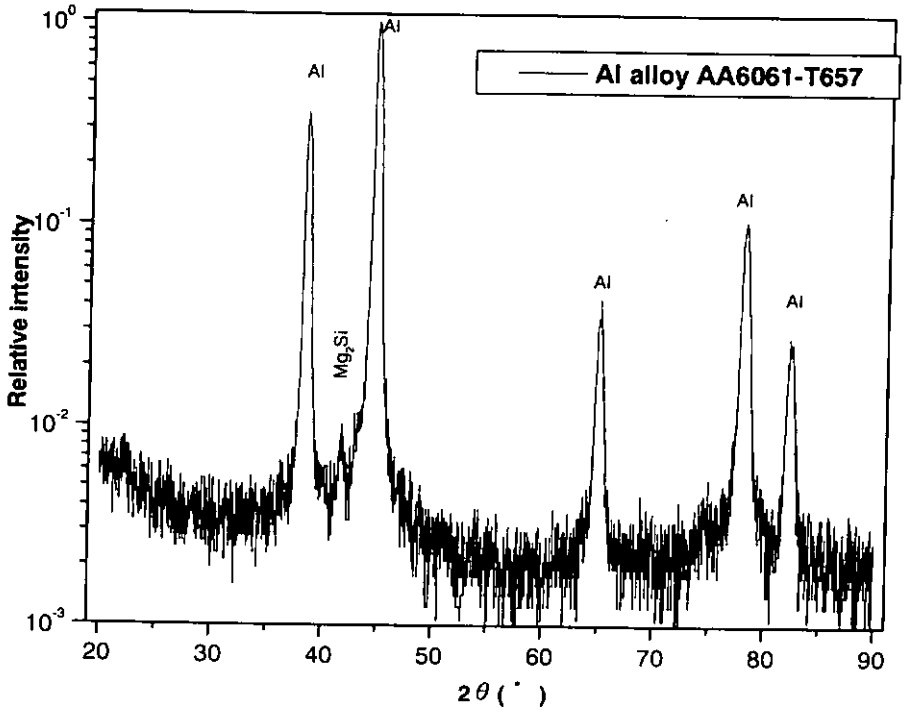

Figure 4.25a X-ray diffraction spectra of Al alloy AA6061-T657.

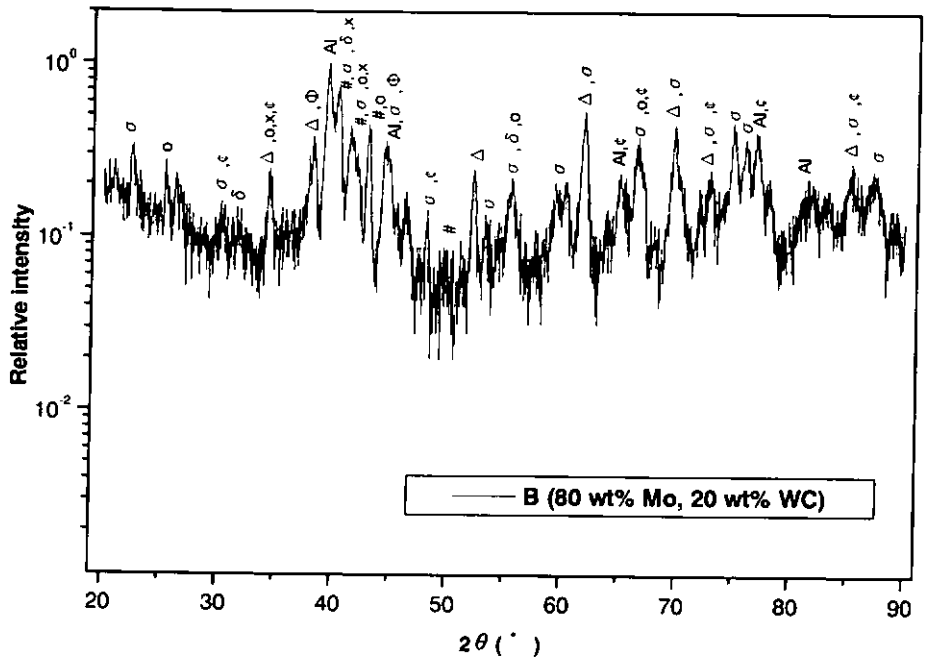

Figure 4.25 b X-ray diffraction spectra of laser clad specimen B.

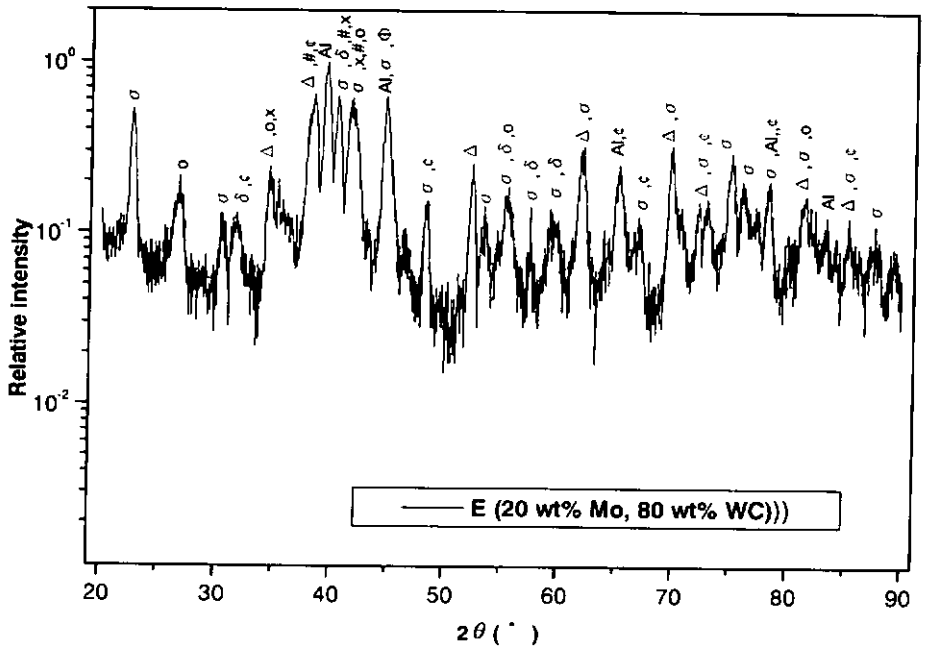

Al=Al, ¢ = WC ; o =Al_5Mo ; x = $Al_{17}Mo_4$; # = $Al_{22}Mo_5$; σ = (Al_5W)12H ; δ = Al_4C_3 ; Δ = α-Mo_2C ; Φ = WAl_{12}

Figure 4.25c X-ray diffraction spectra of laser clad specimen C.

4.6 *LASER CLADDING OF Mo /TiC ON ALUMINUM ALLOY AA6061*

In this part, laser cladding of Mo/TiC system on AA6061 alloy is discussed. The results in section 4.5 confirmed that WC in the Mo/WC system would partially dissolve in the clad layer and has a tendency to sink into the bottom of the clad. In this study, TiC was chosen as the ceramic binder for combining with the Mo metal powder, because TiC has lower density and more stable when compared with WC.

For successful clad layer to be formed, the optimum processing parameters were found to be 3 mm laser beam size, 17 mms^{-1} beam scanning speed, 1.3 kW laser power at work and 0.25mm pre-placed layer thickness. A 50% overlapping on each track was practiced to make up a surface. Using the same laser processing conditions, the typical clad thickness was in the range of 180-200 μm for Mo/TiC clad layer with different powder mixing ratio. The thickness of each clad layer is shown in Table 4.6. Under this set of parameters, all specimens were of high integrity, no porosity and free of cracks. The laser cladlayers formed a good metallurgical bond with the substrate alloy.

Figures 4.26a, 4.27a, 4.28a, 4.29a & 4.30a show the cross-sections of the laser clad Mo/TiC on Al alloy at different ratio of powders in the paste coating. Good metallurgical bonding between the substrate and the coating interface was observed. Figures 4.27b, 4.28b and 4.29b are EDX line scan across specimen Bb, Cc and Dd. These figures reveal the amount fluctuations of Al, Mo and Ti. The line fluctuations of Al and Mo are almost coherent and indicate that Al and Mo form intermetallic compounds along the clad layer. such as Al_5Mo, $Al_{17}Mo_4$, $Al_{22}Mo_5$ and $Al_{22}Mo$. The results were proven by the X-ray diffractometry studies. Ti and Mo occur alternatively and this shows that TiC is embraced by Al_xMo_y intermetallic compounds. In some region, Al, Ti and Mo are co-exited. The high melting point TiC (3065 ℃) is partially dissociated under the high power laser

irradiation. Al-Mo and Al-Mo-Ti intermetallic compounds are also found on the melt pool. Only small amount of Al was detected on these line scan figures. This indicates that the dilution rate is low in the Mo/TiC clad samples. Fig 4.30a, specimen TiC6 (100% TiC pasting powder), TiC particles are well distributed and perfectly embedded as a smooth layer, which is up to 250 μm thick on the surface. TiC particles were small and uniformly dispersed in the melt pool. Excellent bonding between the clad layer and substrate and it is free of crack and porosity. Figure 4.30b is the line scan of 100%TiC pasting powder.

A lot of new phases were found after laser cladding (Figure 4.31 a-c). From the X-ray diffractograms of specimen Bb, Cc, Dd which were laser clad with different composition of Mo and TiC powder. Under laser irradiation, the reaction of Mo and Al form intermetallic compounds, such as Al_5Mo, $Al_{17}Mo_4$, $Al_{22}Mo_5$, $Al_{22}Mo$. This was proved by previous research work [53]. TiC was decomposed into Ti and C, and partially dissolved in the melt pool and precipitated during solidification. The dissolution of Mo and Al combines with the dissociated Ti or C to form intermetallic compounds, such as $AlMoTi_2$ or Al_2Mo_3C. The Al Alloy substrate material had small amount of Si, so small amount of Ti_3SiC_2 was found from the data of X-ray diffractograms. The incorporation of Mo and TiC into the laser clad layers resulted in an increase of microhardness considerably. The hardness increased from 85 Hv to 950 Hv of the 100% TiC pre-placing powder clad layer. The detail microhardness of different composition is shown in Table 4.6.

The distribution of the particulates was highly affected by the Marangoni flow and the mass transportation of the powder particle. If the Marangoni flow is not large enough to create turbulence for the homogenization of the powders in the clad layer, the denser particles will tend to sink into the bottom of the clad. The density of Mo is 10220 kg/ m^3 . which is 2 times of TiC and 4 times of Al alloy. So, it is obvious that a lot of Mo exists at

zone B (Figure 4.32). In zone A, Al-Mo intermetallic compounds were formed and TiC was embraced between the Al_xMo_y dendritic arms. Under supercooling condition, the grains have a tendency to grow away from the heat source and align toward the heat flow direction [63]. The Al_xMo_y dendritic structures grow from the lower part of the Mo rich region of the clad, as can be seen in the SEM micrograph (Figure 4.32a). Energy dispersive X-ray (EDAX) analysis data in Table 4.7 indicates that 3.38 wt% and 8.81 wt% of Ti exist in the grey color grain and white color grain (Figure 4.32d). This means that Ti and C were decomposed during laser irradiation. The intermetallic compound is $AlMoTi_2$, which is confirmed by the data of XRD diffractograms. The dark-grey color particulate was found as the un-dissolved TiC particle.

Partial dissociation of TiC and re-precipitation of the dispersed phase improve the particle distribution and enhance the strength of the matrix. Figure 4.31b shows the evidence of the TiC particles. The partially melted TiC particles did not grow and form aggregates as other ceramics, such as WC [112-118]. Figure 4.33 shows the SEM mapping of the cladding layer. Figure 4.33a is the SEM diagram and Figure 4.33 b-d show the uniform dispersion of Al, Mo, and Ti in the melt pool.

Table 4.6 % of Mo and %TiC in the 0.25 mm thick powder paste and the clad layer hardness and thickness. (carbon was not detected)

Specimens	Pre-placing composition		Composition after laser cladding			Average microhardness	Thickness
	Wt% of Mo	Wt% of TiC	Wt% of Al	Wt% of Mo	Wt% of Ti	$VHN_{(200g)}$	(μm)
A	100	-	80	20	-	230	240
Bb	50	50	37	20	43	430	180
Cc	40	60	27	20	52	660	200
Dd	30	70	26	17	57	750	200
TiC6	-	100	4	-	96	950	240

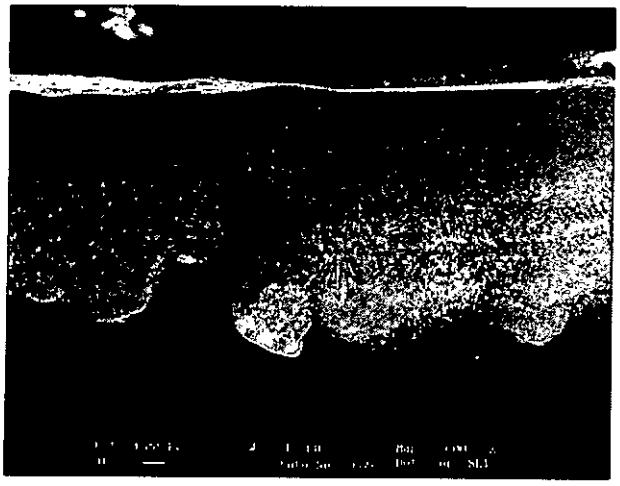

Figure 4.26a Cross-section of specimen A, layer clad with 100% Mo pre-placing powder.

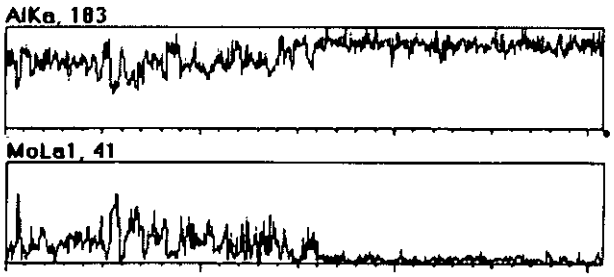

Figure 4.26b EDX line scan across the clad layer of specimen A.

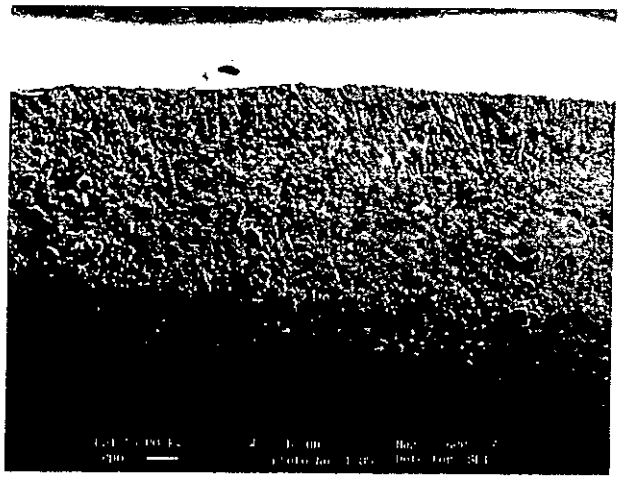

Figure 4.27a Cross-section of specimen Bb, layer clad with 50% Mo and 50% TiC powder.

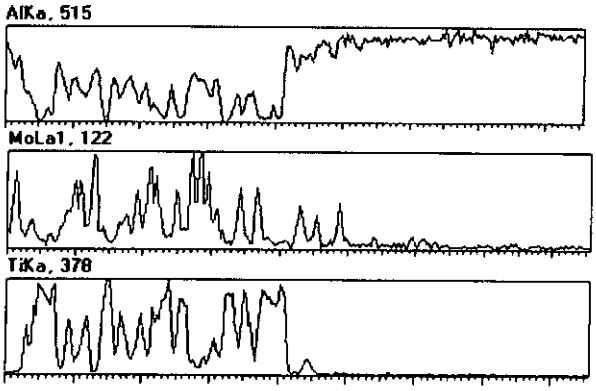

Figure 4.27b EDX line scan across the clad layer of specimen Bb.

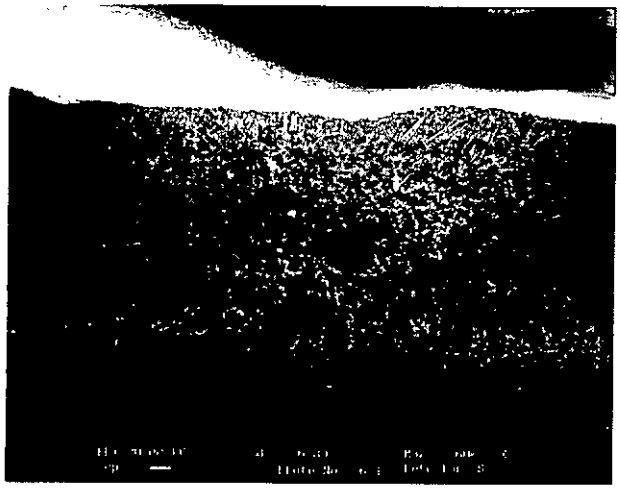

Figure 4.28a Cross-section of specimen Cc, layer clad with 40% Mo and 60% TiC powder.

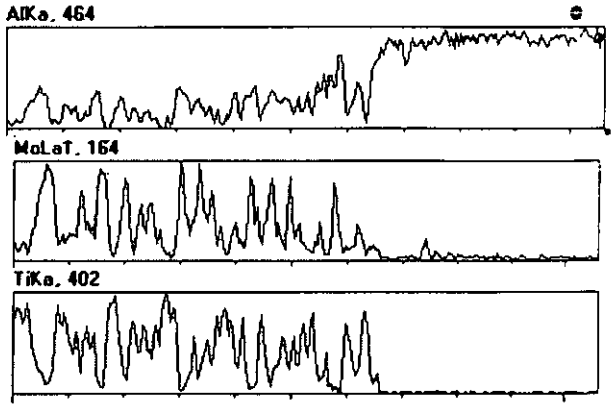

Figure 4.28b EDX line scan across the clad layer of specimen Cc.

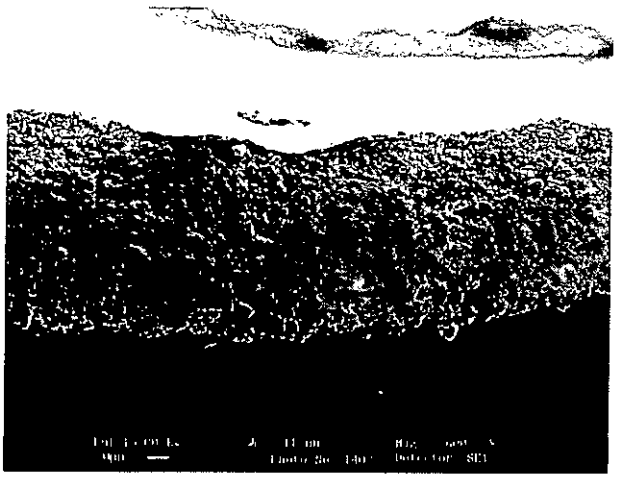

Figure 4.29a Cross-section of specimen Dd, layer clad with 30% Mo and 70% TiC powder.

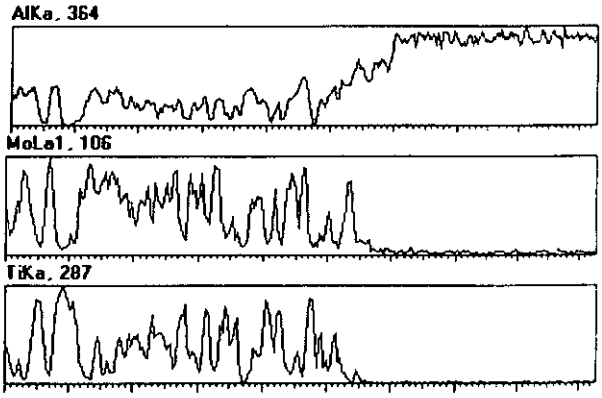

Figure 4.29b EDX line scan across the clad layer of specimen Dd.

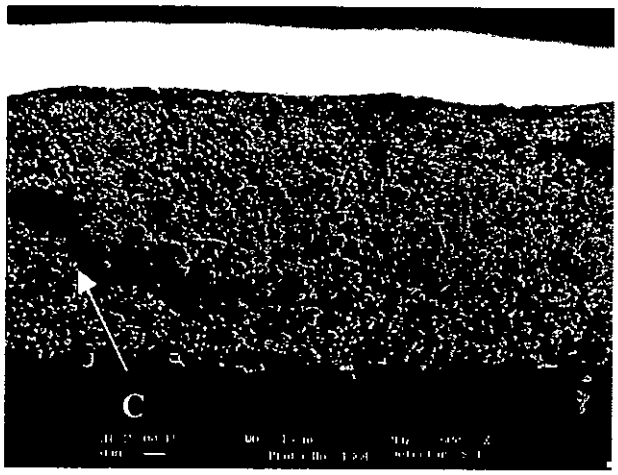

Figure 4.30a Cross-section of specimen TiC6, layer clad with 100% TiC pasting powder.

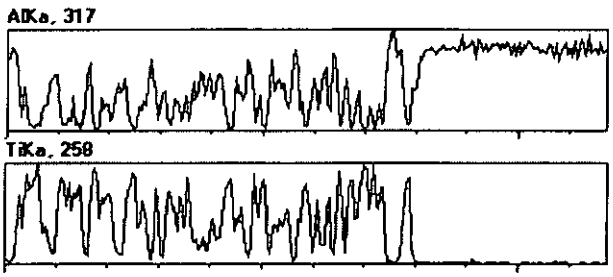

Figure 4.30b EDX line scan across the clad layer of specimen TiC6.

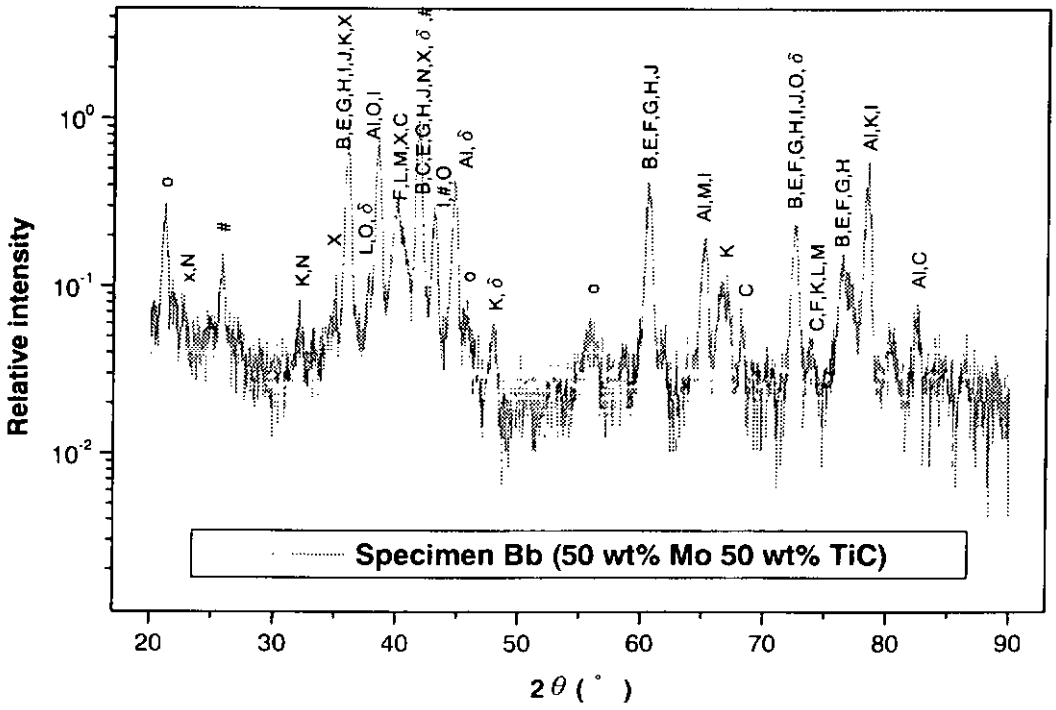

Figure 4.31a X-ray diffraction spectra of laser clad specimen Bb.

Al=Al, o =Al_5Mo ; x = $Al_{17}Mo_4$; # = $Al_{22}Mo_5$; δ = $Al_{22}Mo$, B = TiC, C = $TiAl_3$, D = Ti_3Al, E = Ti_8C_5, F = Ti_3SiC_2, G = $Ti_6C_{5.75}$, H = $Ti_{5.75}C_{3.72}$, I = $(Mo_{0.54}Ti_{0.46})C$, J = $Ti_{0.98}Mo_{0.02}C_{0.6}$, K = MoC, L = Mo_2C , M = $AlMoTi_2$, N = Al_2Mo_3C

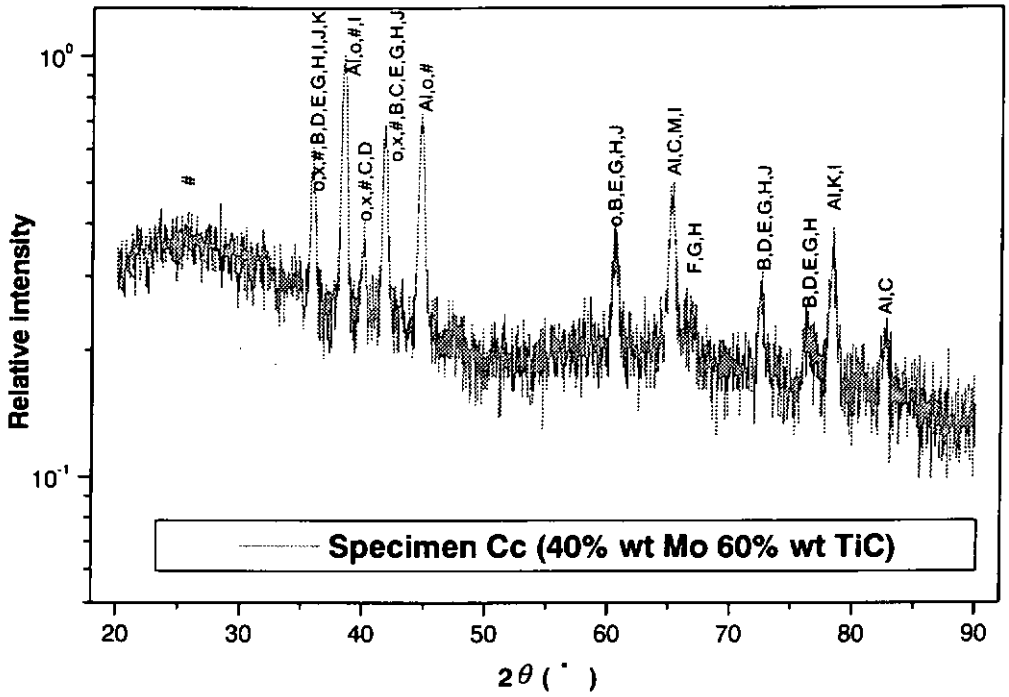

Figure 4.31b X-ray diffraction spectra of laser clad specimen Cc.

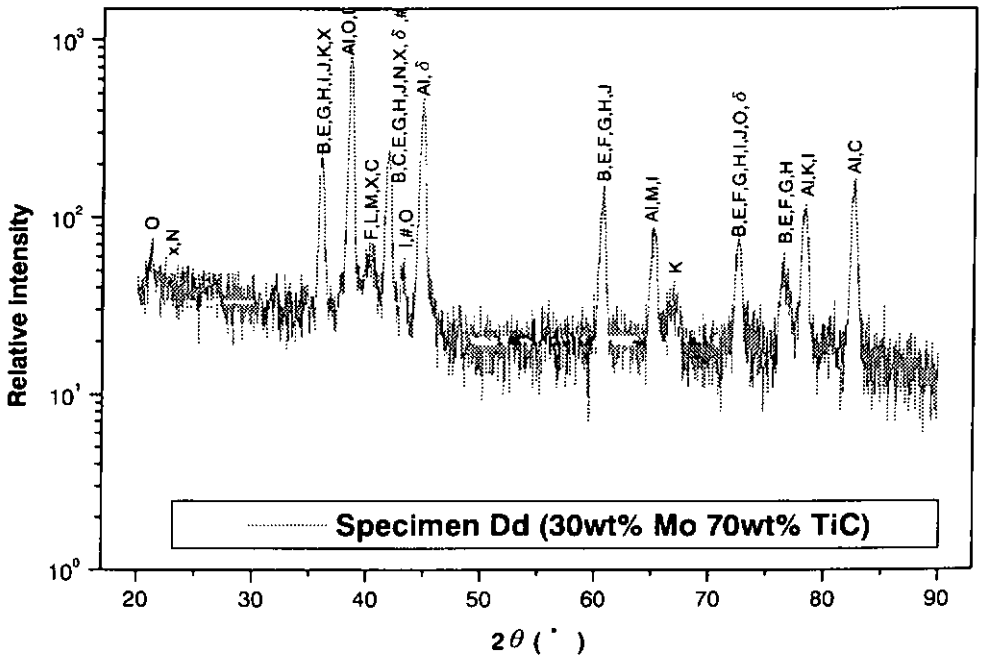

Figure 4.31c X-ray diffraction spectra of laser clad specimen Dd.

Al=Al, o =Al_5Mo ; x = $Al_{17}Mo_4$; # = $Al_{22}Mo_5$; δ = $Al_{22}Mo$, B = TiC, C = $TiAl_3$, D = Ti_3Al, E = Ti_8C_5, F = Ti_3SiC_2, G = $Ti_6C_{5.75}$, H = $Ti_{5.75}C_{3.72}$, I = $(Mo_{0.54}Ti_{0.46})C$, J = $Ti_{0.98}Mo_{0.02}C_{0.6}$, K = MoC, L = Mo_2C , M = $AlMoTi_2$, N = Al_2Mo_3C

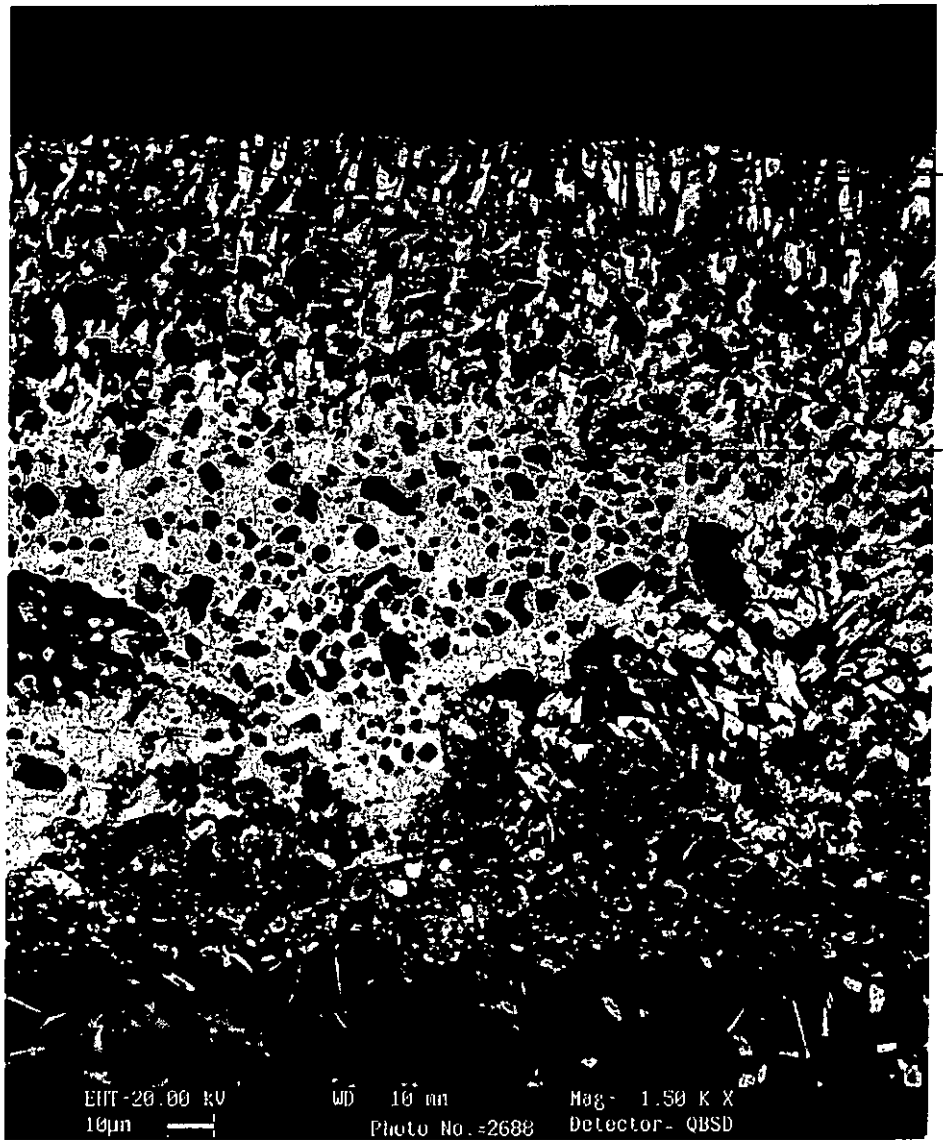

Figure 4.32a Distribution of the Mo/TiC clad layer in specimen Cc.

Table 4.7 Composition of the grey and white phases in Figure 4.32d. (carbon was not detected)

	Al wt%	Mo wt%	Si wt%	Ti wt%
White color phase	8.24	88.16	0.22	3.38
Grey color phase	28.11	62.44	0.64	8.81
Dark-grey color particulate	0	0	0	100

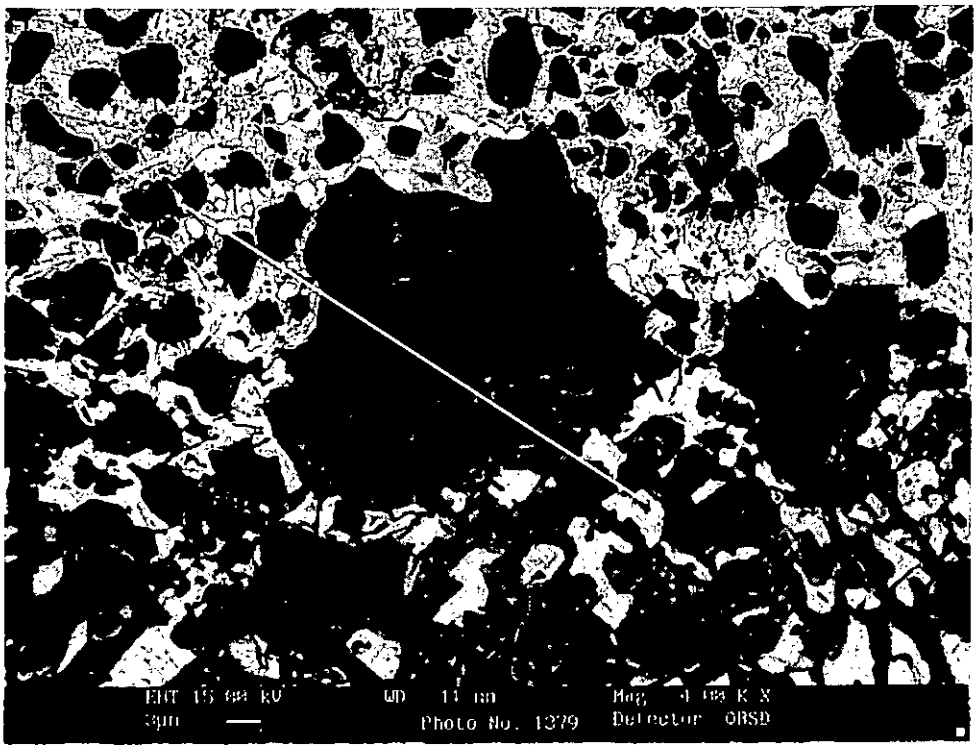

Figure 4.32b Dissociation behaviors of TiC particles in specimen Cc.

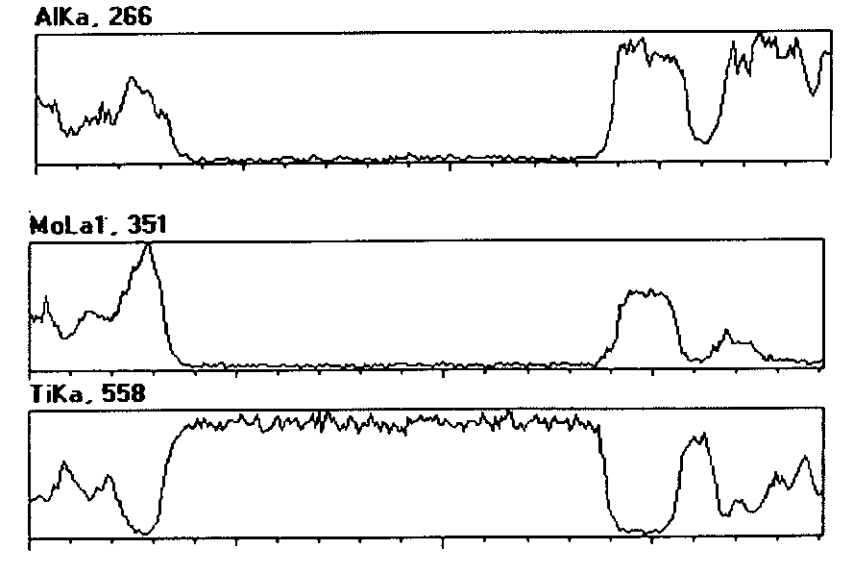

Figure 4.32c EDX line scan of Figure 4.32b.

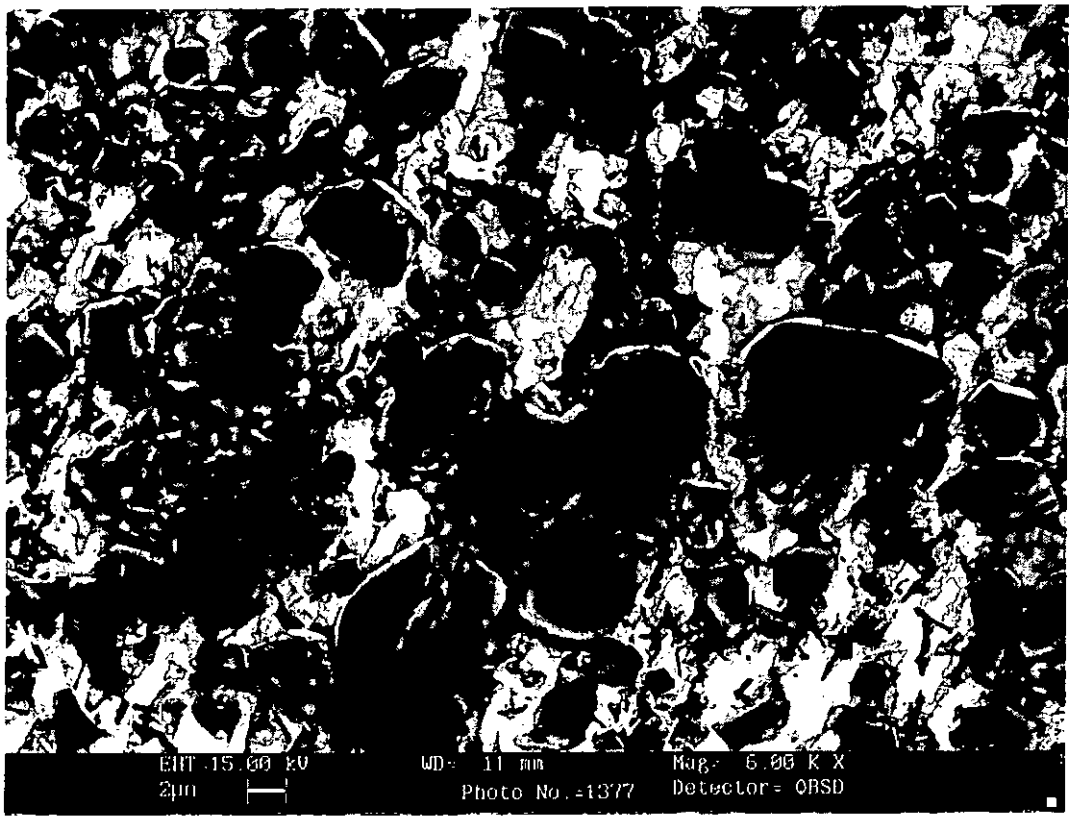

Figure 4.32d Higher magnification of specimen Cc (zone B of Figure 4.32a).

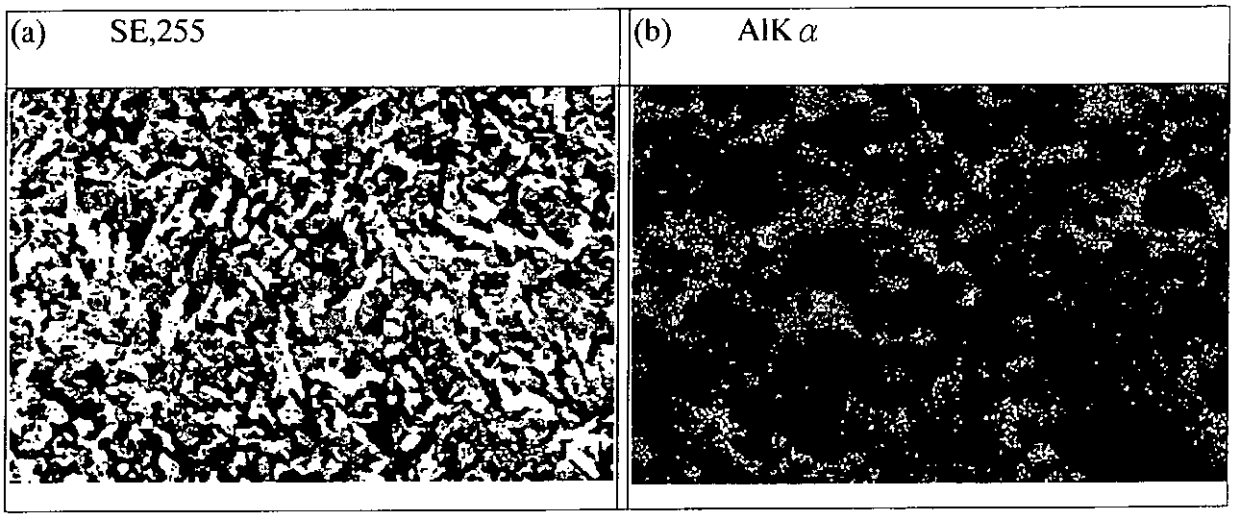

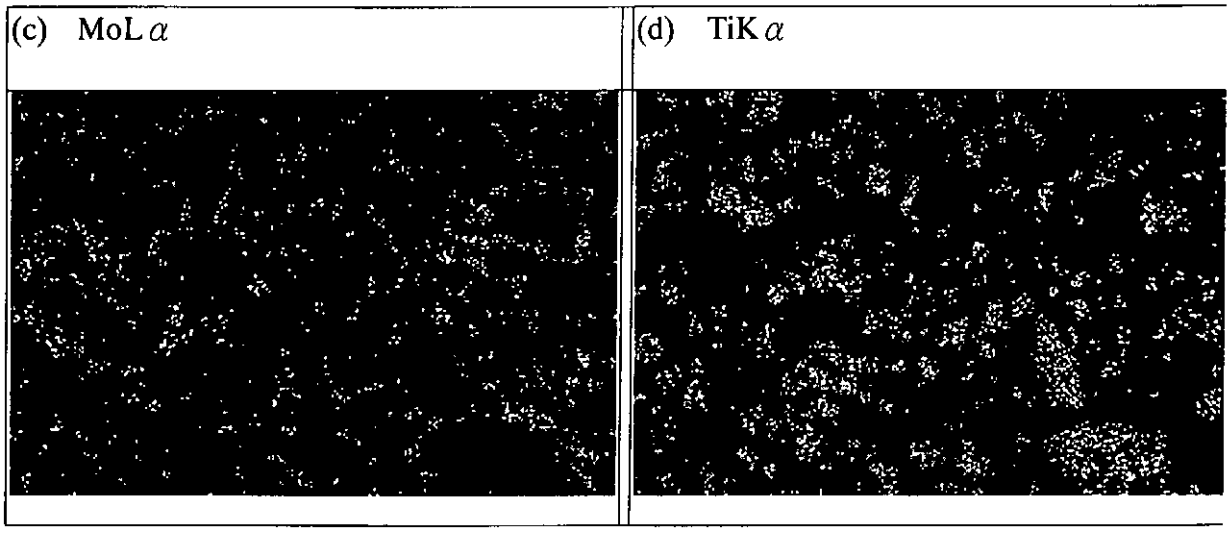

Figure 4.33a-d Distribution of Mo/TiC particles in the melt pool under SEM mapping examination of specimen Bb.

4.7 OTHER SYSTEMS STUDIED

WC, TiC, Mo laser cladding systems were studied at the initial stage and found that all of these could form a good clad layer with good integrity of bonding between the surface layer. Then Mo/WC and Mo/TiC were studied for the fabrication of MMC layer. In this section, some preliminary studies on Si_3N_4 , Mo/ Si_3N_4 , TiC/ Si_3N_4 have also been examined.

4.7.1 LASER CLADDING OF Si_3N_4 ON ALUMINUM ALLOY AA6061

The thickness of the coatings studied was in the range of 0.1 mm and 0.2 mm thick. Process parameters of 1-1.5 kW laser power, 8-20 mm/s scanning speed and 3 mm beam diameter were used in order to achieve the pre-placing 100% Si_3N_4 laser-clad layer. Laser

cladding of Si_3N_4 on Al alloy was found to be difficult to form a good layer without porosity or cracking. From the study of Miyamoto [55], the temperature at the laser irradiated region was found to be higher than 2000 K, which is very close to the melting point of Si_3N_4 (2273 K). Under laser irradiation, Si_3N_4 is easily dissociated into Si and N. The release of N_2 gas causes a lot of porosity on the surface of the clad layer. From this study, it was found that Si_3N_4 is not a good cladding material for Al alloy.

(a) Thickness of Si_3N_4 coating

For 0.1 mm thick pre-placed layer, the Si_3N_4 is too thin to form a clad layer on the surface of Al alloy. Once the laser energy irradiated this thin layer of Si_3N_4 , Si_3N_4 particles decomposed into Si and N instantly and it is no longer able to form a successful clad layer onto the Al alloy surface.

For 0.2 mm thick pre-placed layer, all of the specimens show a lot of small hole on the surface and poor surface roughness. Because of the excessive melting of the substrate during the process, the surface has undergone vigorous melting and resulted in poor surface roughness and porosity. Figure 4.34 shows the surface appearance of specimen S8 has 100% Si_3N_4 pre-placing powder with 0.2mm clad thickness on Al alloy AA6061.

(b) Characteristic study of specimen S8

Figure 4.35a shows the uneven distribution of Si_3N_4 particles on specimen S8. Figure 4.35 b is the line scan pattern of Figure 4.35 a. A lot of cracks occur in the clad layer. Si_3N_4 particles have high tendency to form clusters. Cluster formation may cause inhomogeneous distribution in the clad layer. As in MMC reinforcement, ceramic plays the role as reinforced phase and improves the hardness of the clad layer. However, the clad

layer still needs tough phase to improve its ductility. Once the clad layer solidified and contracted, the residual stress was induced. So, sufficient amount of Al was required to improve its toughness and prevent cracking in laser-clad layer. Moreover, cracking of the clad layer is also related to some extent to the difference in physical properties between the cladding layer and the substrate. Zone Z in Figure 4.35 b is the crack region of specimen S8. A sudden drop of aluminum content in the zone A of the line scan diagram. It can be easily observed that the sudden increase of the Si content at the interface may indicate the accumulation of the Si_3N_4 , which causes cracking. Table 4.8 shows the composition distribution of specimen S8. High dilution rate occurs on this process. The silicon content in the substrate is about 1 wt%, but in the clad layer is 8.19 wt %. This proved that some of the Si_3N_4 particles have dissociated into the clad layer and some of the Si_3N_4 left in the alloyed zone too.

Figure 4.36a shows the SEM micrograph of the specimen S8. Figure 4.36b and 4.36c are the cross-section appearance of specimen S8 at a higher magnification. Figure 4.36b is the matrix region in which the cellular structure formed. The cellular structure mainly composed of AlN and Al-Si. The hardness in zone SS is 245Hv. Some white color grain and flower like structure grow in-between the grain boundary of the cellular structure. The wt% of Si in this white color grain increases to 14.5 and 15.6. The results show that some of the Si_3N_4 particles trapped in-between the cellular gain before they solidified. Figure 4.36c is the magnification of zone S in Figure 4.36a, in which the white color gain and grey color grain may be the Si_3N_4 clusters and Al-Si-N intermetallic compounds respectively. The hardness value in this zone is 450Hv. Typical X-ray diffractograms show that Al, AlN (f.c.c.), AlN(H), Si_3N_4 phases were formed in Figure 4.37.

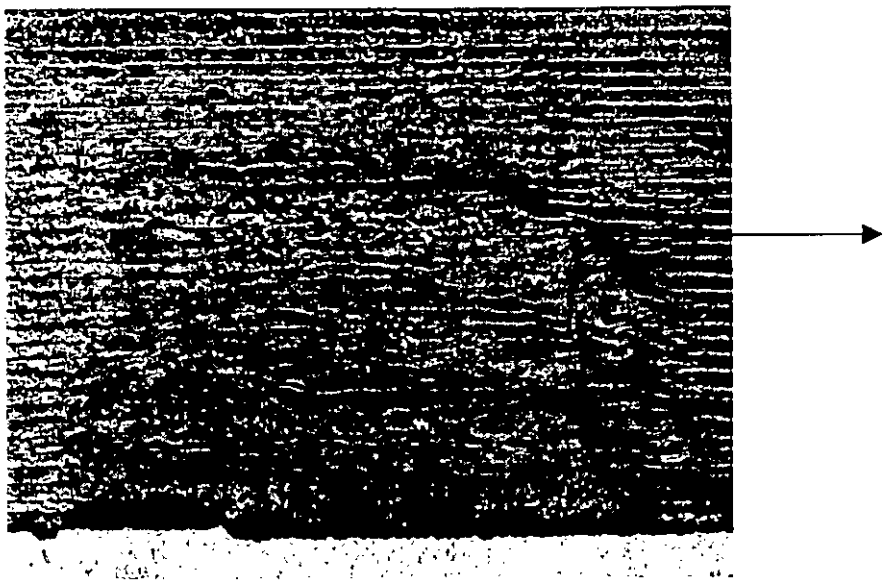

Figure 4.34 The surface appearance of 100% Si_3N_4 (pre-placing powder) on Al alloy AA6061.

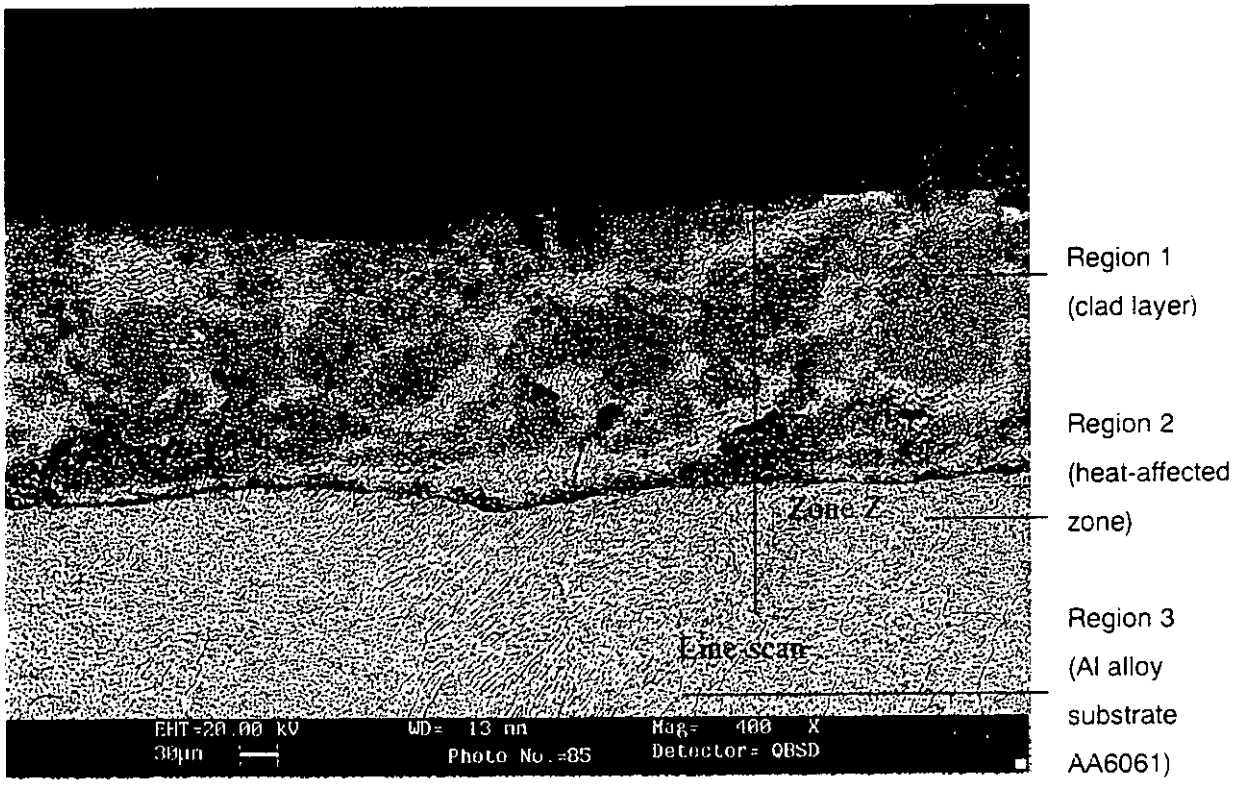

Figure 4.35a The clad layer of specimen S8 with 100% Si_3N_4 pasting powder.

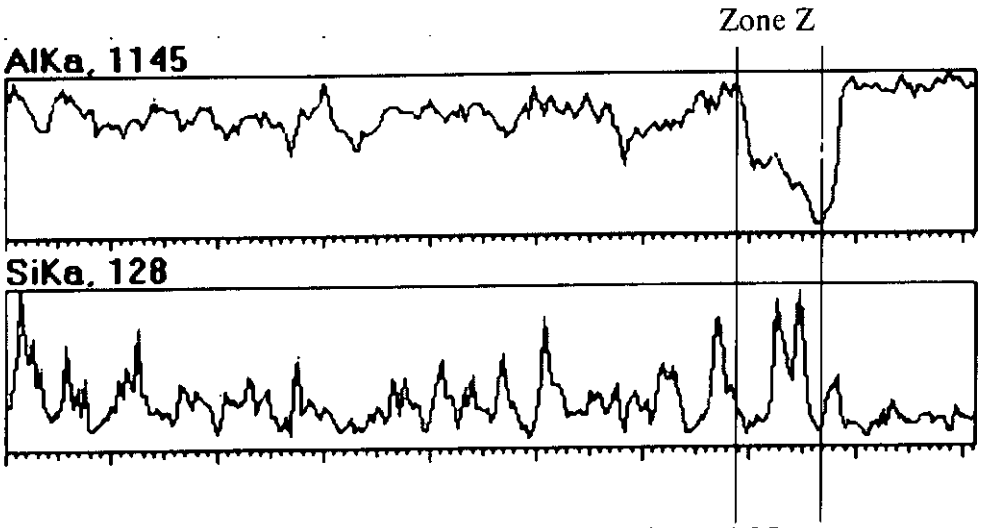

Figure 4.35 b EDX line scan of Figure 4.35a.

Table 4.8 The composition distribution of the clad layer

	Al wt %	Si wt%	N wt%	O wt%
Region 1 (clad layer)	84.1	8.2	3.7	4
Region 2 (heat-affected zone)	90.9	2.9	3.0	3.2
Region 3 (Al alloy substrate)	91.1	3.6	2.7	2.6

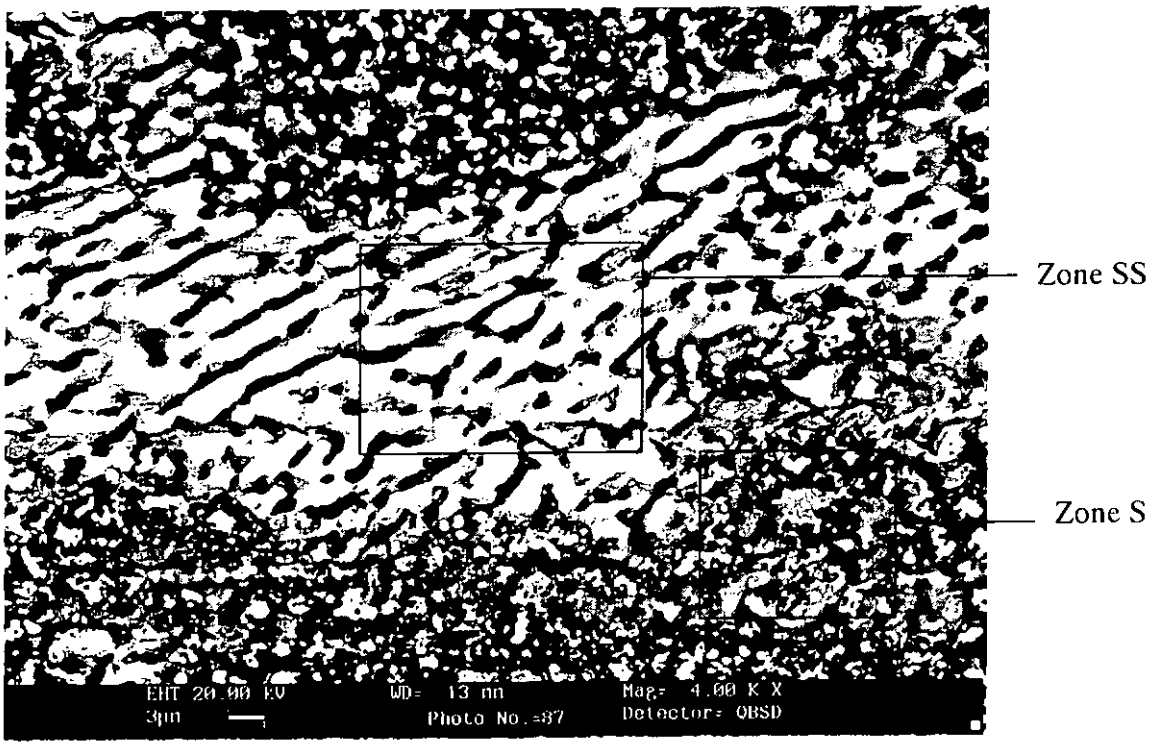

Figure 4.36a The microstructure of specimen S8.

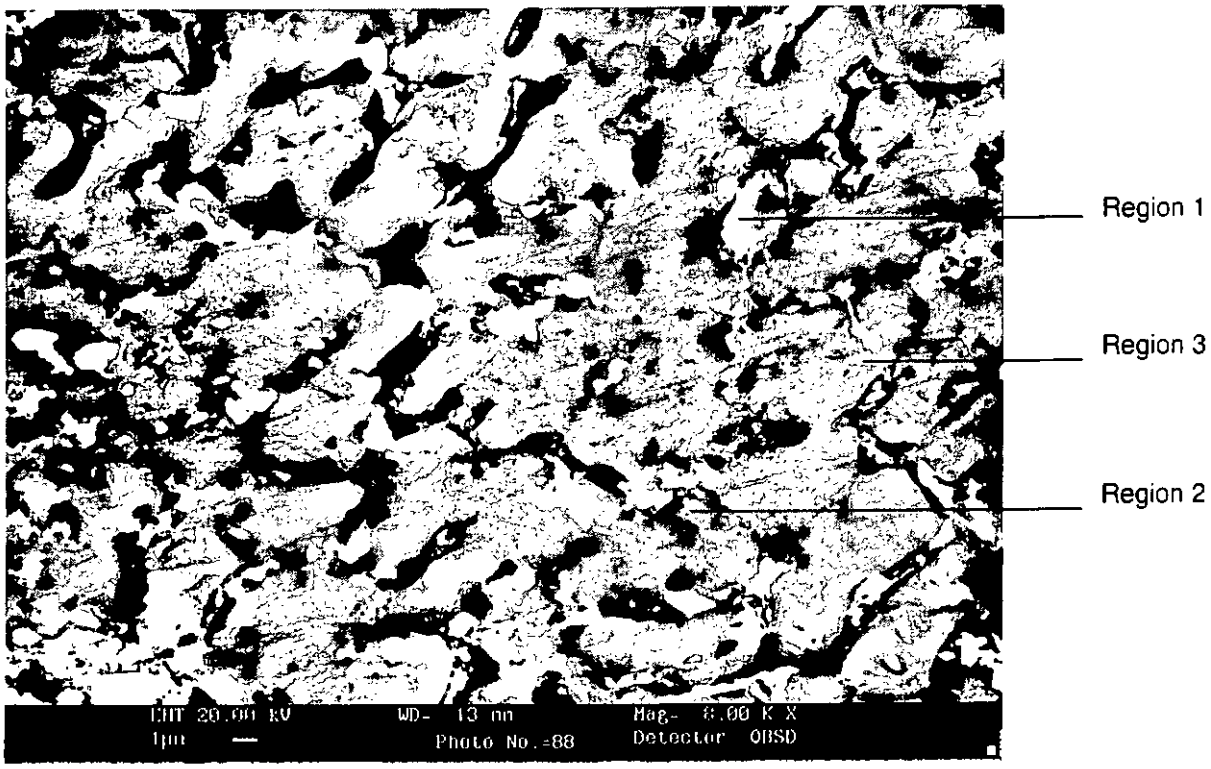

Figure 4.36b The cellular structure of zone SS in the 100% pre-placing Si_3N_4 cladding.

Table 4.9 The composition analysis of Figure 4.35b

	Al wt %	Si wt%	N wt%	O wt%
Region 1 (white color)	78.7	14.5	3.3	3.5
Region 2 (white flower)	75.6	18.6	2.8	3
Region 3 (grey color)	87.8	7.5	2.7	2

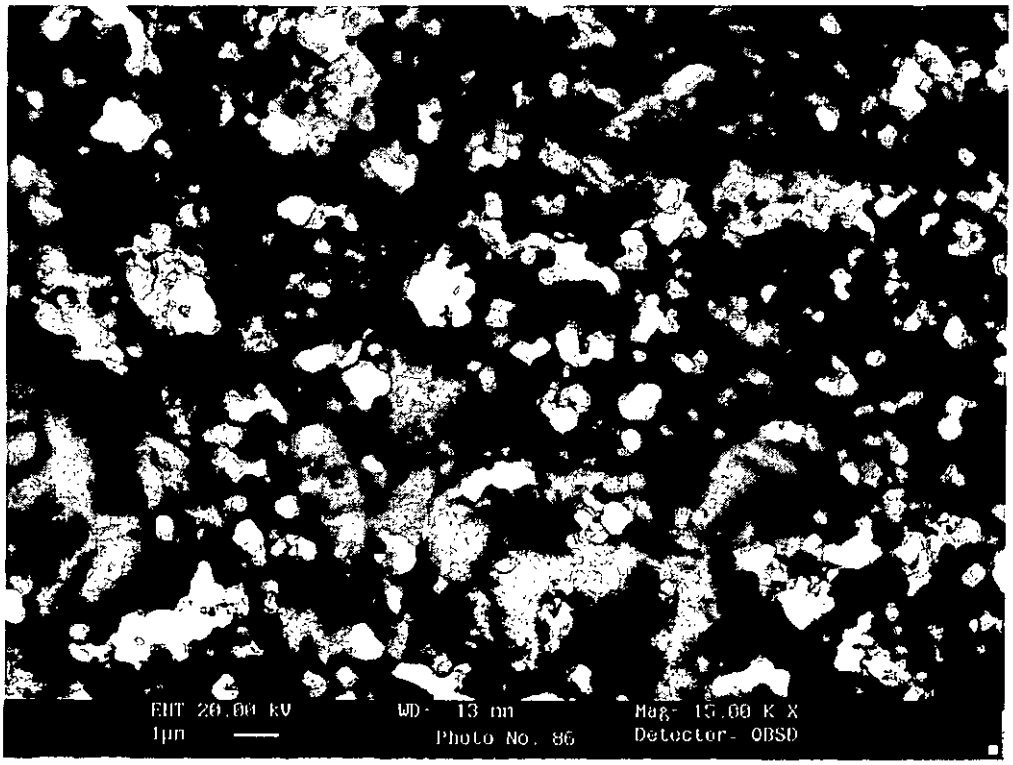

Figure 4.36c SEM micrograph of zone S in Figure 4.36a.

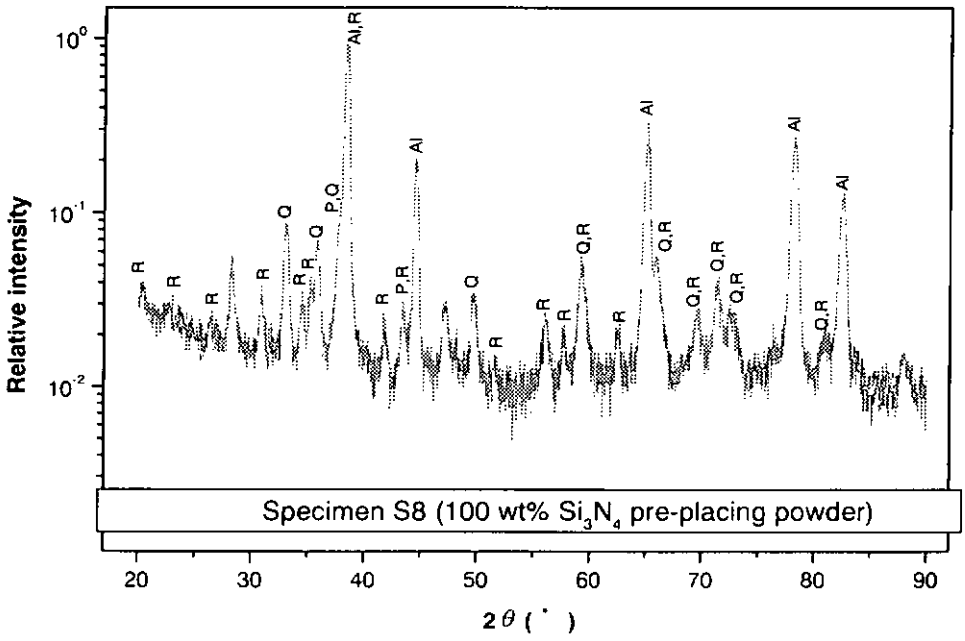

Al = Al, P = AlN (fcc), Q = AlN (H), R = Si_3N_4

Figure 4.37 X-ray diffraction spectra of laser clad specimen S8.

4.7.2 *LASER CLADDING OF Mo/ Si_3N_4 ON ALUMINUM ALLOY AA6061*

As shown in Section 4.7.1, it was found that Si_3N_4 is not a good cladding material for Al alloys. In this section, powders of 50wt % Mo and 50wt % Si_3N_4 ceramic were mixed and pasted on Al alloy. The thickness of the paste was approximately 0.2 mm thick. Process parameters of 1.5 kW laser power, 14 mm/s scanning speed and 3 mm beam diameter were used. The results show that Mo/Si_3N_4 is also a difficult-to-clad system on Al alloy.

Figure 4.38 shows the cross section of laser clad specimen SA10, with 50%Mo 50%Si_3N_4 pre-placed powder. The alloyed zone is about 900 μm. It was found that the melt tracks were quite homogeneous and a good degree of mixing was achieved after the laser treatment. Composition profile of specimen SA10, measured by EDAX, is shown in Figure 4.39a. It seems that the concentration of Mo, Al and Si are evenly distributed through the alloyed zone. It is about 20wt% of Mo at the top of the alloyed layer and then it drops to 3 wt% at 0.2 mm away from the surface. Figure 4.39b shows some un-melted Mo in the alloyed layer. Because the equilibrium solubility of Mo in Al is very low (~0.08 wt%), Mo is quickly rejected by the solidifying liquid and producing large constitutional supercooling and the dendritic structure nucleates. The concentration of alloyed layer is evenly distributed. The presence of intermetallic particles at the fusion boundary was also observed (Figure 4.39c). The concentration of Si keeps at around 4 – 6 wt%. This means that some of the Si_3N_4 has dissolved into the alloyed zone, as the Al alloy AA6061-T657 substrate only contains about 1wt% Si.

From the hardness measurement of specimen SA10, the hardness values are almost uniform in the alloyed zone and slightly higher than the Al substrate (Figure 4.40). The

hardness value of the substrate is about 75 Hv and the alloyed zone is about 114 Hv. It means that small amount of Si and Mo were dissolved and formed solid solution with Al in the alloyed layer, which made its hardness value higher than the substrate. Figure 4.40a shows the columnar dendritic grains, which is about 114 Hv. The columnar dendritic grain starts to grow at the fusion boundary along the general direction of heat flow. The columnar growth was epitaxial, with some grain boundaries being continuous, from the HAZ in the substrate, through the melt zone to the free surface (Figure 4.41a & b). From the study of McMahon and Vilar [87], cooling rates were estimated to be of the order of 10^6 K/s during solidification adjacent to the fusion boundary and increased to the order of 10^7 K/s just below the surface.

Some un-melted Mo cluster was dragged into the melt pool as shown in Figure 4.42a & b. The melting point of Mo is very high and sometimes the laser energy may not be large enough to melt it completely. Also, it may not have sufficient time in the melt for the Mo to melted completely. The hardness of this un-melted Mo cluster is about 850 Hv. Figure 4.43 is an X-ray diffraction diagram of the specimen SA10, which laser alloyed with 50% Mo 50% Si_3N_4 powder paste.

In this figure, it seems that there are some Al_xMo_y phases in the alloyed zone: Al_5Mo, $Al_{17}Mo_4$, $Al_{22}Mo_5$, $Al_{22}Mo$ and Si_3N_4. The result agrees to the result of SEM analysis.

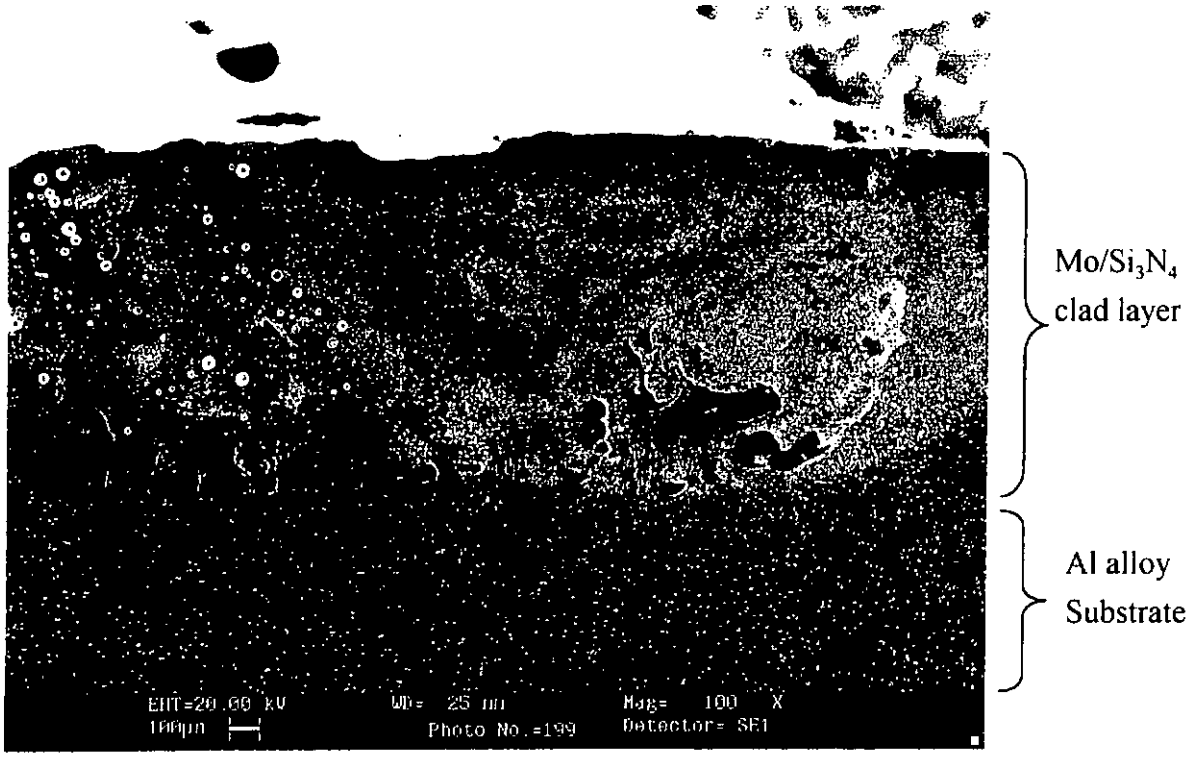

Figure 4.38 Cross-section of specimen SA10, layer alloyed with 50% Mo and 50% Si_3N_4 powder.

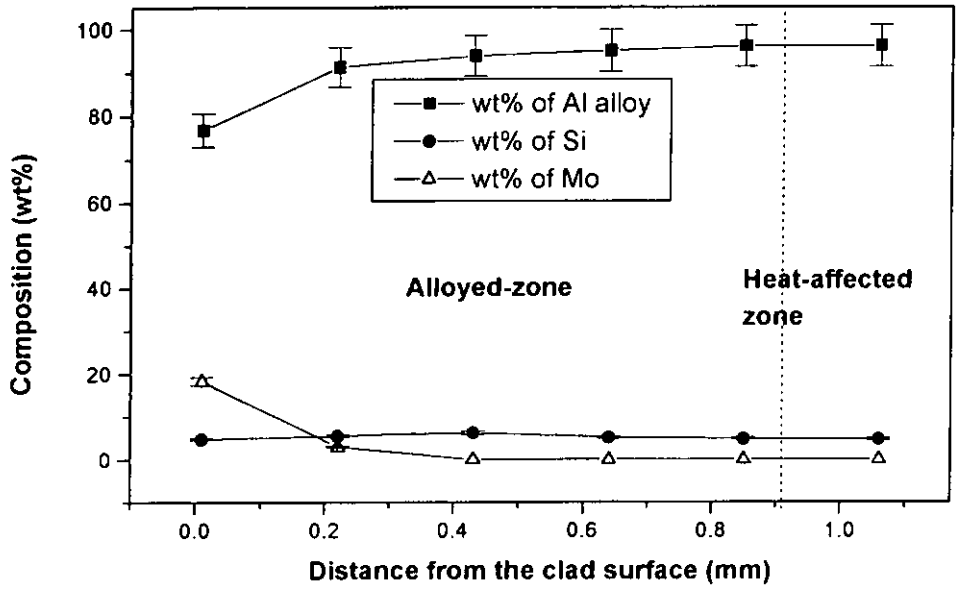

Figure 4.39a EDX composition analysis of specimen SA10.

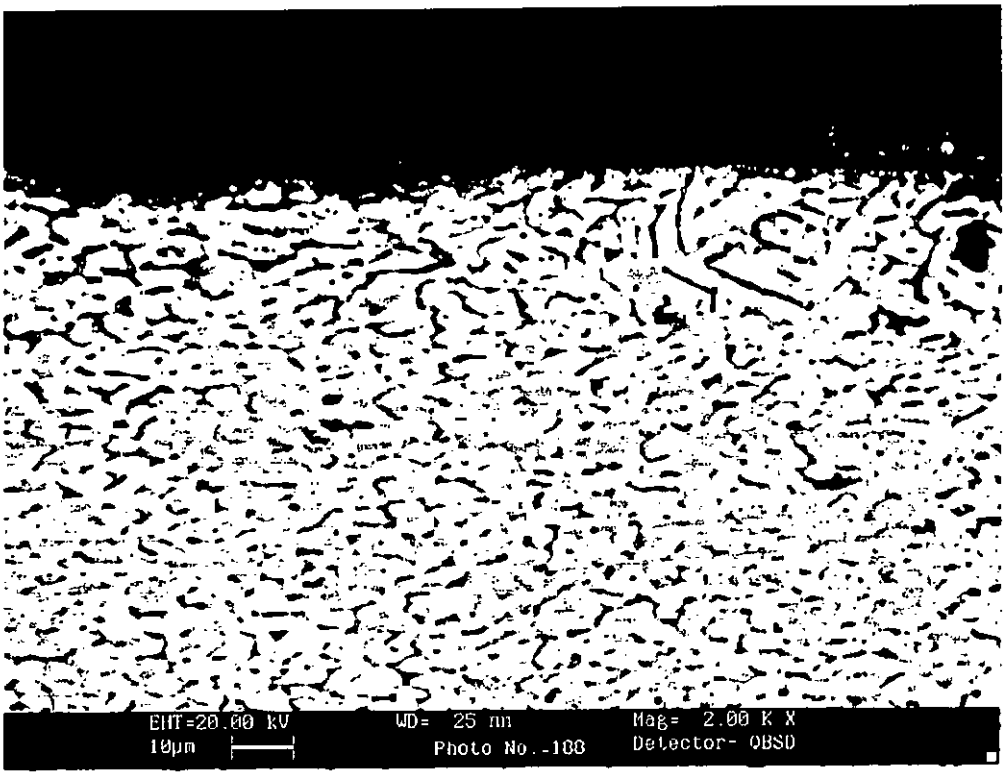

Figure 4.39 b Black scattered SEM micrograph showing the alloyed layer, in which the white color spots are some un-melted Mo.

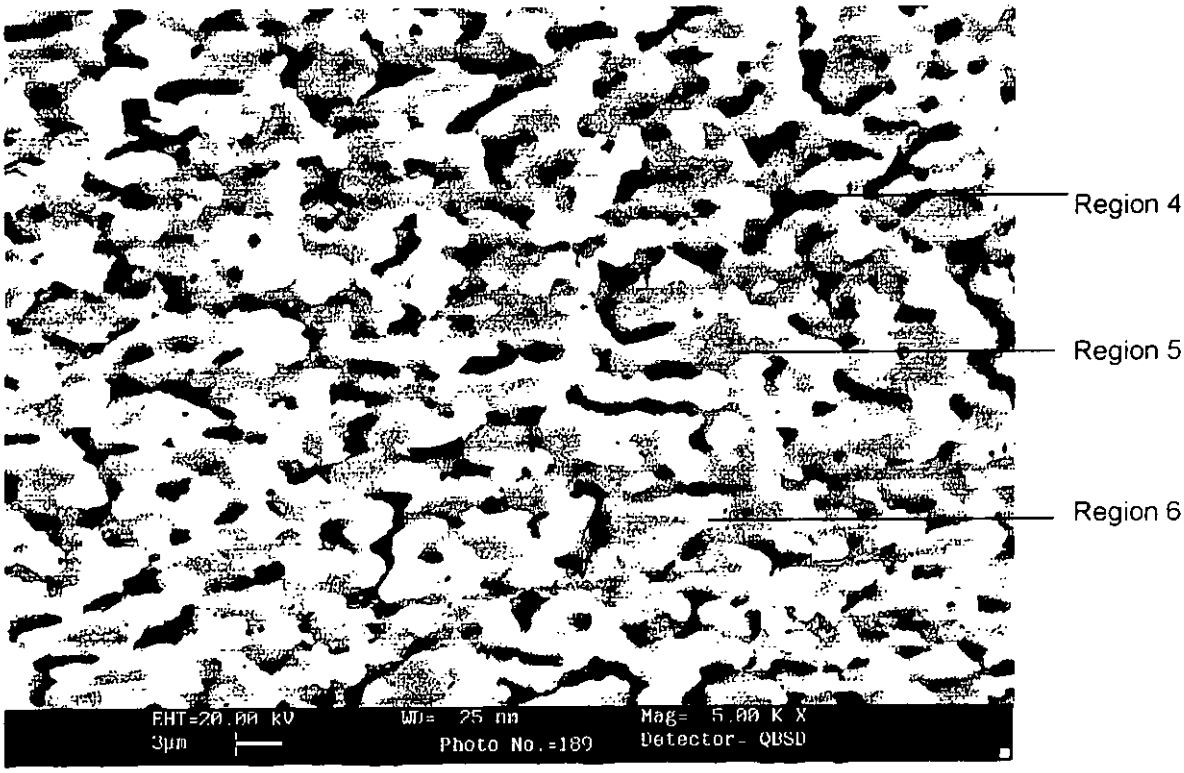

Figure 4.39c Black scattered SEM micrograph shows the higher magnification of Figure 4.39b.

Table 4.10 The composition analysis of the alloyed region in Figure 4.39c

	Al wt %	Si wt%	Mo wt%
Dark line (Region 6)	95.05	3.02	1.57
Grey color grain (Region 6)	95.86	3.03	1.02
White color grain (Region 6)	73.96	3.29	22.42

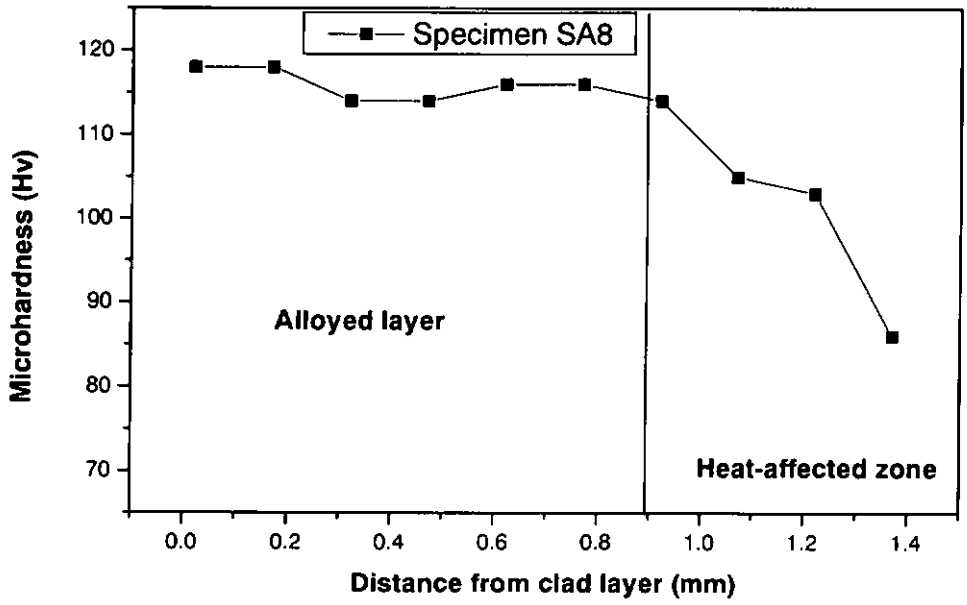

Figure 4.40 The hardness distribution along the specimen SA10.

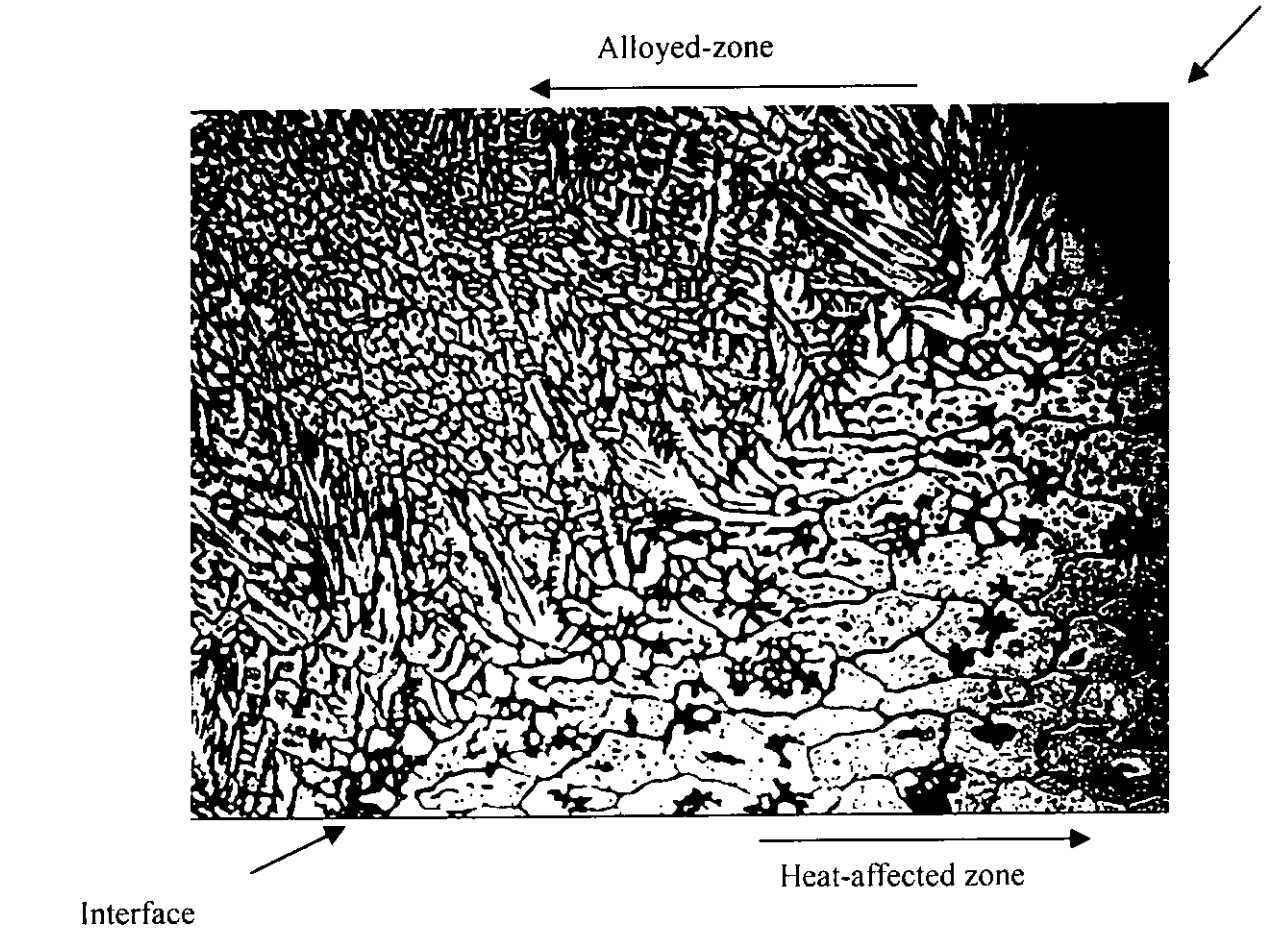

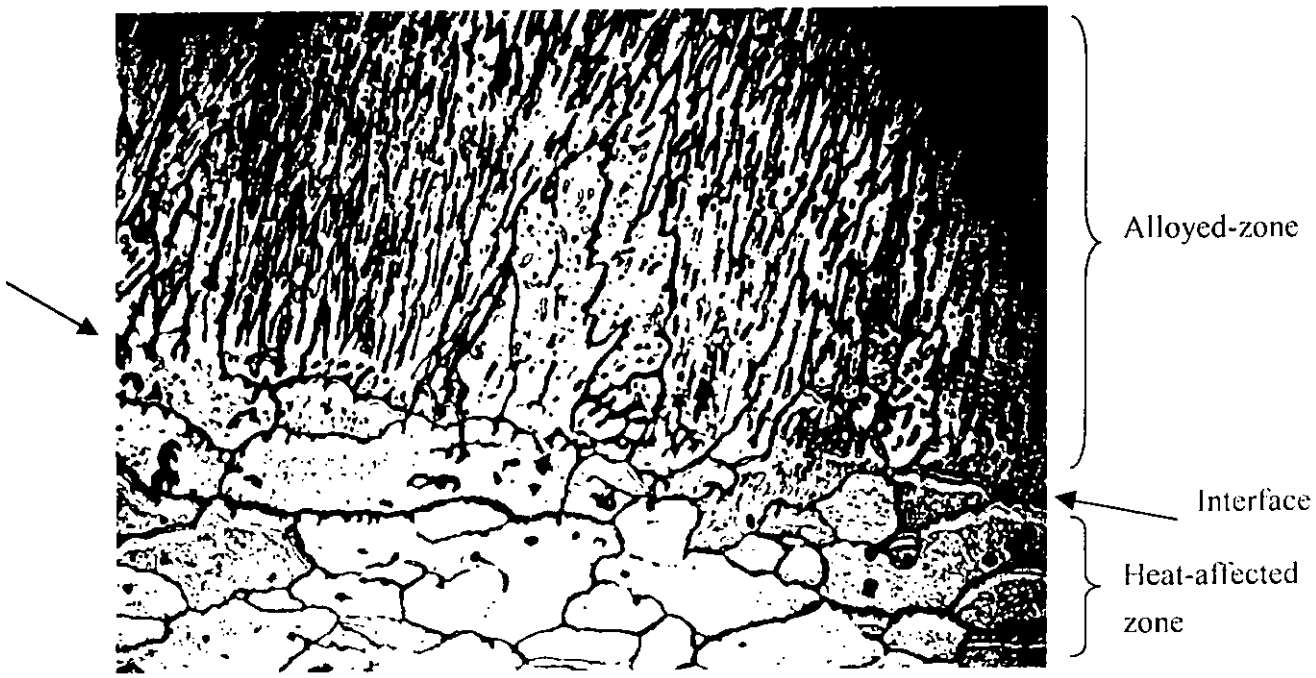

Figure 4.41 a & b The optical microscope of gain structure in alloyed zone.

Figure 4.42a The un-melted Mo cluster.

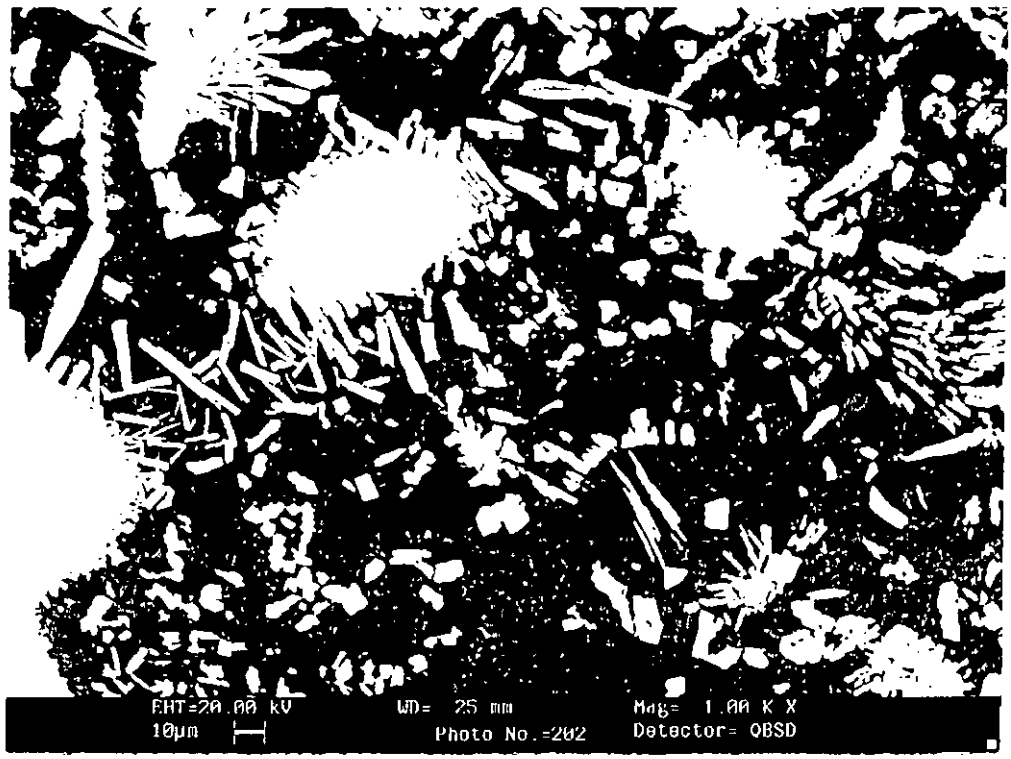

Figure 4.42 b The un-melted Mo and Al-Si-Mo intermetallic compounds in Mo/ Si_3N_4 alloyed layer.

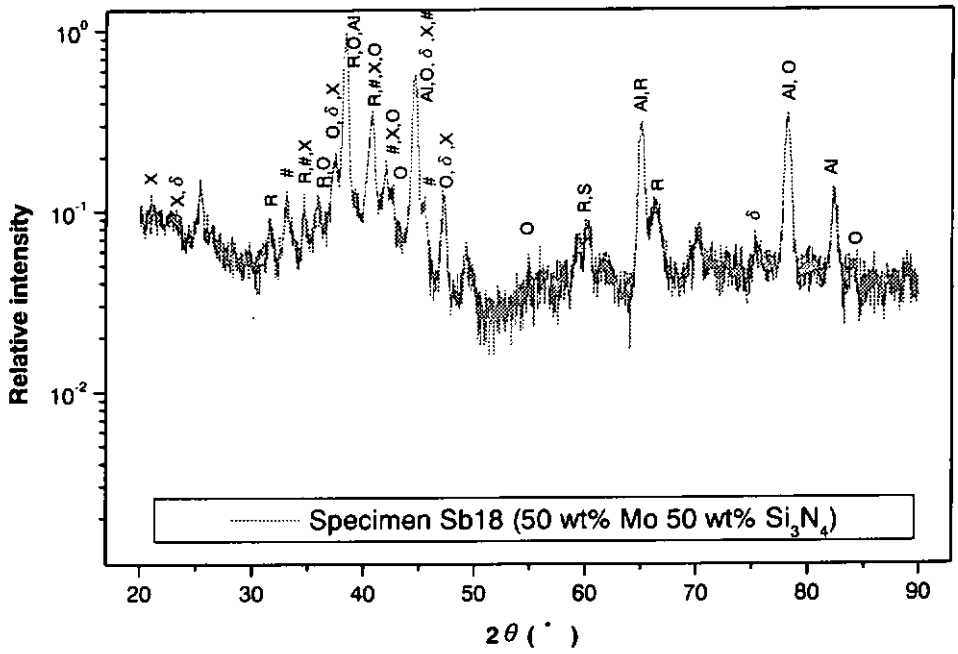

o =Al_5Mo ; x = $Al_{17}Mo_4$; # = $Al_{22}Mo_5$; δ = $Al_{22}Mo$, R = Si_3N_4

Figure 4.43 X-ray diffraction spectra of laser clad specimen SA 10.

4.7.3 LASER CLADDING OF TiC / Si_3N_4 ON ALUMINUM ALLOY AA6061

Laser cladding technique can produce in-situ novel surface with extended solid solution and without being restricted by equilibrium phase diagram, because of the rapid heating and cooling in the laser surface modification. A high cooling rate (~10^{60} K/sec) often leads to extension of solubility of the solute atoms, thus producing novel metastable materials. This process is dependent on energy, momentum and mass transport. The mass transport in the laser melted pool is dominated by convection. TiC and Si_3N_4 were chosen as the cladding material in this part of study, because the densities between them are close to each other, TiC is 4904 kgm^{-3} and Si_3N_4 is 3200 kgm^{-3}, so they were appropriate cladding material to produce homogenized clad layer.

This section is the preliminary study of the feasibility of laser cladding 50% TiC 50% Si_3N_4 pre-placing layer on Al alloy AA6061-T651. The thickness of the paste coatings was approximately 0.2 mm thick. Process parameters of 1.1 kW laser power, 17 mm/s scanning speed and 3 mm beam diameter were used.

Because the coating material and the substrate have different physical and mechanical properties, failure of the clad layer is commonly associated with the interfacial bond. In this section of study, the main problem associated with the strength of the clad layer is the occurrence of cracking at the interface (Figure 4.44). Table 4.11 shows the composition distribution of the specimen SA6. The composition of Si and Ti in the clad layer is the ratio of 1:1. Figure 4.45 shows the SEM micrograph of the microstructure of specimen SA6. The hardness of this clad layer is 410 Hv. From the EDAX analysis, the grey color particle (Y) is TiC particle, because 100 wt% Ti was recorded. The other dark grey particle (X) maybe Si_3N_4 particle and some Al-Si-Ti intemetallic compounds. As the concentration of Si

in this region is very high, i.e. it contains almost 91 wt%, this particle is likely to be Si_3N_4. The other minor compositions are 7 wt% Al and 2 wt% Ti and they may be some Al-Ti-Si intermetallic compound.

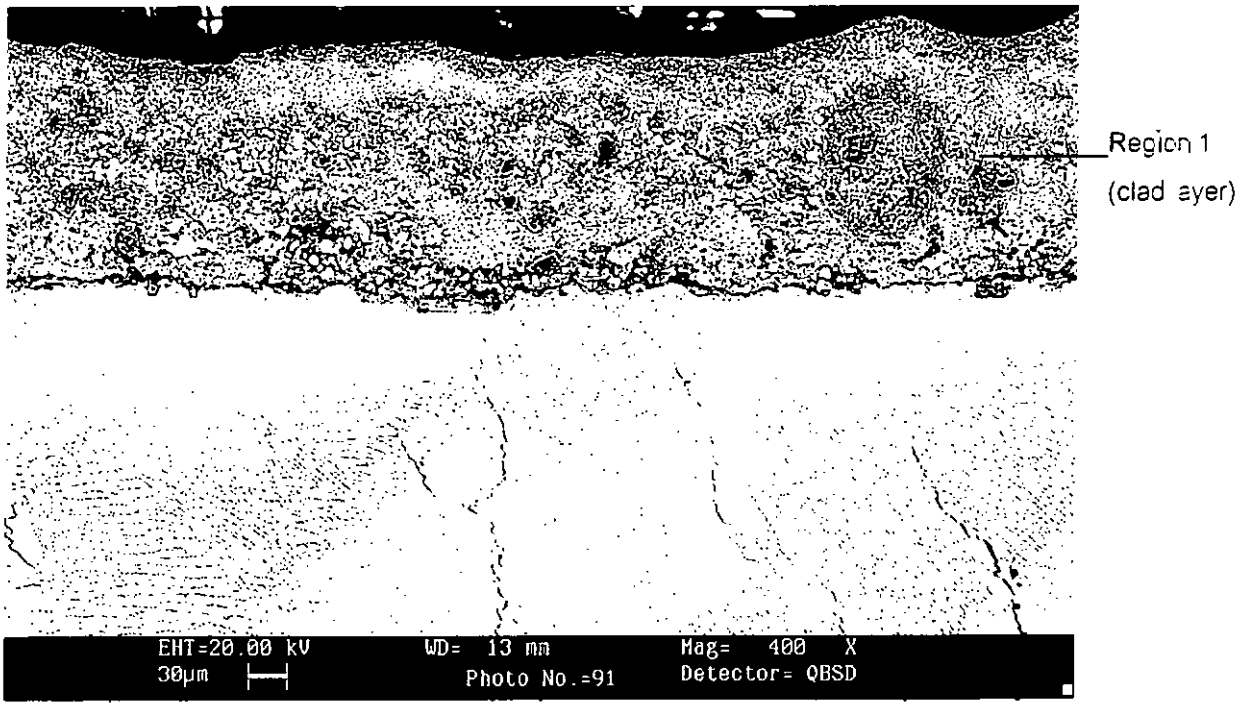

Figure 4.44 Cross-section of specimen SA6, layer alloyed with 50%TiC and 50% Si_3N_4 powder.

Table 4.11 The composition distribution of the clad layer.

	Al wt %	Si wt%	Ti wt%	N wt%	O wt%
Region 1 (clad layer)	57.74	19.94	18.59	0.73	3

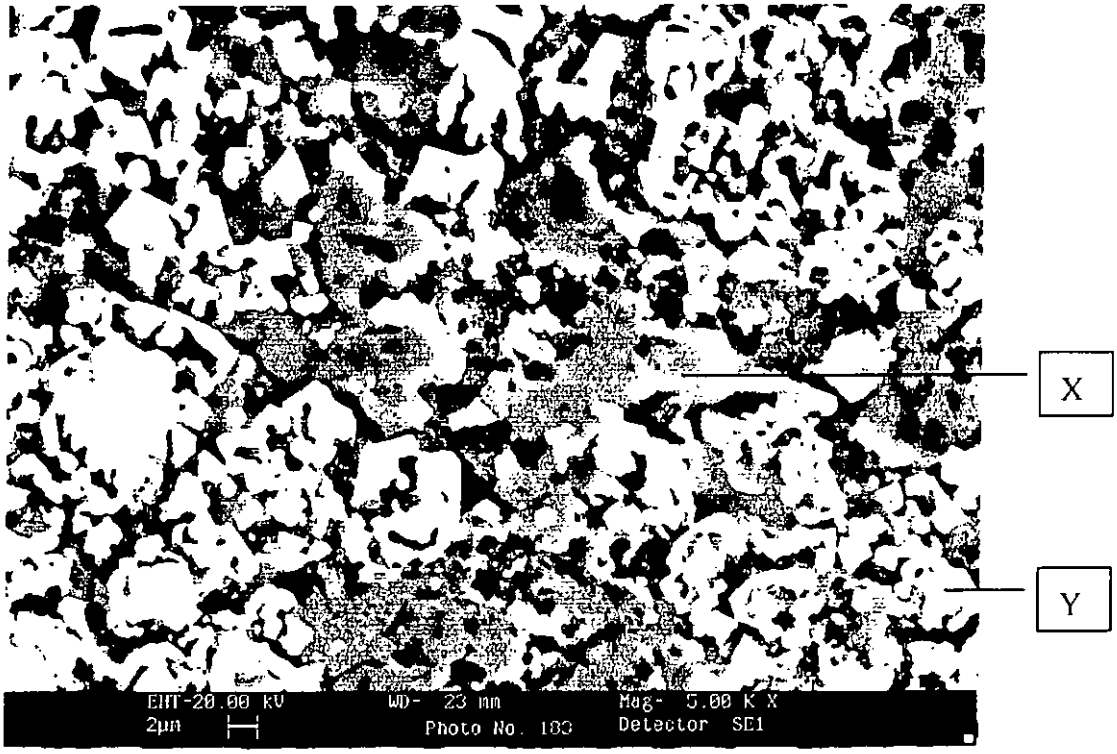

Figure 4.45 SEM micrograph of the microstructure of specimen SA6.

Chapter 5

Results and Discussions –

Wear Resistant Properties of the Laser Cladding of MMC on Al Alloy AA6061

5.1 INTRODUCTION

The objective of the present study is to verify the feasibility of MMC claddings as a candidate wear-protective material for various applications, such as the engines or pistons usage. Abrasive wear test for the laser clad WC, TiC, Mo, Mo/WC and Mo/TiC systems were carried out and this chapter will discuss their wear resistance properties.

5.2 WEAR RESISTANCE ANALYSIS OF LASER CLADDING Mo, Mo/WC, WC ON ALUMINUM ALLOY

Table 5.1 shows the average mass loss of aluminum alloy AA6061 and the laser clad specimens. Figure 5.1 shows the mass loss of the as-received alloy and the clad specimens against time of the wear test. The severe wear of the as-received Aluminum alloy AA6061 is characterized by rapid material removal by the abrasive paper. Large metallic debris of the material were being cut away layer by layer. Figure 5.2 shows the average mass loss of the laser clad specimens of Mo4, B, C, D, E and WC 6 using a different scale in the vertical axis. Mass loss for specimen E is about 40 times lower than that of Al alloy AA6061. The reinforcement with WC is efficient in enhancing the wear resistance against the SiC

abrasive paper. Figure 5.2 also indicates that specimens C, D, E and WC6 have similar wear behaviour when WC content exceed 40%. The wear mechanism of such coating is affected by the wear of the metal matrix followed by the pullout of the hard phase. The observed high wear resistance of the clad layer was the combined results of the tough Mo and Al matrix, distribution of the hard WC particles and the good bonding between the WC particles and matrix. Abrasive particles of SiC were not able to plough into the clad matrix because of the existence of the hard phase particles of WC. Actually, the hard WC particles delayed the transition load such that the weight loss of the clad samples was reduced greatly.

Table 5.1 Average mass loss (g) of specimens from the moving pin-on-disc experiment after 1414 m sliding distance (per 5 min test cycle).

Specimen	AA6061 -T651	Mo4 (100% Mo)	B (80%Mo, 20%WC)	C (60%Mo, 40%WC)	D (40%Mo, 60%WC)	E (20%Mo, 80%WC)	WC 6 (100% WC)
Average mass loss (g)	0.1982	0.0281	0.0171	0.0047	0.0053	0.0031	0.0029

Since this is a kind of pin-on disc abrasive wear test, the load carrying capacity of the hard-phase structure is an important factor for the improvement of wear resistance. In the experiment, 300g loading was used. In the case of Al alloy, loading is initially and mostly applied onto the abrasive particles because of the deformation of the soft surface Al. The SiC abrasives are able to plough deeply into the surfaces and causes microcutting. On the other hand, the hard-phase MMC coatings form a load support system that greatly reduces the load applied to the abrasives and limits the micro-cutting process [132].

In order to understand the wear mechanisms of the specimens, the result of the SEM examination of the worn surface were shown in Figure 5.3-5.6. It is clearly shown that

the worn surface of the Al alloy AA6061 (Figure 5.3) was characterized by deep and fairly long continuous grooves, where the material was removed from the surface during wear. Figure 5.4, shows the worn surface of specimen Mo4 which has less cutting grooves than in figure 5.3. Because the hard phases exist in the clad layer, the wear resistance is significantly improved. Figure 5.5 shows that the worn surface of specimen E. Carbide particles and the hard intermetallic phases have high resistance on the microcutting process of the moving SiC abrasive disc, so the wear loss of this specimen is very low. Figure 4.4 clearly shows that a good interfacial bond between the ceramic particles and matrix exists and this can help resist the pull out force on the WC particles. However, the gradual wearing of the matrix by the hard SiC abrasive particles will reduce the holding force of the matrix that exerts on the WC particles. Under the shearing stress that acted on the protruding WC particles, some of the WC particles were torn off from the matrix. Once the WC particle was pulled, those dendrites that grew epitaxially on the WC particles, as shown in figure 4.16 and were torn out together. So, a number of micro-holes were found surrounding the cavity of the WC particle, as shown in figure 5.5b. Figure 5.6 shows the worn surface of specimen WC6 (100% WC in pasting powder). After the wear test, the worn surface shows that cracking was found to occur at the overlapping region of the clad tracks. This is due to the weak matrix exists at the overlapping region. This may cause problem if the tests were to run for a long time. The clad layer may peel off should the cracks extend deep into the matrix. Thus, it is not recommended that 100% WC particles should be used for cladding even though the wear resistance is excellent.

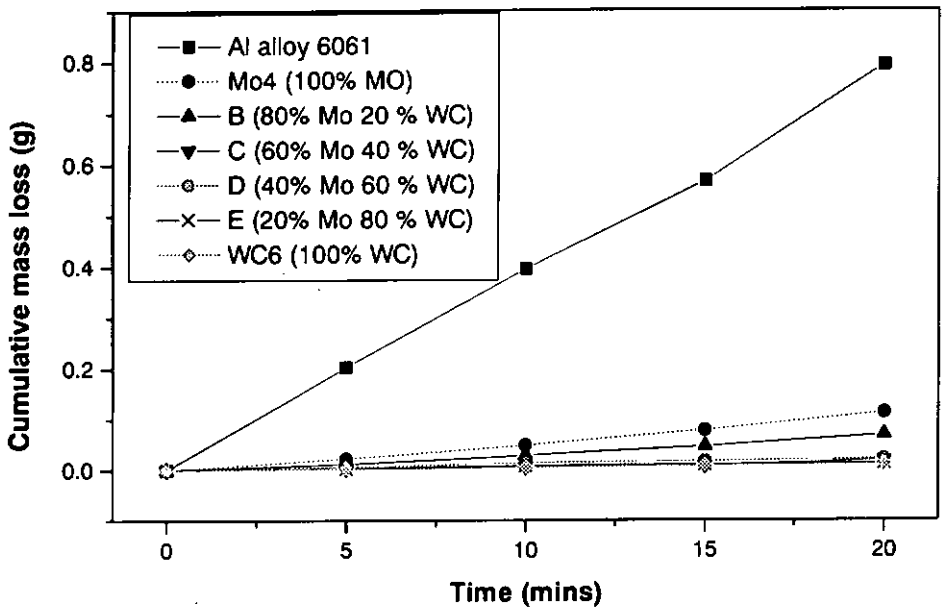

Figure 5.1 Wear test results of cumulative mass loss on the laser clad specimens and the as-received Al alloy AA6061.

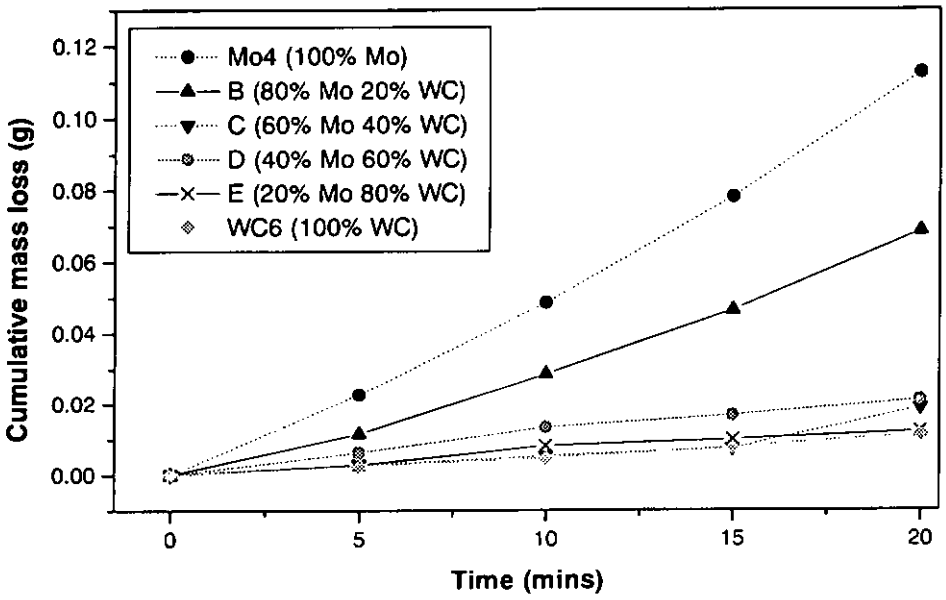

Figure 5.2 Results of cumulative mass loss on the laser clad specimens. (note the scale of the vertical axis)

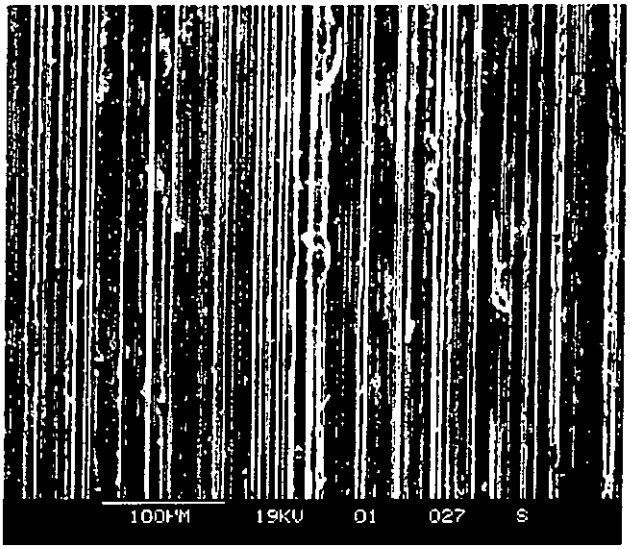

Figure 5.3a Scanning electron micrograph of the worn surface of Al alloy AA6061 surface.

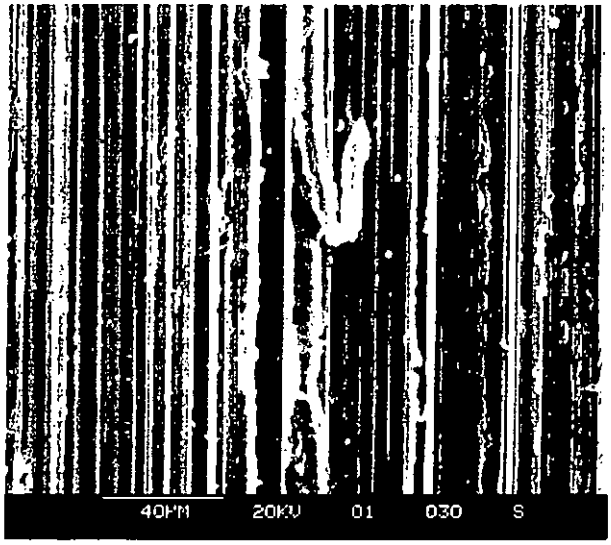

Figure 5.3b Higher magnification of the aluminum alloy AA6061 worn surface.

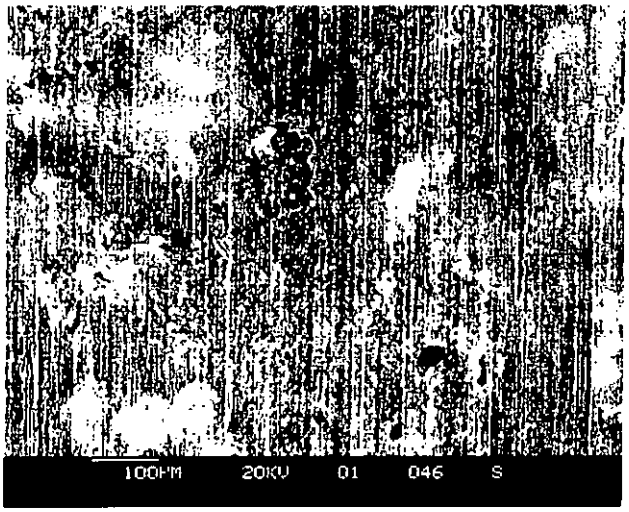

Figure 5.4a Scanning electron micrograph of the worn surface of specimen Mo4 (100% Mo pasting powder).

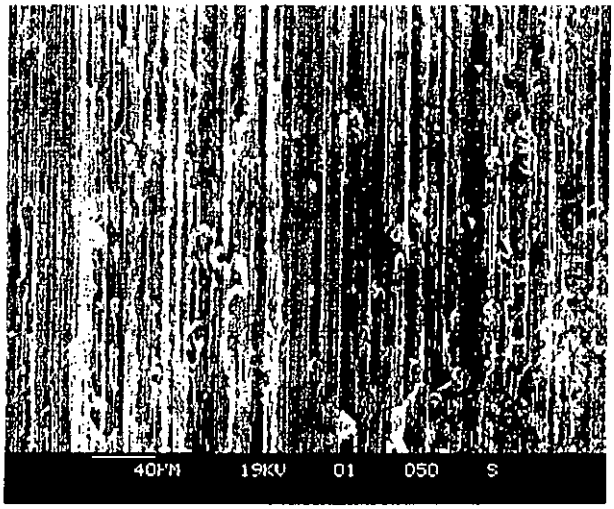

Figure 5.4b Higher magnification of the worn surface of specimen Mo4 (100% Mo pasting powder).

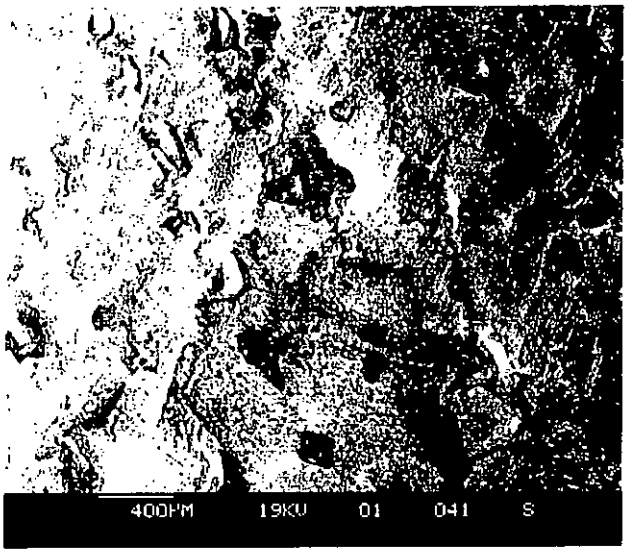

Figure 5.5a Scanning electron micrograph of the worn surface of the specimen E (20%Mo 80%WC in pasting powder).

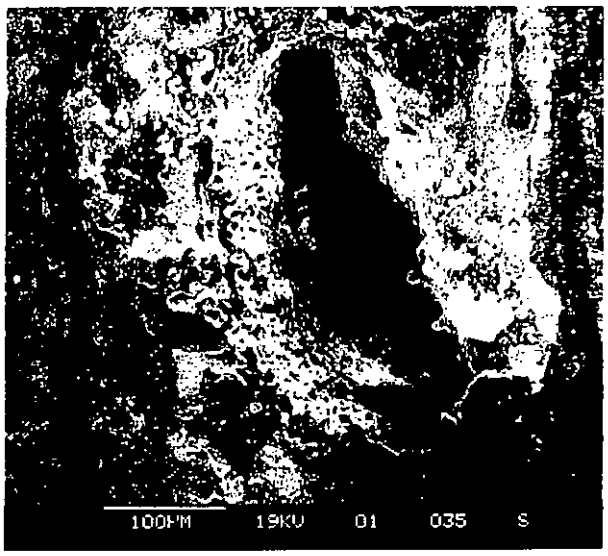

Figure 5.5b WC torn off after the abrasive wear test.

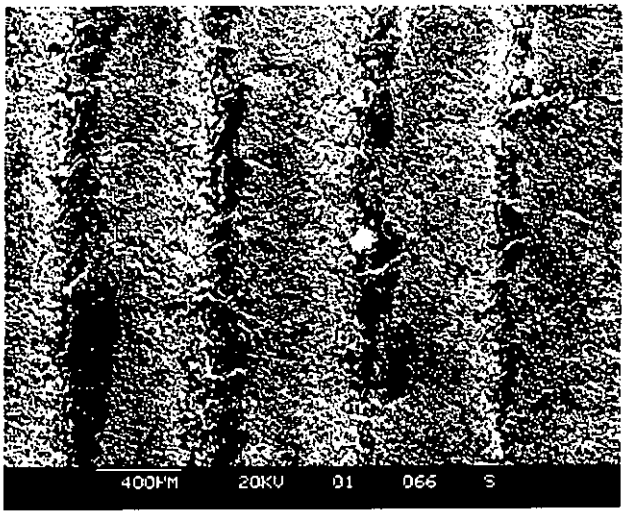

Figure 5.6a Scanning electron micrograph of the worn surface of the specimen WC6 (100%WC in pasting powder)

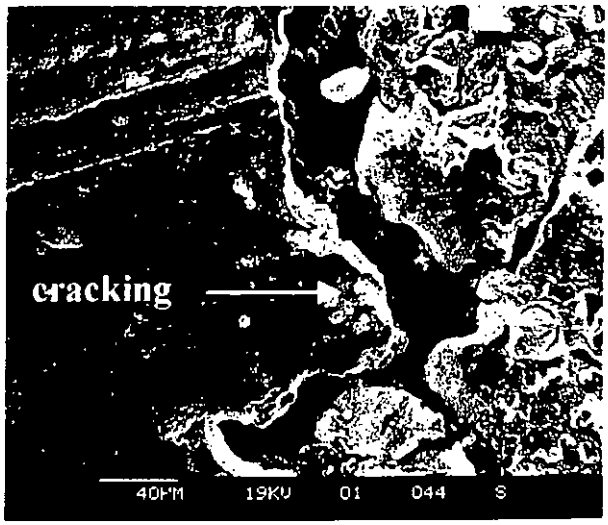

Figure 5.6b Cracking occurred on the worn surface of specimen WC6.

5.3 WEAR RESISTANCE ANALYSIS OF LASER CLADDING Mo, Mo/TiC, Ti ON ALUMINUM ALLOY AA6061

For most cases, the microhardness is directly related to the wear resistance. It means that the higher hardness, the higher wear resistance and lower cumulative mass loss. But it is more complicated for the mechanism of MMC abrasive wear test. The wear properties completely differ from those of the single constituents and depend on microstructural configuration. High wear resistance of the clad layer was combined with the results of the hard phases of TiC particles and soft matrix of Al-Mo / Al-Mo-Ti. Moreover, the better bonding strength between the TiC particle and the soft matrix, the lesser its mass loss.

Wear tests were performed on the laser clad surfaces which had been treated using 70% overlapping of single tracks. The wear behaviors were compared with the as-received sample. Figure 5.7 indicates that the MMC clad surfaces have less mass loss than the un-treated sample. Figure 5.8 shows the average mass loss of the laser clad specimens of Mo, Bb, Cc, Dd and TiC6 using a different scale in the vertical axis. Table 5.2 shows that the mass loss of the un-treated sample is 4 times higher than sample Mo (100% Mo pasting powder). The Mo clad specimen only has AlxMoy intermetallic material at the clad layer, and its hardness is about 230Hv. All the samples clad with different percentage of Mo and TiC showed great improvement on mass loss after the 20 minutes test. 20-28 times improvement was recorded when the specimen TiC and Bb were compared with the as-received alloy.

This indicates that the enhanced wear resistance is mainly attributed by the undissolved TiC particles. The incorporation of TiC particles enhances the resistance to plastic deformation and delays the occurrence of delamination.

Figure 5.9 is the worn surface of Al alloy AA6061. It is clearly shown that delamination occurs, and the material is removed from the surface during wear. As the Al alloy has relatively low hardness and poor wear resistance, the abrasive particles are able to plough deeply into the surfaces and cause microcutting and grooving. Figure 5.10 is the worn surface of 70%TiC 30% Mo pre-placing powder clad layer. In this sample, no such kind of grooving occurs. The soft matrix Al-Mo/ Al-Mo-Ti provides a good embedding environment for the hard TiC particles which are evenly distributed on cladding layer. Figure 5.11 shows the surface morphology of the worn surface of specimen TiC6 (100% TiC) after the abrasive wear test. The delamination wear mechanism appears and cracking occurs constantly at the surface. As the clad surface was built up by successive overlapping tracks, TiC free region was found at the overlapping interface (Figure 5.12, region 2). Figure 5.13 shows the inter-track zone of 100% TiC clad specimen. This is the weakest part of the cladding track and cracking occurs at the zone on the worn surface after 20 minutes abrasive wear test (Figure 5.11b). This phenomenon also occurs on WC6 (100% pre-placing WC powder) as well. The average mass loss of specimens Bb, Cc, Dd and TiC6 are similar, but cracking occurs significantly on the surface of specimen TiC6 (100% pre-placing TiC). Under this circumstance, composition of 70% TiC 30% Mo as pasting coating (specimen Cc) is suggested as the optimum powder composition for laser cladding of Mo/TiC on Al alloy to withstand abrasive wear.

Table 5.2 Average mass loss (g) of specimens from the moving pin-on-disc experiment after 1414m sliding distance (per 5 mins test cycle).

Specimen	AA6061-T651	Mo (100% Mo)	Bb (50%Mo, 50%TiC)	Cc (40%Mo, 60%TiC)	Dd (30%Mo, 70%TiC)	TiC6 (100%TiC)
Average mass loss (g)	0.4538	0.1125	0.0227	0.0202	0.0176	0.0161

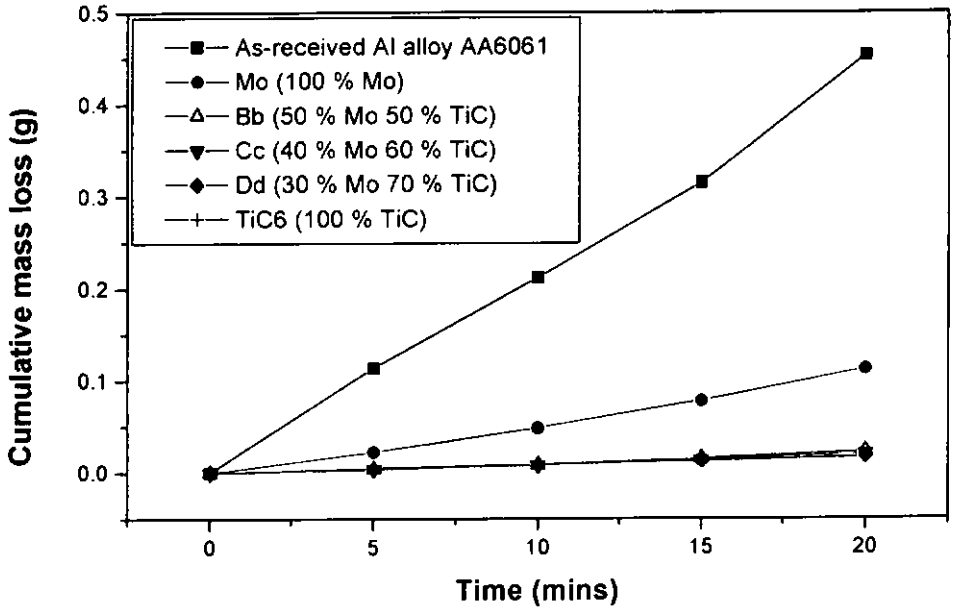

Figure 5.7 Wear test results of cumulative mass loss on the laser clad specimens and the as-received Al alloy AA6061.

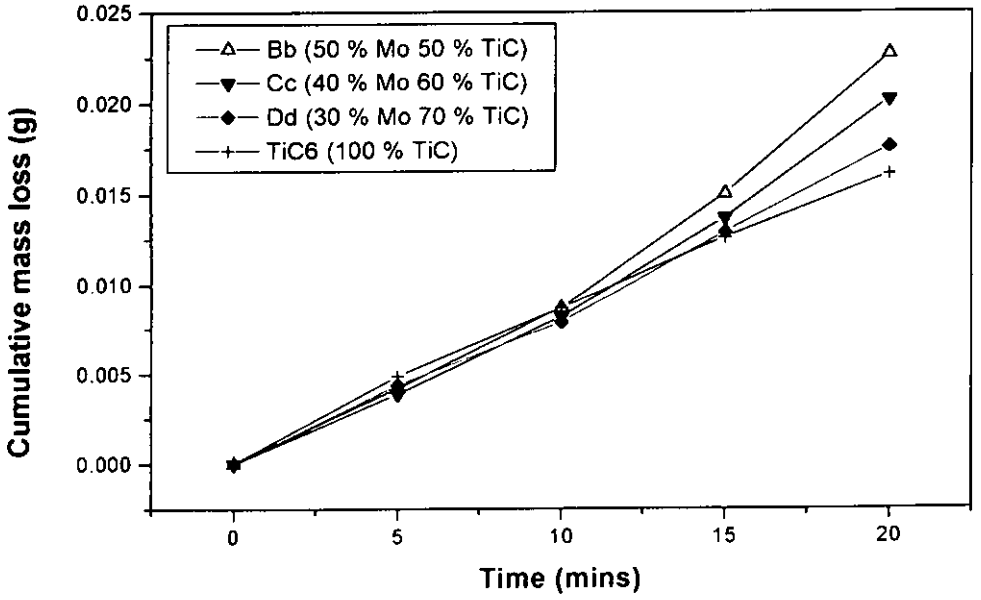

Figure 5.8 Results of cumulative mass loss on the laser clad specimens.

(note the scale of the vertical axis)

Figure 5.9 Worn surface of the as-received Al alloy AA6061.

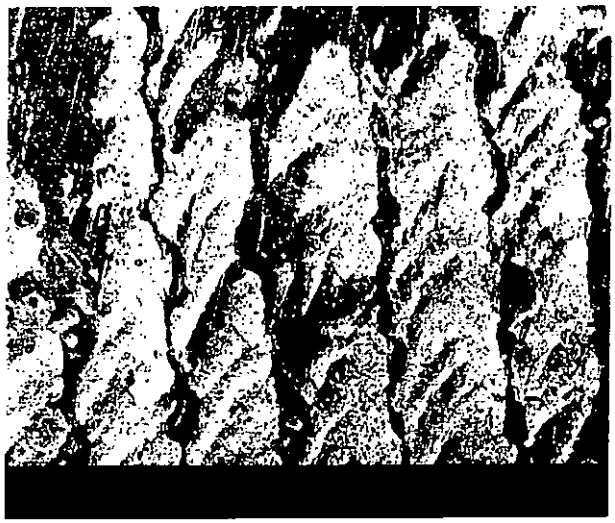

Figure 5.10 Scanning electron Micrograph of the worn surface of specimen D (30%Mo 70% TiC pre- placing powder).

Figure 5.11a Scanning electron micrograph of the worn surface of specimen TiC6 (100% TiC pre-placing powder).

Figure 5.11b Cracking occurred at the overlap track interface.

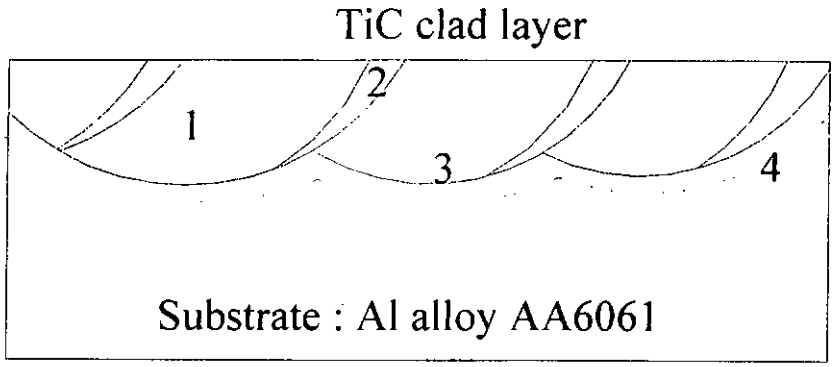

Figure 5.12 Schematic view of a transverse cross-section of the TiC clad layer. (1) clad zone, (2) overlap track interface zone, (3) substrate clad layer interface , (4) heat affected zone in substrate.

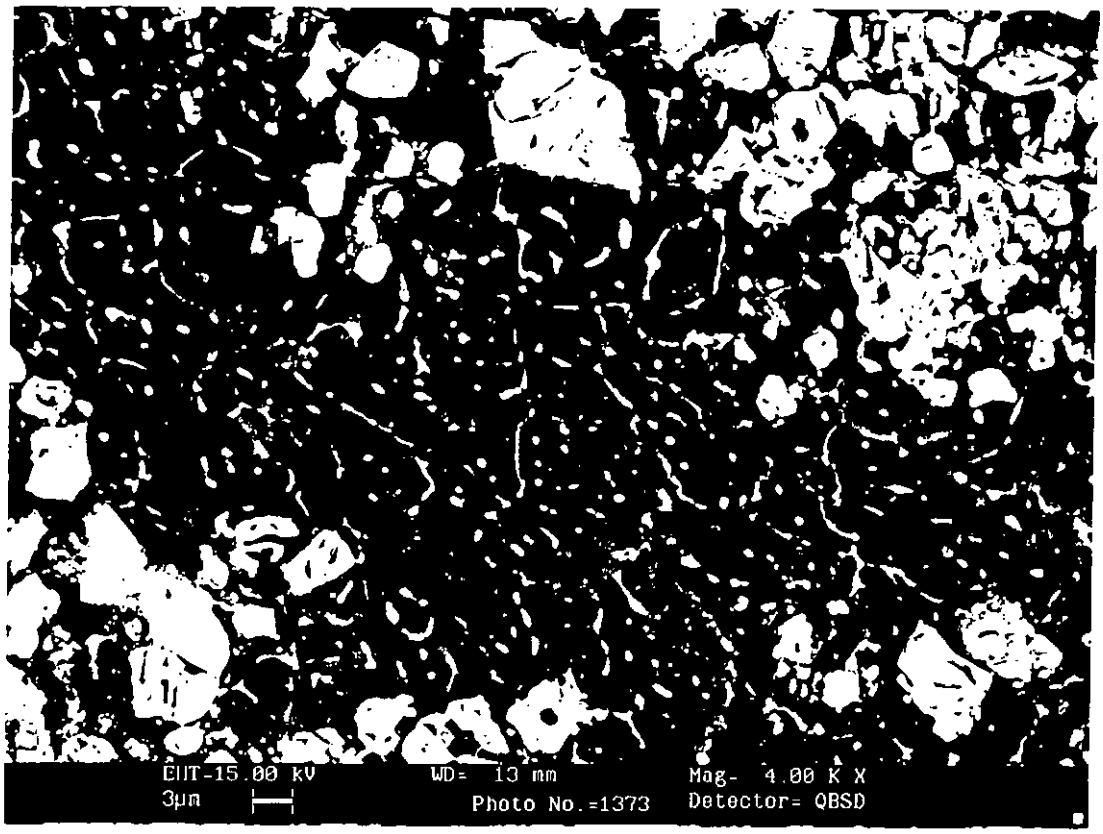

Figure 5.13 The overlap track interface zone of 100% TiC clad specimen.

(Note: the depletion of TiC particles in this zone)

5.4 *WEAR RESISTANCE ANALYSIS BY USING ARCHARD EQUATION*

Archard equation is widely used to express the sliding or abrasive wear behavior of metals and alloys.

$$V = (kPL)/H \qquad \text{Archard equation [136,137]}$$

Where V is volume loss, P is the applied load, L is the sliding distance, H is the Vickers hardness and k is the wear constant.

From the equation, V volume loss is inversely proportional to the Vickers hardness. It means that higher hardness will have lower volume loss and this imply to lower wear rate. However, this equation may not be suitable to apply directly to the abrasive wear property of the laser clad MMC layer. The strength of the matrix and the interfacial strength between the two phases of a composite play critical roles in the performance of the composite. The volume loss of the specimen studied after the abrasive wear test should not only be related to the hardness of the material. Figure 5.14 & 5.15 show the relationship of cumulative mass loss of the MMC layers versus the hardness value. The cumulative mass loss is not inversely proportional to the microhardness for both Mo/WC and Mo/TiC clad systems. It must be emphasised that the assumption of constant density was used in the MMC layer. In fact, the density varies between each specimen and within the specimen itself. A more detail investigation in this property is needed for future work.

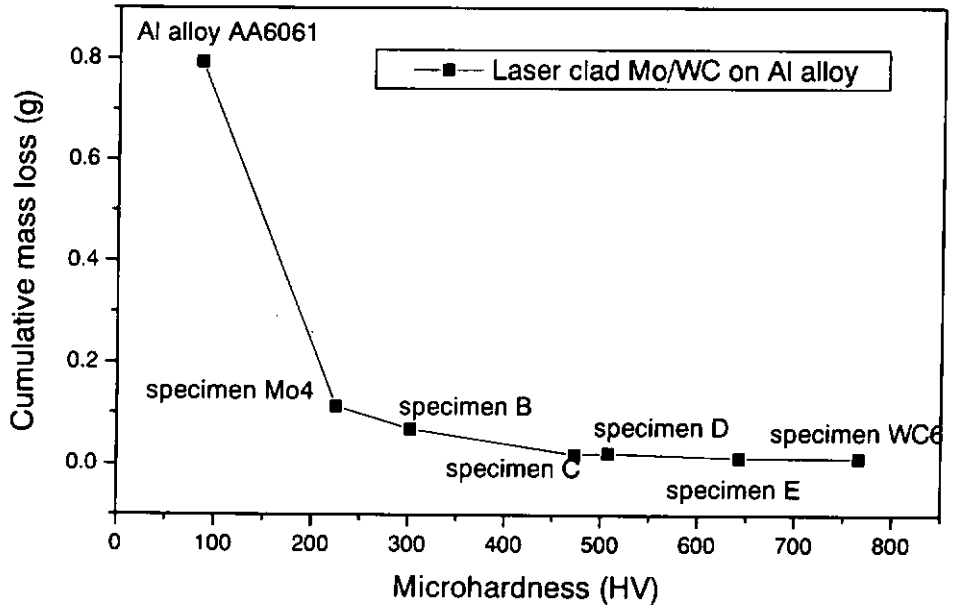

Figure 5.14a The relationship of cumulative mass loss of the as-received Al alloy and laser clad Mo/WC MMC system versus the hardness value.

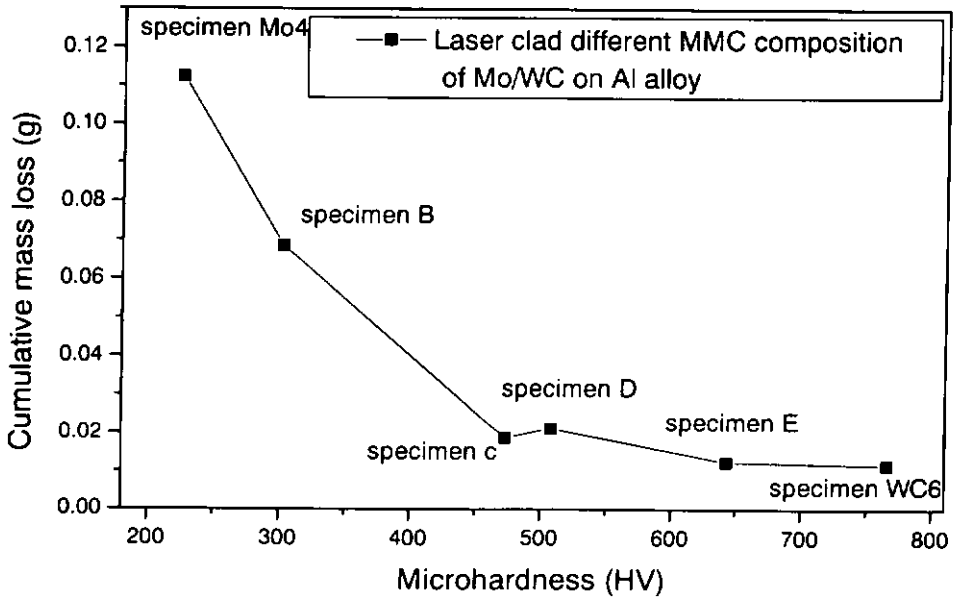

Figure 5.14b The relationship of cumulative mass loss of the laser clad Mo/WC MMC layers versus the hardness value.

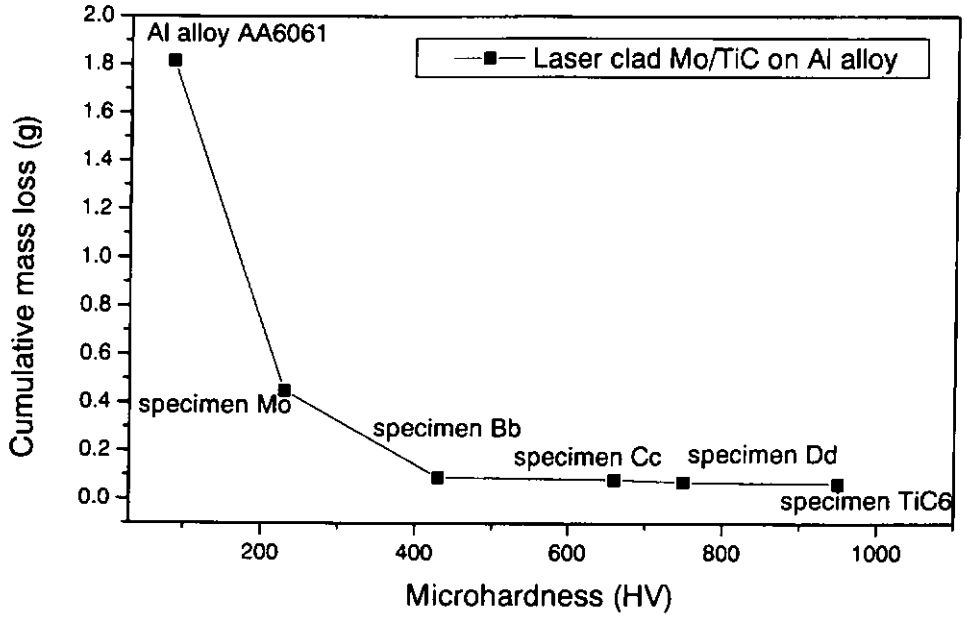

Figure 5.15a The relationship of cumulative mass loss of the as-received Al alloy and laser clad Mo/TiC MMC system versus the hardness value.

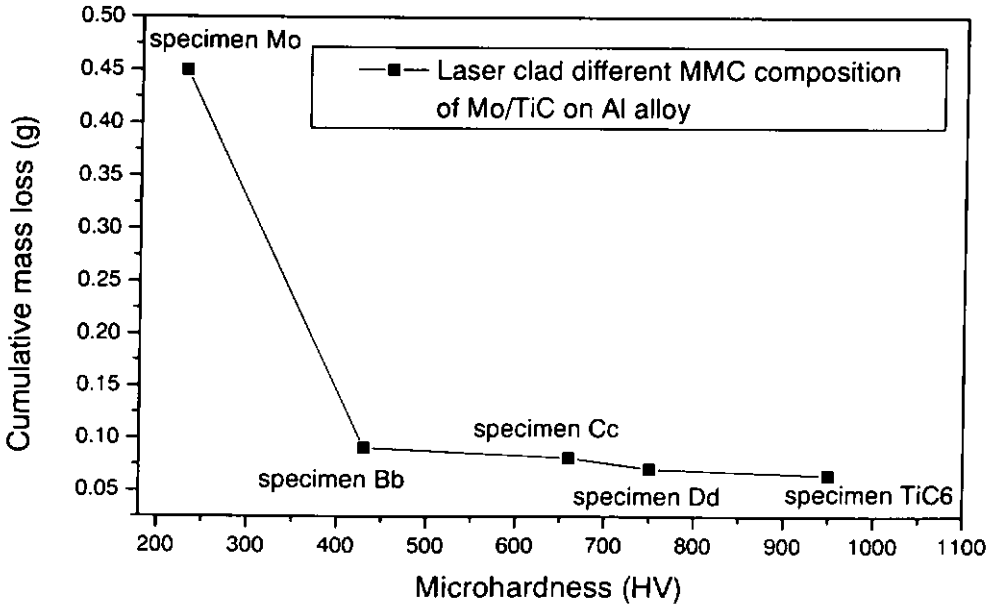

Figure 5.15b The relationship of cumulative mass loss of the laser clad Mo/TiC MMC layers versus the hardness value.

Chapter 6

Conclusion

The fabrication of a Mo/WC surface MMC on aluminum alloy substrate can be achieved using laser cladding of pre-pasted powders of Mo and WC. The processing parameters were 17 mm/s beam scanning speed, 3 mm beam diameter and 1.4 kW laser power at the workpiece and 0.3 mm pre-placed layer thickness. Different ratios of Mo and WC in the powder paste were studied and the clad layers of all ratios were free of crack and porosities. Excellent interface between the surface MMC and the substrate was formed. The interface between the reinforced WC phase and the Mo/Al matrix is enhanced by the epitaxially grown dendrites on the partially melted surface of the WC particles. The hardness and wear resistant properties of the Mo/WC surface MMC were significantly better than the Al alloy.

The fabrication of a Mo/TiC surface MMC on aluminum alloy substrate can be achieved using laser cladding of pre-pasted powders of Mo and TiC. The optimum processing parameters were 3 mm laser beam size, 17 mm/s beam scanning speed, 1.3 kW laser power at work and 0.25 mm pre-placed layer thickness. The clad surface was built up by 70% overlapped single tracks. A smooth MMC layer can be produced with well-embedded particles in the layer under this operation condition. Excellent interfacial bonding between the whole series of Mo/TiC clad specimens and the Al substrate was found. The microhardness of laser claddings with different pre-mixed compositions of Mo/TiC and with pure TiC is 5-10 times higher than that of the as-received Al alloy. Compared with the as-received Al alloy AA6061, the cumulative wear loss of the laser clad specimens with 50 % to 100% TiC pre-placed powder is 20-28 times better. However, there

was a weak region in-between the overlapping track interface. Hard TiC particles were displaced away and a TiC particle free region existed in the overlap track interface. These weak regions cracked during abrasive wear test. It was found that clad layers with a powder paste of 70% TiC with 30% Mo provided the best abrasive wear resistant properties.

Preliminary studies on cladding with Si_3N_4 , Mo/Si_3N_4 and TiC/Si_3N_4 on Al alloy were also carried out. The results show that Si_3N_4 is not a good cladding material for Al alloy. Under laser irradiation, Si_3N_4 is easily dissociated into Si and N, and the release of N_2 gas causes porosity on the surface of the clad layer. For the Mo/ Si_3N_4 system, Mo cannot form good bonding with Si_3N_4 because of the decomposition of Si_3N_4. So, only a laser alloying layer could be formed. For 50%Mo 50%Si_3N_4 pre-placed powder, the alloyed zone was about 800μm. It was found that the melt tracks were quite homogeneous and a good degree of mixing was achieved after the LSA treatment. Finally, the TiC/ Si_3N_4 system was studied. Failure of the clad layer is commonly associated with the clad layer interface. As the coating material and the substrate have different physical and mechanical properties, failure of the clad layer is commonly associated with the interfacial bond.

The results of this project are useful for the fabrication of a surface MMC on the Al alloy for improving the wear resistant property of the Al alloy.

Chapter 7

Suggestions for Further Study

1. The results of the present study have highlighted that Al alloy can be modified to form a surface MMC that possesses excellent abrasive wear resistance. The addition of Mo/WC, Mo/TiC was favorable for enhancing the abrasive wear resistance. Abrasive wear test and adhesive wear test of the laser clad sample should be studied in detail.
2. All MMC systems and their processing parameters should be optimized. The size, shape and purity of the metal powders, ceramic powders, process optimization, and characterization of the coatings should be investigated in detail.
3. To investigate the corrosion property of the clad specimens. The ideal clad layer should always be wear resistant with corrosion resistant.
4. More detail microstructural examinations of the microstructure of the clad layer in order to understand the alloy compositions and formation mechanism.
5. Coaxial nozzle with powder feeding system is suggested for the further development. Laser cladding by powder injection is superior to alternative processes and is the most practical way for industrial usage. Coaxial nozzle can provide better shielding for laser cladding and rapid alloy prototyping. Among the recent developments in laser cladding, rapid prototyping and rapid alloy prototyping are particularly exciting.
6. Higher laser power with larger beam size should be used for achieving thicker MMC cladding.

References

1. William M. Steen, Laser Material Processing, Springer-Verlag, London, p.27 (1998).
2. G. M. Beford and P. Richards, Proc. Eng. Surf. Conf. London, Institutes of Metals, London, May, (1996)
3. K. Holmberg and A. Watthews, Coatings Tribology: Properties Techniques and Applications in Surface Engineering, Elsevier Sequoia, Amsterdam, (1994).
4. D.S. Rickerby and A. Matthews (Eds), Advanced Surface Coatings: A Handbook of Surface Engineering, Blackie, Glasgow, (1991).
5. C. Dawes, Surface Engineering, Vol. 7 , p.29(1991).
6. HMSO, Wear Resistant Surfaces in Engineering, London, (1986).
7. Bell, T, Metals Mater. ,Vol. 7, p.478, (1991).
8. J.S. Burnell-Gray and P. K. Datta, Surface Engineering Casebook: Solutions to corrosion and wear-related failure, Woodhead Publishing (1996).
9. D. Hemsley, Engineering, Vol.235, No.9, pp.25-27, (1994).
10. Plating and Electroplating, ASM Material Handbook: Surface Engineering Vol.5, Materials Park, Ohio : ASM International, 10th ed., pp.167-285, (1990).
11. G. Sundararajan, D. Srinivasa Rao, D.Sen and K. R. C. Somaraju, "Tribological Behaviour of Thermal Sprayed Coatings", Surface Modification Technologies XI (1998) pp.872-886.
12. S. Rangaswamy and H. Herman, "Metallurgical Characterization of Plasma Sprayed WC-Co Coatings" , Proceedings of the Eleventh International Thermal Spraying Conference, Pergamon Press, pp.101-110, (1986).

13. M.E. Vinayo, F. Kassabji and P. Fauchais, "Advances in Thermal Spraying", Proceedings of the Eleventh International Thermal Spraying Conference, Pergamon Press, pp.93-96, (1986).
14. R.W. Kaufold, A.J. Rotolica, J. Nerz and B.A. Kushner, "Thermal Spray Research and Applications", Proceedings of the Third National Thermal Spray Conference, U.S.A. pp.561-574, (1990).
15. Thermal Spray Coatings, ASM Material Handbook Vol.5, Materials Park, Ohio : ASM International, 10th ed., pp. 498-509, (1990).
16. F.L.Riley, 2nd European Symposium on Engineering Ceramics, Elsevier Applied Science, USA, pp.61-73, (1989).
17. B.C. Oberlander and E. Lugsheider, "Comparison of Properties of Coatings Produced by Laser Cladding and Conventional Methods", Materials Science and Technology, Vol. 8 , pp.657-665, (1992).
18. S. Nowotny, A. Richter and K. Tangermann, "Surface Protection of Light Metals by One-Step Laser Cladding with Oxide Ceramics", Journal of Thermal Spray Technology, Vol.8 (2), pp.258-262, (1999).
19. G.Y. Liang and T. T. Wong, "Investigate of Microstructure of Laser Cladding Ni-WC layer on Al-Si Alloy", Journal of Materials Engineering and Performance Vol. 6, pp.41-45, (1997).
20. G.Y. Liang, J.Y. Su, "The Microstructure and Tribological Characteristics of Laser-Clad Ni-Cr-Al Coatings on Aluminum Alloy", Materials Science and Engineering A. Vol. 290, pp.207-212, (2000).
21. T.T. Wong, G.Y. Liang, B.L. He, C.H. Woo, "Wear Resistance of Laser-clad Ni-Cr-B-Si Alloy on Aluminum Alloy", Journal of Materials Processing Technology Vol.100

pp.142-146, (2000).

22. Kenneth G.Budinski, "Overview of Surface Engineering and Wear", Effect of Surface Coatings and Treatments on Wear, ASTM STP 1278, S. Bahadur, Ed., American Society for Testing and Materials, pp.4-21, (1996).
23. F.J. Pérez , E. Otero, M.P. Hierro, C. Gómez, F. Pedraza, J. L. de Segovia, E. Román, "High Temperature Corrosion Protection of Austenitic AISI 304 Stainless Steel by Si, Mo and Ce Ion Implantation", Surface and Coating Technology, pp.127-131, (1998).
24. P. Sioshansi, Thin Solid Films Vol. 118, pp61-71, (1984).
25. William M. Steen, Laser Material Processing, Springer-Verlag London Limited, p.27, (1998).
26. E.V. Locke & R. A. Hella, IEEE J. Quantum Electron. QE-10, p.179, (1974).
27. X. M. Zhang, H.C. man, H.D. Li, "Wear and Friction Properties of Laser Surface Hardened En 31 Steel", Journal of Materials Processing Technology Vol. 69, pp.162-166, (1997).
28. R. Colaco, R. Vilar, "Laser Surface Melting and Post-heat Treatment of AISI 420 Stainless Tool Steel", Surface Modification Technologies XI, The Institute of Materials, London, pp. 600-606, (1998).
29. R. Vilar, F.J.Solgado., S.R.Figuira, "Laser Surface Melting of Cast Iorn, Ecalt – 90", Germany, pp593-604, (1990).
30. K.G. Watkins, M.A. McMahon, W.M. Steen, "Microstructure and Corrosion Properties of Laser Surface Processed Aluminum Alloys: A Review" , Materials Science and Engineering A, Vol. 231, pp.55-61, (1997).
31. H. J. Hegge, J.T.M. De Hosson, Scripta Metallurgica et Materialia, Vol. 24, pp.293, (1990).

32. U. Luft, H.W. Bergmann, B.L. Mordike, in: B.L. Mordike (Ed), Laser Treatment of Materials, DGM Informationsgesellschaft mbH, Oberursel, Germany, p.147, (1987).

33. J. Lasek, P. Bartuska, V. Synecek, 3 rd international Conference on Aluminum Alloys, Trondheim, Norway, pp.22-26, (June 1992).

34. P.W. Leech, Thin Solid Films, Vol.177, pp.133, (1989).

35. M. Pierantoni, M. Gremaud, P. Magnin, D. Stoll, w. kurz, Acta Metallurgica et Materialia Vol.40 , p.1637, (1992).

36. M. Rappaz, C. Charbon, R. Sasikumar, Acta Metallurgica et Materialia 42, p.2365, (1994).

37. Muneharu KUTSUNA & Yoshihiro INAMI, "Study on Surface Remelting of Aluminum Alloy Castings by CO2 Laser Using a Rotating Optical Device", Proceedings of the International Congress on Applications of Lasers and Electro-Optics (ICALEO), pp.689-698, (1995).

38. H. Simiddzu, S. Katayama, A. Matsunawa, Proceedings of the International Congress on Applications of Lasers and Electro-Optics (ICALEO), Laser Institute of America, Orlando, FL, p.492 , (1990).

39. S. Katayama, H. Muraki, H. Simidzu, A. Matsunawa, Proceedings of the International Congress on Applications of Lasers and Electro-Optics (ICALEO), Laser Institute of America, Orlando, FL, p.352, (1991).

40. A. Munitz, Metallurgical Transactions, Vol. 11B, p.563, (1980).

41. Olaineck C., Luhrs D. , "Laser Camshaft Remelting", Lasers and Power Beam Processing, pp.15-16, (1996).

42. Mordike S., "Laser Surface Remelting of Camshafts", Lasers in Engineering, (1993).

43. E.M. Breinan, B.H. Kear, and C. M. Banas, Physics Today , p.44, (November 1976).

44. John F. Ready, Industrial Applications of Lasers, Academic press, pp.89, 331, 380-381, (1997).

45. Toshihide Taeda, Kaoru Adachi, Hideo Hisada, "Laser Alloying of Aluminum Alloy Substrate", In: Proceedings of LAMP' 92, pp.795-800, (June1992).

46. P. Vanhille, S. Tosto, J. M. Pelletier, A. Issa, A. B. Vannes, B. Criqui, "Electron Beam and Laser Surface Alloying of Al-Si Based Alloys", Surface and Coatings Technology, Vol. 50 , pp.295-303, (1992).

47. Ernst Wolfgang Kreutz, Maria Rozsnoki and Norbert Pirch, "Surface Remelting and Alloying of Al-Based Alloys with CO2 Laser Radiation", Proceedings of LAMP'92 Nagaoka, pp.787-793, (June, 1992).

48. P. Sallamand and J. M. Pelletier, "Laser Cladding on Aluminum-base Alloys: Microstructural Features", Materials Science and Engineering A, Vol. 171, pp.263-270, (1993).

49. A. Almeida, R. Vilar, R. Li, M. G. S. Ferreira, K. G. Watkins, W. M. Steen, "Laser Alloying of Aluminum and 7175 Aluminum Alloy for Enhanced Corrosion Resistance", Proceedings of the International Congress on Applications of Lasers and Electro-Optics (ICALEO), pp.903-911, (1993).

50. W. J. Tomlinson and A.S. Bransden, "Laser Surface Alloying of Al-12 Si", Surface Engineering, Vol. 11, pp. 337-344, (1995).

51. Z. Liu, C. S. Xie, K. G. Watkins, W. M. Steen, R. M. Vilar and M. G. S. Ferreira, "Microstructure and Pitting Behaviour of Al-Ti-Ni Laser Alloyed Layers in 2014 Aluminum Alloy Substrates", Proceedings of the International Congress on Applications of Lasers and Electro-Optics (ICALEO), pp.431-439, (1995).

52. Y. Liu, J. Mazumder and K. Shibata, "Microstructural Study of the Interface in Laser-

Clad Ni-Al Bronze on Al Alloy AA333 and Its Relation to Cracking", Metallurgical and Materials Transactions A, Vol. 26A, pp.1519-1533, (June 1995).

53. A. Almeida and R.Vilar, "Laser Alloying: A Tool to Produce Improved Al-Mo Surface Alloys", Proceedings of the International Congress on Applications of Lasers and Electro-Optics (ICALEO), pp.123-131, (1996)
54. Z. Liu, K. G. Watkins, M. A. McMahon and W. M. Steen, "Characteristics and Corrosion Behaviour of the Overlapped Area in Laser Surface Melted and Alloyed Aluminum Alloys", I Proceedings of the International Congress on Applications of Lasers and Electro-Optics (ICALEO), Section A pp.151-160, (1996).
55. Isamu Miyamoto, Satoshi Fujimori and Katsuhito Itakura, "Mechanism of Dilution in Laser Cladding with Powder Feeding", Proceedings of the International Congress on Applications of Lasers and Electro-Optics (ICALEO), pp.1-10, (1997).
56. M. Ignatiev, C. Dupuy, X. Sola, E. Thevenet, I. Yu. Smurov, L. Covelli, Laser and Electron Beam Alloying of Al with Fe and Sn, Applied Surface Science, Vol. 109, pp.137-142, (1997).
57. Z. Liu, K.G. Watkins, W.M. Steen, R. Vilar and M.G. Ferreira, "Dual Wavelength Laser Beam Alloying of Aluminum Alloy for Enhanced Corrosion Resistance", Journal of Laser Application, Vol. 9, pp. 197-204, (1997).
58. Zhiyue Xu, Keng H. Leong and Paul g. Sanders, "Laser Surface Alloying of Silicon into Aluminum Casting Alloys", Journal of Laser Applications, Vol. 12, No.4, pp.166-170, (2000).
59. Yongqing Fu, A. W. Batchelor. Yanwei Gu, K.A. Khor, Huting Xing, "Laser Alloying of Aluminum alloy AA6061 with Ni and Cr. Part 1. Optimization of Processing Parameters by X-ray Imaging", Surface & Coating Technology, Vol. 99, pp.287-294,

(1998).

60. N. Pirch, G. Backes, E. W. Kreutz, X. He, A. Weisheit, B. L. Mordike, "Laser Surface Alloying of Al and AlSi10Mg with Ti and Ni ", Proceedings of the International Congress on Applications of Lasers and Electro-Optics (ICALEO), pp.189-196, (1998).
61. J. Kelly, K. Nagarathnam, and J. Mazumder, "Laser Cladding of Cast Aluminum-Silicon Alloys for Improved Dry Sliding Wear Resistance", Journal of Laser Applications,Vol. 2 No. 2, pp.45-54.
62. A.H. Wang, C.S. Xie and H. Nie, "Microstructural Characteristics of Iron Based Alloy Laser Clad on Al-Si Alloy", Materials Science and Technology, Vol. 15, pp.957-964, (Aug 1999).
63. R. Vilar, "Laser Alloying and Laser Cladding", Materials Science Forum, Vol. 301, pp.229-252, (1999).
64. R. Vilar, "Laser Cladding", Journal of Laser Application, Vol. 11 No.2, pp.64-79, (April 1999).
65. C.L. Sexton and G. Byrne, "Alloy Development by Laser Cladding: An Overview", Journal of Laser Applications, Vol. 13, No. 1, pp.2-11, (Feb 2001).
66. Steffen Nowotny, Anne Müller, Anja Techel, Ulrich Franz, Fraunhofer Institut für Werkstoff-und Strahhltechnik, Dresden, Laser Surface Cladding of Aluminum with Oxide Ceramics, Germany, pp.37-44, (1997).
67. C. Chan, J Mazumder and M.M. Chan, "A Model for Surface Tension Driven Fluid Flow in Laser Surface Alloying", Lasers in Materials Processing, ASM, pp.150-157, (1983).
68. T. Chande and J. Mazumder, Metallurgical Transactions B, Vol. 14, pp.181-190,

(1983).

69. P. Gilgien and W. Kurz, "Microstructure and Phase Selection in Rapid Laser Processing", in Laser Processing: Surface Treatment and Thin Film Deposition, J. Mazumder, O. Conde, R. Vilar and W. Steen Editors, Kluwer Academic Publishers, Dordrecht, pp.77-92, (1996).
70. O. Grong, Metallurgical Modelling of Welding, The Institute of Materials. London, (1994).
71. Yune-Hua Shieh, Jia-Tzann Wang, Han C. Shin and Shinn-Tyan Wu, Surface Coating Technology, Vol. 58, pp.73-77, (1993).
72. T. N. Baker, H. Xin, C. Hu and S. Mridha, "Design of Surface In Situ Metal-Ceramic Composite Formation Via Laser Treatment", Materials Science and Technology, Vol. 10 , pp.536-544, (1994).
73. H. C. Man, C. T. Kwok and T. M. Yue, "Cavitation Erosion and Corrosion Behaviour of Laser Surface Alloyed MMC of SiC and Si_3N_4 on Al Alloy AA6061", Surface and Coatings Technology, Vol. 132 , pp.11-20, (2000).
74. C.Hu, T.N. Baker, "Laser Processing to Create in-situe Al-SiCp Surface Metal Matrix Composites", Journal of Materials Science, Vol.30 , pp.891-897, (1995).
75. A. Hinse-Stern, D. Burchards and B.L. Mordike, "Laser Cladding with Pre-placed Wires, Presented in Laser Treatment of Materials", DGM Metallurgy Information, pp.223-228, (1992).
76. F. Hensel, C. Binroth and G. Sepold, "A Comparison of Powder-fed and Wire-fed Laser-beam Cladding", Presented in Laser Treatment of Materials, DGM Metallurgy Information, pp.39-44, (1992).
77. Zhenda Chen, Chew Leong Lim, Ming Qian, "Laser Cladding of WC-Ni Composite",

Journal of Material Processing Technology, Vol. 62, pp.321-323, (1996).

78. Minlin Zhong, Kefu Tao, Wenjin Liu, Qiang Ma, "High Power laser Cladding Stellite 6 + WC with Various Volume Rate", Proceedings of the International Congress on Applications of Lasers and Electro-Optics (ICALEO), pp.114 –123, (2000).
79. D. Pantelis, A. Tissandier, P. Manolatos and P. Ponthiaux, "Formation of Wear Resistant Al-SiC Surface Composite by Laser Melt-particle Injection Process", Materials Science and Technology, Vol. 11, pp.299-303, (1995).
80. András Roósz, J. Sólyom, I. Teleszky, "Some Observations Made in the Structure of Laser-Remelted Layer of TiC- and WC-Alloyed Al-Alloy", Prakt. Metallogr ,Vol. 35, pp.449-455, (1998).
81. J. Lin and W.M. Steen, "Design Characteristics and Development of a Nozzle for Coaxial Laser Cladding", Journal of Laser Application, Vol. 10, No2, pp.55-63, (1998)
82. Jehnming Lin, "Laser Attenuation of the Focused Powder Steams in Coaxial laser Cladding", Journal of Laser Applications, Vol.12, No. 1, pp.28-33, (2000).
83. William F. Smith, Principles of Materials Science and Engineering, McGraw-Hill, pp.536-538, (1996).
84. Serope Kalpakjian, Manufacturing Engineering and Technology, Addison-Wesley Publishing Company, 3 rd Edition, pp.178-180, (1995).
85. M. Murphy, C. Lee and W.M. Steen, "Studies in Rapid Prototyping by Laser-Surface Cladding", in ICALEO 93 Laser Materials Processing, 1994, Bellingham: Spie – International Soc. Optical Engineering, pp. 882-892, (1993).
86. Alexander G. Grigoryants, Basic of Laser Material Processing, Advances in Science and Technology, Mir Publishers, pp.281-306.
87. M. A. McMahon, K.G. Watkins, M.G.S. Ferreira, R. M. Vilar, and W.M. Steen, "Laser

Surface Alloying of 2014 Aluminum Alloy with Molybdenum for Enhanced Corrosion Resistance", In: Proc. NATO Advanced Study Institute, Sesimbra, Portugal (July 3-16, 1994).

88. R. Li, M.G.S. Ferreira, A. Almeida, "Localized Corrosion of Laser Surface Melted 2024-T351 Aluminum Alloy", Surface Coating technology, Vol. 81, pp.290-296, (1996).

89. M.G.S. Ferrira, R. Li, J. S. Fennandes, A. Almeida, R. Vilar, K.G. Watkins, "Pitting Corrosion of Laser Surface Modified Aluminum Alloys", Material Science Forum, pp.421-432, (1995).

90. G.L.Goswami, D. Kumar, A.L. Pappachan, A.K. Grover and K. Sridhar, "Characterization of Chromium Bearing Surface Alloys Produced by Laser Alloying on Low carbon Steel Substrates", Journal of Laser Applications, Vol. 7, pp.153-161, (1995).

91. C. Hu, L. Barnard, S. Mridha, T.N.Baker, "The Role of SiC Particulate and Al_2O_3 (Saffil) Fibers in Several Alloys During the Formation of in situ MMCs Developed by Laser Processing", Journal of Materials Processing Technology, Vol.58, pp.87-95, (1996).

92. P. H. Chong, H. C. Man, T. M. Yue, " Microstructure and Wear Properties of Laser Surface-cladded Mo-WC MMC on AA6061 Aluminum Alloy", Surface and Coatings Technology, Vol.145, pp.51-59 (2001).

93. E. Gaffet, J. M. Pelletier, S. Bonnet-Jobez, "Laser Surface Alloying of Nickel Film on Aluminum-based Alloy", Apply Surface Science, Vol.43, pp.248-255, (1989).

94. D.K. Das, K.S. Prasad, A.G. Paradkar, "Evolution of Microstructure in Laser Alloying of Aluminum with Nickel", Material Science Engineering A, Vol.174, pp.75-84,

(1994).

95. L.S. Wang, P.D. Zhu, K. Cui, "Effect of Ni Content on Cracking Susceptibility and Microstructure of Laser Clad Fe-Cr-Ni-B-Si Alloy", Surface Coating Technology, Vol. 80, pp.279-282, (1996).
96. D.K. Das, "Surface Roughness Created by Laser Surface Alloying of Aluminum with Nickel", Surface Coating Technology, Vol. 64, pp.11-15, (1994).
97. J. L. Sun, Z. Liu, C. Lee, W. M. Steen, K.G. Watkins and W. P. Brown, "Realization and Characterization of Al-Sn Alloy Layers Deposited on Mild Steel by Laser Cladding", Proceedings of the International Congress on Applications of Lasers and Electro-Optics (ICALEO), pp.640-649, (1995).
98. Hui Wang, Weiming Xia, Yuansheng Jin, "A Study on Abrasive Resistance of Ni-based Coatings with a WC Hard Phase", Wear, Vol.195, pp. 47-52, (1996).
99. Q. Li, T.C. Lei, W.Z. Chen, "Microstructural Characterization of WCp reinforced Ni-Cr-B-Si-C Composite Coatings", Surface and Coatings Technology, Vol. 114, pp.285-291, (1999).
100. M. Brandt, S. W. Huang and M. Samandi, "Pulsed Nd:YAG Laser Deposition of WC/Ni Clad Layers", Proceedings of the International Congress on Applications of Lasers and Electro-Optics (ICALEO), pp.133-140, (2000).
101. Beidi Zhu, Xiaoyan Zeng, Zengi Tao, Shuguo yang, Kun Cui, "Coarse Cemented WC Particle Ceramic-Metal Composite Coatings Produced by Laser Cladding", Wear, Vol. 170, pp.161-166, (1993).
102. R.C. Gassmann, "Laser Cladding with (WC+W2C)CoCrC and (WC+W2C)/NiBSi Composites for Enhanced Abrasive Wear Resistance", Material Science Technology, Vol. 12, pp.691-696, (1996).

103.C. Yang and X. Chen, "Laser Cladding of WC-Co Powder", Proceedings of the International Congress on Applications of Lasers and Electro-Optics (ICALEO), Orlando, FL (1990)

104.B. Grunenwald, J. Shen, F. Dausinger, and S. Nowotny, "Laser Cladding with a Heterogeneous Powder Mixture of WC/Co and NiCrBSi", Proceedings of the European Conference on Laser Treatment of Materials ECLAT'92, Göttingen. Oberursel : DGM, pp.441-416, (1992).

105.S. Nowontny, A. Techel, A. Luft, W. Reitzenstein, "Microstructure and Wear Properties of Laser Clad Carbide Coatings", Proceedings of the International Congress on Applications of Lasers and Electro-Optics (ICALEO), pp.985-993, (1993).

106.M. Cadenas, R. Vijande, Hontes and J. M. Sierra, "Wear Behaviours of Laser Cladded and Plasma Sprayed WC-Co Coatings", Wear, Vol. 212, pp.244-253, (1997).

107.P. Z. Wang, J. X. Qu, and H. S. Shao, "Cemented Carbide Reinforced Nickel-based Alloy Coating by Laser Cladding and the Wear Characteristics", Materials & Design, Vol. 17, pp.289-296, (1996).

108.R.C. Gassmann, S. Nowotny, A. Luft, W. Reitzenstein, and J. Shen, "Laser Cladding of Hard Particles Rich Alloys", Proceedings of the International Congress on Applications of Lasers and Electro-Optics (ICALEO), Orlando, FL, pp.288-300, (1992).

109.Ying-jiao Liang, Wu ji wu re li xue shu ju shou ce, Dong-bei da xue chu ban she, Shen-yang shi, pp. 43,239,419, (1993).

110.J.D. Ayers and T.R. Tucker, "Particulate-TiC-Hardened Steel Surfaces By Laser Melt Injection", Thin Solid Film, Vol.73, pp.201-207, (1980).

111.E. Lugsheider and H.Bolender, "One-Step-Powder Cladding of Oxide Ceramics on

Metal Substrates with CO_2 Laser Radiation", ECLAT'94 –European Conference on Laser Treatment of Materials, Bremen-Vegesack, Germany, (1994).

112.Q.Li, T.C.Lei, W.Z. Chen, "Microstructural Characterization of Laser-Clad TiCp-reinforced Ni-Cr-B-Si-C Composite Coatings on Steel", Surface and Coatings Technology, Vol.114, pp.278-284, (1999).

113.K.P. Cooper, P. Slebodnick, E. D. Thomas, "Seawater Corrosion Behavior of Laser Surface Modified Inconel 625 Alloy", Materials Science and Engineering A, Vol.206, pp.138-149, (1996).

114.G. Abbas, W.M. Steen and D.R.F. West, "Microstructure and Crack Formation Studies of Laser Produced Deposits", Proceedings of the International Congress on Applications of Lasers and Electro-Optics (ICALEO), pp.150-161, (1998).

115.H.C. Man, S. Zhang, F.T. Cheng and T.M. Yue, "In situ synthesis of TiC reinforced surface MMC on Al6061 by laser surface alloying", submitted to the Scripta Materialia (2001).

116.Xiaolei Wu, "In situ Formation by Laser Cladding of TiC Composite Coating with a Gradient Distribution", Surface and coatings Technology, Vol. 115, pp.111-115, (1999).

117.J. H. Ouyang, Y. T. Pei, T. C. Lei, Y. Zhou, "Tribological Behaviour of Laser-clad TiCp Composite Coating", Wear, Vol. 185, pp.167-172, (1995).

118.T.C. Lei, J.H. Quyang, Y.T. Pei, Y. Zhou, "Microstructure and Wear Resistance of Laser Clad TiC Particle Reinforced Coating", Materials Science and Technology, Vol. 11, pp.520-525, (1995).

119.Chong-Cheng Huang, Wen-Ta Tsai, Ju-Tung Lee, "Microstructure and Electrochemical Behaviour of Laser Cladded Fe-Cr-Mo-Si-N Surface Alloys on Carbon Steel", Materials Science and Engineering A, Vol.196, pp.243-248, (1995).

120.Chong-Cheng Huang, Wen-Ta Tsai, Ju-Tung Lee, "The Effect of Silicon Nitride on the Surface Alloying with Fe-Cr-Si_3N_4 Powders", Scripta Metallurgica et Materialia, Vol. 32, No.9 , pp.1465-1470, (1995).

121.X.M. Zhang, H.C. Man, H.D. Li, "Wear and Friction Properties of Laser surface hardened En31 Steel", Journal of Material Processing Technology, Vol. 69, pp.162-166, (1997).

122.Raymond G. Bayer, Mechanical Wear Prediction and Prevention, Marcel Dekker, New York. pp.11-36.

123.Huei-Long Lee, Wun-Hwa Lu and Sammy Lap-Ip Chan, "Abrasive Wear of Powder Metallurgy Al Alloy 6061-SiC Particle Composites", Wear, pp. 223-231, (1992).

124.A. Kagawa and Y. Ohta, "Wear Resistance of Laser Clad Chromium Carbide Surface Layers", Materials Science and Technology, Vol.11, pp.515-519, (1995).

125.Zang, X. D., Y. J. Bi and M. H. Loretto, "Structure and Stability of the Precipitates in Melt Spun Ternary Al-Transition Metal Alloys", Acta Metallurgical Material, Vol. 41 pp.849, (1993).

126.Polesya, A. F. and A. I. Stepina, Phys. Met. Metallogr. (Engl. Transl.), Vol.30, pp.35, (1970).

127.Chang, C. P. and M. H. Loretto, "The Annealing Behaviour of Rapid Solidification Processed Al-Mo Alloys", Material Science and Engineering, Vol. 98, p.185, (1988).

128.Bi, Y. J. and M.H. Loretto, "The Influence of Iron on Precipitation from Supersaturated Al-Mo Solid Solutions", Material Science and Engineering A, Vol.134, p.1188, (1991).

129.The Handbook of Binary Phase Diagrams, General Electric, Vol.1.

130.JCPDS Powder Diffraction Data, International Center for Diffraction Data, (1989).

131.L. J. Yang, "Pin-on-disc Wear Testing of Tungsten Carbide with a New Moving Pin Technique", Wear, pp.557-562, (1999).

132.A. G. Wang, I.M. Hutchings, "Wear of Alumina Fiber Aluminum Metal Matrix Composite by Two-body Abrasion", Material Science Technology, Vol.5, pp.71-76, (1989).

133.W. Kurz and D.J. Fisher, "Fundamentals of Solidification", Trans. Tec. Publications, Aedermansdorf , p.242, (1986).

134. A.B. Kloosterman and J. Th. M.De Hosson, "Characterization of a Metal Matrix Composite Produced with Laser Particle Injection", Surface Modification Technologies XI, pp. 625-633, (1998).

135.Chong-Cheng Huang, Wen-Ta Tsai, Ju-Tung Lee, Laser Surface Alloying of Carbon Steel with Fe-Cr- Si_3N_4 Powders, Scripta Metallurgica et Materialia, Vol. 30, No.11, PP1461-1466, (1994)

136. D. Scott, "Treatises on Materials Science and Technology", Vol.13, Wear, Academic Press, New York, pp.221-222, (1997).

137. L. J. Yang, Pin-on-disc Wear Testing of Tungsten Carbide with A New Moving Pin Technique, Wear, Vol 225-229, pp.557-562, (1999).

Appendix I

Laser Cladding of WC on various alloys

Author	Substrate	Coating/ adding material	Year	Finding	Remarks	Ref.
				WC cladding		
Yang	Low carbon steel	WC/Co-base	1990	Microstructure of coating varies considerably with processing conditions, coating hardness of 1725 Hv and wear resistance increased by a factor of 5.	Wear test	103
Grunenwald	Low carbon steel	WC/Co-base	1991	Similar to Yang		104
Gassmann	Steel	Stellite 21, Cr, Mo	1992	The commercial stellite alloys are not always suited for cladding in combination with WC. The production of crackless coatings requires a Co matrix alloy, such as Stellite 21, but with lower contents of Cr and Mo.		108
Beidi Zhu	20Ni4Mo steel	WC particle (600-900 ì m),Ni-base flux alloy powder	1993	The microhardness of the laser cladded surface was 13.7-16.2GPA and with uniform distribution of the ceramic particles. The abrasive wear results showed that laser cladded coating have superior wear resistance to atomic hydrogen welded coating.	CO_2 laser, pre-placed powder with chemical binder	101
Nowotny	16MnCr5 case hardening steel	Stellite 21, NiBSi, WC	1993	The optimized WC/Co-NiBSi system yields the best results with respect to wear, flaws and cost. Claddings with Stellite 21 binder showed that minimum wear at contents of 35vol% hard material, though cracking and debonding spoil the over-all performance.	CO_2 laser, 2 separate powder feeding	105
H. Wang	Nodular cast iron, phosphor-cast iron	Ni-WC	1996	The best laser-treated plasma-sprayed Ni60%+60% WC coating had significant improvement on wear resistance.	Plasma spraying with laser post-treatment	98
Gassmann	Mild steel	(WC+W_2C) CoCrC, (WC+W_2C)/ NiBSi	1996	Coatings with up to 40% carbides had excellent bonding and no cracks for enhanced abrasive wear resistance.	CO_2 laser, powder injection	102

P.Z. Wang	AISI 1045 steel	Nickel base powder, WC-Co	1996	Block-on-ring dry sliding wear test and rubber wheel slurry erosive abrasive wear test have been conducted to study wear properties. The WC-CO cladded samples were showed to have superior wear and corrosion resistance.		107
Chen	AISI 1020 mild steel	Ni-WC	1996	Maximum hardness, superior wear resistance and low dilution (<5%) were achieved.	CO_2 laser, powder injection	77
Cadenas	AISI 1043	WC-Co	1997	Compared with plasma spray and laser clad process, the wear rate of the latter was 34% lower than the former.	CO_2 laser, powder injection	106
G. Y. Liang	Al-Si cast alloy surface	Ni-WC	1997	The highest microhardness 1027 Hv was found in the high nickel-region.	Plasma spraying with CO_2 laser post-treatment	19
András Roósz	Al alloy	TiC, WC	1998	Result showed that WC with much higher density, so it has a tendency to sink into the bottom of the clad. While, TiC was agglomerated at the surface of the sample. Because TiC particles did not penetrate the oxide layer of Al alloy.	CO_2 laser, powder injection	80
Q. Li	1045 steel	WCp/ Ni-Cr-B-Si-C	1999	30vol.% WCp / Ni-Cr-B-Si-C composite coatings were deposited on AISI 1045 steel by laser cladding. It was found that WC would partially dissolved on the surface of particulates in the melt pool.	CO_2 laser, pre-placed powder with chemical binder	99
M. Brandt	H13 tool steel	WC/Ni	2000	1 mm thick, fully dense and crack-free clad layer were produced. The average microhardness of the coating was 650Hv and abrasive wear resistance was up to 10 times higher than the heat-treated H13 steel.	Nd:YAG laser, powder injection	100
T. T. Wong	$AlSi_8Cu_1Mg$	Ni-Cr-B-Si and Ni-Cr-B-Si+WC	2000	Laser-clad plasma-sprayed specimen has higher hardness and better abrasion wear resistance than plasma sprayed specimen. The author proved that the Ni-Cr-B-Si+WC laser clad specimen without significant improvement in wear resistance when compared with laser-clad Ni-Cr-B-Si sample.	Plasma spray coating and post-treatment by 5kW CO_2 Pin-on-disc abrasion wear tester is used	21
Minlin Zhong	E24 low carbon steel	Stellite + WC	2000	No cracking was appeared until WC volume over 18%. The average hardness and cracking increased when increase of the volume % of WC.	Duel powder feeding system	78

Appendix II

Laser Cladding of TiC on various alloys

		TiC				
J. D. Ayers	304 Stainless Steel	TiC	1980	Partial dissolution of the carbide particles increased the microhardness of the austenitic matrix to 200 – 250Hv.	CO_2 laser, powder injection	110
T.N. Baker	Titanium alloy	SiC, in situ formation of TiC	1994	This proved that the wear resistance of laser cladded Ti was increased by 2 times.	CO_2 laser, powder injection	74
Lugsheider	mild steel	TiC, Stellite 6	1994	Powder premixed in single hopper was the effective method for producing high grade wear resistance coating on stressed components.	Powder premixed in single hopper	111
T.C. Lei	1045 steel substrate	TiC–Ni	1995	The partially dissolution and aggregation of the original TiC particles during melting of the Ni alloy and showed that TiC particles would significant enhanced wear resistance.	CO_2 laser, pin-on-ring fricton and wear test	118
J.H. Ouyang	1045 steel	TiC–Ni	1995	Studied its tribological behaviour by using pin-on-ring friction and wear test with lubrication. The results showed that the degree of wear depended mainly on the extend of debonding and removal of TiC.	CO_2 laser, powder injection, pin-on-ring adhesive wear test.	117
K.P. Cooper	Inconel 625 alloy	TiC, WC	1996	Corrosion was occurred in WC particles itself. For TiC, corrosion also occurred in the eutectic carbide. Result showed that corrosive damage was more severe in the WC injected sample than in TiC injected sample and in the laser melted sample. The homogenized microstructure was found and reducing the dissolution of the particle would minimize the sea water corrosion.	CO_2 laser, powder injection	113
András Roósz	Al alloy	TiC, WC	1998	Result showed that WC with much higher density, so it has a tendency to sink into the bottom of the clad. While, TiC was agglomerated at the surface of the sample. Because TiC particles did not penetrate the oxide layer of Al alloy.	CO_2 laser, powder injection	80

A.B. Kloosterman	Ti-6Al-4V	TiC, TiN and SiC powder	1998	TiC and SiC showed that an improvement in bending strength and fracture toughness. The relative wear resistance was relatively higher for SiC particles in Ti-6Al-4V after abrasive were test.	Nd:YAG laser, Powder injection	134
Xiaolei Wu	5CrMnMo steel substrate	In situ reacted TiC, Ni	1999	TiC particles were distribution uniformly. TiC-γ-Ni interfaces were free from any deleterious surface reaction. Micohardness of the clad layer up to 1250 Hv.	CO_2 laser, pre-placed powder, pin-on-disc abrasive wear test	116
Q. Li	AISI 1045	TiC/ Ni-Cr-B-Si-C	1999	The result showed that the partially dissolution of TiC was occurred on melting and the epitaxial growth of the remaining particles took place by the precipitation of TiC upon cooling.	CO_2 laser, pre-placed powder with chemical binder	112
H.C. Man	Aluminum Alloy AA6061	In situ Ti SiC synthesize	2001	The hardness layer reached a value of Hv 650.	Nd:YAG laser, pre-placed powder	115

Appendix III

Laser Cladding of Si_3N_4 on various alloys

			Laser clad Si_3N_4 on substrate			
Chong-Cheng Huang	AISI 1020 carbon steel	Fe-Cr- Si_3N_4	1994	Laser surface alloyed homogeneous stainless steel layers on carbon steel to improve the corrosion resistance of carbon steel. The results proved that Si_3N_4 decomposed after laser alloying.	4.5 kW CO_2 laser, milling a groove then pre-placed powder	135
Chong-Cheng Huang	AISI 1020 carbon steel	Fe-Cr- Si_3N_4	1994	Si_3N_4 reduces the oxidation during LSA. Because the decomposition of Si_3N_4 , it cause the formation of N_2 and decrease of O_2 content. The Fe-Cr/Si_3N_4 mixed powder increase the laser energy absorption and due to high dilution ratio of the surface alloyed layer.	4.5 kW CO_2 laser, milling a groove then pre-placed powder	120
Chong-Cheng Huang	Carbon steel	Fe/Cr/Mo, Fe/Cr/Si_3N_4 and Fe/Cr/Mo/ Si_3N_4	1995	Pre-mixed Fe/Cr/Mo, Fe/Cr/Si_3N_4 and Fe/Cr/Mo/ Si_3N_4 powders to the surface of carbon steel and to introduce Fe-Cr-Mo, Fe-Cr-Si-N and Fe-Cr-Mo-Si-N stainless layers. The addition of molybdenum is to increase the resistance of stainless steels to localized corrosion. This research focused on alloying Mo plus-N into a stainless steel surface layer by LSC and incorporating Fe/Cr/Mo/Si_3N_4. The polarization resistance of the laser cladded Fe-Cr-Mo-Si-N layer was proven higher than the other layers	CO_2 laser, pre-placed powder	119
H. C. Man	Alumimum Alloy AA6061	SiC/Si_3N_4	1999	The cavitation erosion resistance of 100% Si_3N_4 was improved by 3 times than that of monolithic AA6061, whereas no significant improvement in specimen cladded with 100% SiC.	2kW Nd-YAG laser, pre-placed with PVA paster	73